UNIVERSITÀ POLITECNICA DELLE MARCHE

FACOLTÀ DI INGEGNERIA

Corso di Laurea Magistrale in Ingegneria Civile

Ruolo delle polveri Sahariane sugli episodi meteorologici estremi nel Mediterraneo

The role of Saharan dust on extreme weather episodes within Mediterranean region

Relatore:
Prof. Ing. Giorgio Passerini

Correlatore:
Dott. Umberto Rizza

Tesi di laurea di:
Eleonora Brega

Anno accademico 2018/2019

INDEX

Abstract

L'inquinamento atmosferico da aerosol ha una stretta correlazione con i cambiamenti climatici che si stanno verificando sul pianeta Terra negli ultimi decenni.

Le particelle di aerosol modificano il bilancio energetico globale attraverso l'assorbimento e la deviazione delle radiazioni solari e terrestri (effetti diretti), ed influenzano la microfisica atmosferica agendo come nuclei di condensazione per il vapore d'acqua, con conseguenti variazioni nella formazione di nuvole e nelle precipitazioni (effetti indiretti).

Gli aerosol naturali sono quantitativamente superiori rispetto a quelli antropogenici, in particolare le polveri (*mineral dust*) costituiscono più del 75% degli aerosol presenti nell'atmosfera. Le loro emissioni sono dovute all'azione erosiva del vento soprattutto su superfici del suolo aride tipiche di aree desertiche o bacini alluvionali effimeri. La sorgente principale è costituita dal deserto del Sahara.

Una volta immesse in atmosfera, le particelle possono essere trasportate per lunghe distanze. Una delle regioni maggiormente colpite da intrusioni di polveri Sahariane è il bacino del Mediterraneo. Qui, molti degli eventi meteorologici estremi che avvengono, sono caratterizzati dalla presenza di polveri.

Ad oggi, la quantificazione degli effetti radiativi degli aerosol nel Mediterraneo è in una fase iniziale e i conseguenti effetti sul clima regionale devono ancora essere ben definiti.

Allo scopo di fornire ulteriori delucidazioni in merito, è stato scelto come oggetto d'indagine la tempesta "Vaia" che tra il 27 e il 30 ottobre 2018 ha imperversato sulla penisola Italiana provocando ingenti danni a causa delle forti raffiche di vento e delle abbondanti precipitazioni. L'evento è stato caratterizzato anche da elevati valori di umidità e da un'intensa intrusione di polveri Sahariane; quindi esso costituisce un valido caso studio per migliorare la conoscenza riguardo all'influenza degli aerosol sulla meteorologia (a breve termine) e sul clima (a lungo termine), oltre che per valutare la capacità di previsione da parte del modello numerico, essendo questa una fase fondamentale per lo scopo prefissato.

L'analisi sinottica dell'evento ha rivelato che si è trattato di un ciclone extra-tropicale, generato da un minimo depressionario formatosi al centro del Mar Mediterraneo in seguito all'irruzione di un fronte freddo proveniente dall'oceano Atlantico.

Sono state eseguite differenti simulazioni con il modello WRF-Chem, implementando al suo interno lo stesso setup per la microfisica, ma un diverso schema per l'emissione delle polveri (una volta è stato adottato lo schema GOCART/AFWA e un'altra volta quello proposto da Shao nel 2004).

Per quanto riguarda i parametri atmosferici sono stati indagati i campi riguardanti il vento, il vapore acqueo e le precipitazioni, mentre le informazioni sul carico e sulla distribuzione delle polveri Sahariane sono state ottenute analizzando l'AOD (Aerosol Optical Depth).

I risultati ottenuti dalle simulazioni sono stati confrontati con dati satellitari e dati di rianalisi climatica per valutarne l'attendibilità, e dal confronto sono emerse le seguenti informazioni:

1. Sottostima della velocità del vento a 10 m; ciò suggerisce la necessità di implementare nel modello una parametrizzazione della rugosità marina che consideri la presenza di *sea-spray* in condizioni di vento forte, poiché incide sulla rugosità superficiale. Tale aspetto non è stato considerato in questo studio e può essere causa della sottostima da parte del modello;
2. Leggera sovrastima delle precipitazioni (sia sulla colonna sia a terra); dovuta al fatto che il modello non ha correttamente considerato l'effetto indiretto esercitato dalle polveri Sahariane sulla microfisica atmosferica, poiché esse costituiscono dei nuclei di condensazione, che aumentano il numero di goccioline d'acqua e ne riducono la dimensione, implicando una riduzione delle precipitazioni;
3. I valori elevati di AOD ($\cong$ 3) sono intercettati più facilmente dallo schema AFWA, mentre Shao (2004) tende a sottostimarli; al contrario i valori relativamente più bassi ($\cong$ 1) sono riprodotti in maniera migliore dallo schema Shao (2004), mentre sono sovrastimati dallo schema AFWA. Tale sovrastima è legata al fatto che nello schema AFWA l'impatto del terreno è basso, poiché il flusso verticale di polveri tiene conto solo del contenuto di argilla, quindi ciò può sotto-rappresentare l'importanza del tipo di terreno. Differentemente lo schema Shao (2004) aggiunge

alcune correzioni, ad esempio tiene conto della copertura vegetativa, che influenza la soglia di velocità d'attrito, infatti, quanto maggiore è la vegetazione tanto più alta è la velocità necessaria a far sollevare le particelle di polvere. Un altro fattore correttivo incorporato nel modello Shao (2004) è quello per gli elementi a superficie non erodibile, il che porta indubbiamente a stime inferiori delle emissioni di polvere.

In generale, seppur con queste imprecisioni dal punto di vista quantitativo, il modello ha riprodotto in maniera egregia la distribuzione spaziale sia dei parametri atmosferici sia delle polveri. Sono state identificate come regioni sorgenti le aree desertiche dell'Africa settentrionale, in particolare il Sahara, ma anche la zona a sud della catena montuosa dell'Atlante, tra l'Algeria e la Tunisia, caratterizzata da un sistema di laghi salati effimeri che rimane secco in estate, ma riceve acqua in inverno, giocando un ruolo importante nella modulazione delle emissioni di polveri.

È stata confermata l'esistenza di un'interazione tra le *mineral dust* e i processi atmosferici, attraverso una simulazione eseguita adottando lo schema di microfisica "*aerosol-aware Thompson–Eidhammer*" all'interno del modello WRF-Chem. Ciò ha reso possibile quantificare, seppur in maniera preliminare, il numero di particelle di polvere che hanno agito come nuclei di ghiacciamento, influenzando lo sviluppo dell'evento meteorologico in esame. È probabile che alla violenza dei fenomeni osservati abbia in parte contribuito anche la superficie del Mediterraneo, avente temperature di 1-2 °C sopra la media e una maggiore disponibilità di energia e vapore acqueo, anche se non si sa ancora quanto. A tal proposito, sono in fase di progresso le indagini da parte del CNR-ISAC ed il gruppo di ricerca dell'UNIVPM.

Complessivamente questo studio rappresenta un banco di prova riguardante il potenziale delle informazioni satellitari in merito alla caratterizzazione e al monitoraggio degli eventi meteorologici sull'area Mediterranea e la possibilità di migliorare le capacità di previsione in questa complessa regione.

Introduction

Various scientific studies have consolidated the fact that aerosol emissions into the atmosphere contribute to climate change, due to their direct effects on the global radiation balance and indirect on the properties of clouds, from which semi-direct effects on atmospheric dynamics derive (Forster et al., 2007), and finally for their role in global biogeochemical cycles (Mahowald et al., 2010).

The consequences of climate change are already being felt all over the globe, but some areas are particularly affected. The Mediterranean region has been referenced as one of the most responsive regions to climate change (IPCC, 2013), due to the human activities, including land use changes, industry and population growth, combined with the growth of coastal urban regions (UNEP/MAP-Plan Bleu, 2012). This pressure is further amplified by the development of tourism in highly attractive Mediterranean coastal areas, and rapidly evolving changes in consumption patterns, as a result of increasing development (UNEP/MAP-Plan Bleu, 2012). The Mediterranean Sea is also one of the world's busiest shipping routes (UNEP/MAP-Plan Bleu, 2009). Moreover, the Mediterranean region is exposed to several natural risks, like volcano eruptions, dust outbreaks, fires or droughts.

Some aerosol transport models indicate that the average aerosol load over the Mediterranean basin is dominated by particles from the surrounding continental sources, in particular sulphate from anthropogenic sources (northern Europe) and mineral dust as product of wind erosion in arid areas (northern Africa).

The Sahara Desert is the main source of mineral dust globally (Prospero et al., 2002; Washington et al., 2003): about half of the total emission comes from it (Goudie, 2009; Ginoux et al., 2012). Moreover, among all the aerosol species present in the atmosphere, mineral dust is dominant in quantitative terms (Textor et al., 2006). In addition to the effects mentioned above, they affect human living conditions, influencing air quality, visibility and health, causing respiratory diseases and meningitis (Molesworth et al., 2002, 2003).

All this has led to an increasing demand for prediction of mineral dust outbreak, especially over the Mediterranean basin, and the topic has become of primary importance in the scientific community that deals with the Earth's atmosphere. In particular, the assessment of aerosol influences on climate by means of numerical simulations is essential for interpreting past climate and for projecting future changes for different emission scenarios.

The study and modeling of the emission and transport of Saharan dust are subject to continuous changes due to the complex weather situation in the region and the scarcity of observation measures, which are mainly concentrated in marginal areas, because they are logistically more accessible, while the central part of the Sahara has a low density of measuring/sampling instruments (Knippertz and Todd, 2012).

Consequently, there are still many uncertainties regarding the contribution of mineral dust particles to radiative forcing (RF) (Claquin et al., 1998; Todd et al., 2008), mostly due to their shape (Haapanala et al., 2012), but also their optical properties (Bi et al., 2011) and their chemical composition (Claquin et al., 1999; Scanza et al., 2015).

Recent insights in this field have allowed to have a better understanding of the phenomenon, especially thanks to the use of new satellite instruments including the Spinning Enhanced Visible and Infrared Imager (SEVIRI) installed on the Meteosat Second Generation (MSG) platform (Brindley and Ignatov, 2006; Thomas et al., 2007), the Multi-angle Imaging SpectroRadiometer (MISR) on board the TERRA spacecraft (Kalashnikova and Kahn, 2008; Kahn et al., 2009) and the Cloud-Aerosol LIdar with Orthogonal Polarization (CALIOP) on board the satellite CALIPSO (Cloud-Aerosol Lidar and Infrared Pathfinder Satellite Observations) (Winker et al., 2009), and the introduction of new algorithms, such as the “Deep Blue” in the MODerate-Resolution Imaging Spectroradiometer (MODIS) on board of TERRA and AQUA satellites (Hsu et al., 2013), which have been applied to improve the ability to monitor aerosol processes. Furthermore, the AERONET network (AErosol RObotic NETwork) provides the parameters concerning to the optical and physical properties of aerosols (Dubovik et al., 2000), which are then supplemented with satellite observations obtaining fundamental data on the distribution of natural and anthropogenic aerosols, at planetary level.

The information provided by ground-based and satellite measurements is a basis for evaluating the performance of predictive models of emission dynamics, transport and dust deposition mechanisms, as well as weather conditions and air quality.

In order to obtain simulation results as realistic as possible, it is necessary to know the physical and chemical properties of the aerosols and the processes that influence those properties so that they can be represented, through specific modules, in regional and global climate models (Ghan and Schwartz, 2007).

The uncertainties concerning mineral dust sources, their chemical composition, diffusion and removal mechanisms, nature of the soil and weather conditions, make it difficult to establish parameterization, but lead to continuous changes in modeling. This is evident in the study of Schulz et al. (2009) in which 15 different global aerosol models (AeroCom) were compared, as well as in the most recent work of Basart et al. (2016) where 9 simulations were performed with different regional models of mineral dust in Europe.

In this context, it was decided to study the role played by the Saharan dust in the meteorological event that affected the Italian peninsula between 27 and 30 October 2018.

It was a catastrophic storm, called “VAIA”, which raged on Italy for about three days causing significant economic and environmental damage, as well as to people, due to rainfall, but also to the strong wind, from the south-western dials, which has reached speeds of more than 200 km/h.

This *Scirocco* wind was responsible for the large amount of dust that came in the atmosphere, so much to tint the skies of a yellowish colour, and coming directly from the Sahara desert (https://www.centrometeoitaliano.it/notizie-meteo/sabbia-polvere-deserto-cieli-italia-pulviscolo-arrivo-sahara-29-10-2018-68196/).

A synoptic analysis was then carried out to assess the meteorological situation of the storm, and the intrusion of mineral dust; in particular, the fields of atmospheric pressure, wind, precipitation and AOD (Aerosol Optical Depth) were described, using the reanalysis data provided by ERA5 (ECMWF ReAnalysis-Fifth generation) and satellite data from MODIS.

After that, two simulations of the episode were performed with the WRF-Chem (Weather Research and Forecasting model coupled with Chemistry) model (Grell et al., 2005),

keeping the same configuration within it, except for the dust emission parameterization, which was once represented by the GOCART/AFWA scheme and another time by the Shao scheme (2004).

The results obtained were compared with reanalysis and satellite data. This comparison allowed to assess the ability of the WRF-Chem model to reproduce the meteorology and the transport of Saharan dust during the weather event examined.

A further simulation was performed considering in the physics suite the aerosol-aware Thompson–Eidhammer microphysics scheme, which is designed to include indirect effects of dust aerosols on cloud microphysics. This has enabled WRF-Chem to predict the number of dust particles that acted as ice nuclei, modifying the formation and development of clouds and precipitation during the strong wind and dust event studied.

1. ATMOSPHERIC AEROSOL

Before describing in detail the characteristics of mineral dust, a general overview of atmospheric aerosols should be given, so as to have a clear idea of the topic to which reference is made and the context in which the Saharan dust are inserted with all the problems that derive from them.

1.1. Generality

The atmospheric aerosol is a suspension of fine solid particles or liquid droplets in the air.
It includes a heterogeneous set of particles, having generally very different characteristics between them, whose composition can be different depending on the environment of origin, the period of the year (hot months or cold months), the sources (vehicle traffic, heating, industrial or agricultural emissions, soil particles eroded and carried by wind) and may vary over time. For this reason it is considered to be the most complex of all the components of the atmosphere (https://digilander.libero.it/silvanodgl3/aeropsol_atmosferico1.htm).
An aerosol particle may be defined as a set of molecules capable of preserving their physical and chemical characteristics for a sufficiently long time to be observed and sufficient to enable them to participate in physical and chemical processes as separate entities (http://fst.unife.it/it/orientamento/progetto-lauree-scientifiche/corso-di-eccellenza/allegati/eccellenza2008-DiMatteo.pdf).
Some of the parameters with which to characterize aerosol particles are primarily their size, but also their density, shape, surface and volume. The dimensions of the particles cover a range that extends for more than 4 orders of magnitude: from a few nanometres up to about 100 micrometres.
As for the shape (Fig. 1) they are distinguished in spherical, cubic or filamentous and can be classified according to the aerodynamic equivalent diameter d_{ae}, defined as the diameter of a perfectly spherical particle of unit density having inertial characteristics

equal to the test particle, considering the same conditions of temperature, pressure and relative humidity.

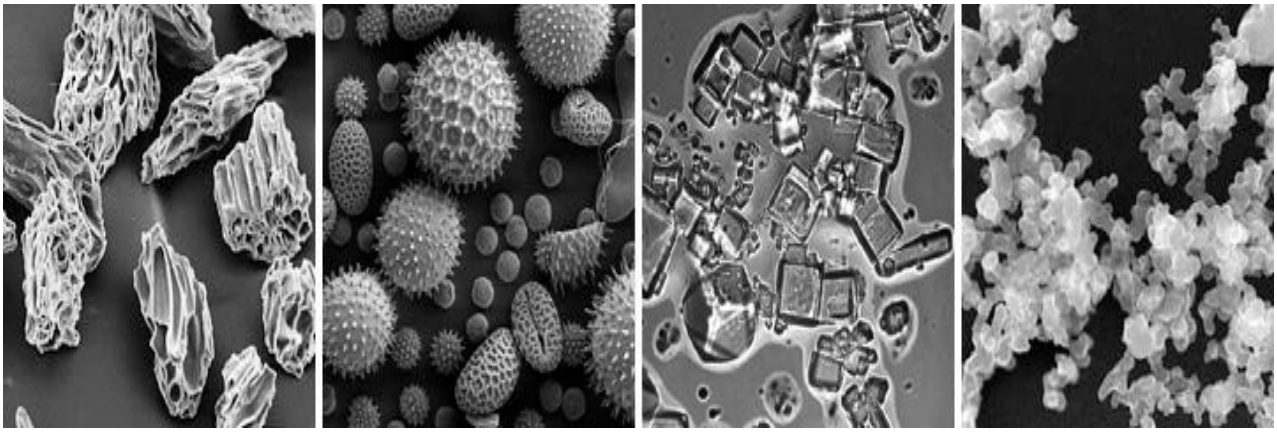

Figure 1. These scanning electron microscope images (not at the same scale) show the wide variety of aerosol shapes. From left to right: volcanic ash, pollen, sea salt, and soot. [Micrographs courtesy USGS, UMBC (Chere Petty), and Arizona State University (Peter Buseck).]

Their release into the atmosphere can occur through different types of sources (Fig. 2):

- Natural phenomena:
  - Transport of mineral dust (large air masses transport hundreds of millions of tonnes of sand from the Sahara to the West and to Europe every year);

  - Sea spray (aerosol particles released into the atmosphere after the explosion of air bubbles produced by the interaction between wind and wave motion of seas and oceans);

  - Volcanic eruptions (they are able to discharge large quantities of aerosols into the atmosphere);

  - Soil erosion;

- Emissions from vegetation;
- Forest fires (biomass burning).

➢ Anthropogenic phenomena:

- Traffic emissions (direct particulate emissions from combustion, but also tyre wear and asphalt);
- Industrial plants of various kinds (metallurgical plants make the largest contribution, followed by the cement industry);
- Dust produced by agriculture;
- Use of fossil fuels (domestic heating, energy production);
- Spreading salt;
- Waste disposal (incinerators).

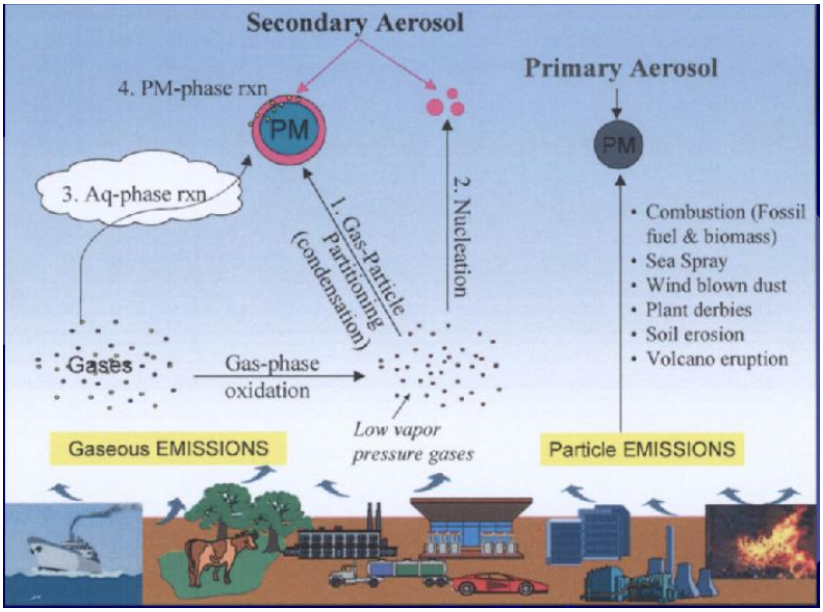

Figure 2. The aerosol sources (http://fst.unife.it/it/orientamento/progetto-lauree-scientifiche/corso-di-eccellenza/allegati/eccellenza2008-DiMatteo.pdf).

The contribution of natural aerosols is greater than that produced by man, which, unlike those of natural origin, can be controlled.

Although the quantity of anthropogenic aerosol is lower than that from natural sources, it is toxicologically more effective on health and tends to concentrate in urban and industrial centres, near the regions where land use changes have led to more dusty areas

(desertification) and where farming practices are common. Consequently, maximum concentrations are found in East America, Europe and East Asia, as well as in some regions of tropical Africa and South America (http://www.climate.be/textbook/chapter4_node3_2.html, Koch et al., 2007).

The diversity of the sources determines a different chemical composition of the particles that make up the environmental dust.

Coarse particles, which belong to the primary aerosol category (they are released directly into the atmosphere), are rich in elements typical of the Earth's crust (Fe, Si, Al, Ca, Mg) and biogenic organic substances (pollen, spores, plant fragments), in fact they are introduced into the environment mainly due to natural phenomena (Fig. 3).

Fine particles, which are mainly the secondary aerosol (they are formed in the atmosphere by chemical oxidation reactions which convert the precursor gases into the liquid or solid phase), are rich in carbon, nitrates and sulphates and derive above all from industrial activities (Fig. 3). However, in the fine fraction there are also compounds of primary origin, due for example to combustion, such as elemental carbon, some heavy metals (Ni, Fe, Cu, As) and PAHs (Polycyclic Aromatic Hydrocarbons).

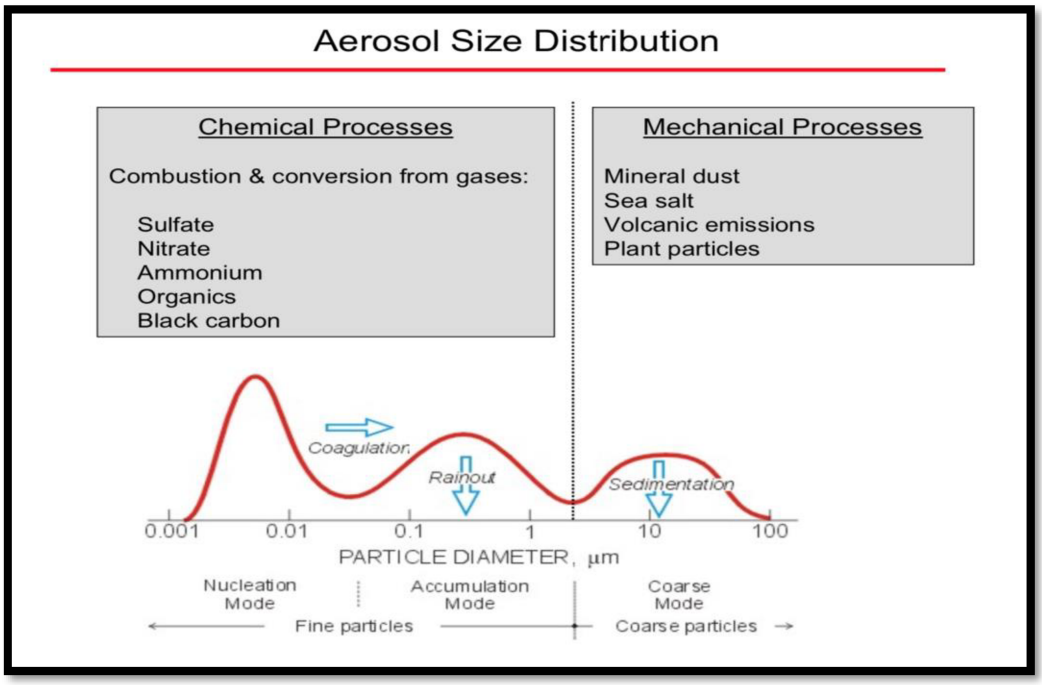

Figure 3. Aerosol particle size distribution and main sources (Rizza, University of Messina, School of Excellence, 22-26 July 2019).

Once the aerosol particles have reached the atmosphere, they undergo a transformation by different mechanisms (Fig. 4), such as:

- condensation (transformation from the gaseous to the liquid or solid state which occurs when the thermodynamic equilibrium of the chemical species between the gaseous and particulate phases moves towards the latter, due to the variation of the external conditions);
- evaporation (inverse process respect to condensation);
- coagulation (occurs by collision between two particles moving by thermal agitation, with the formation of larger particles; as a result, the overall number of particles is lost, but the mass concentration of atmospheric aerosol remains unchanged);
- activation (formation of water droplets when, the water vapour, under oversaturation, tends to condense on aerosol particles).

Finally, the removal of aerosols from the atmosphere may be by dry deposition (direct transfer to the Earth's surface without precipitation) or wet deposition (involves transfer to the Earth's surface in aqueous form: rain, snow or fog).

Dry deposition is the removal mechanism that occurs mainly in the part of the atmosphere close to the ground, while at heights greater than 100 m the scavenging operated by precipitation prevails; moreover, coarse particles (d_{ae} > 1 μm) are more subject to gravitational sedimentation and have a shorter residence time in atmosphere (in the order of minutes or seconds) than those with d_{ae} < 1 μm, which can remain in suspension even for days and are removed more easily by wet deposition, after activation in the clouds and subsequent precipitation (Zender et al., 2003). It should be noted that although a particle may be collected by a water droplet, it will not be removed from the air if the droplet evaporates rather than falls to the ground.

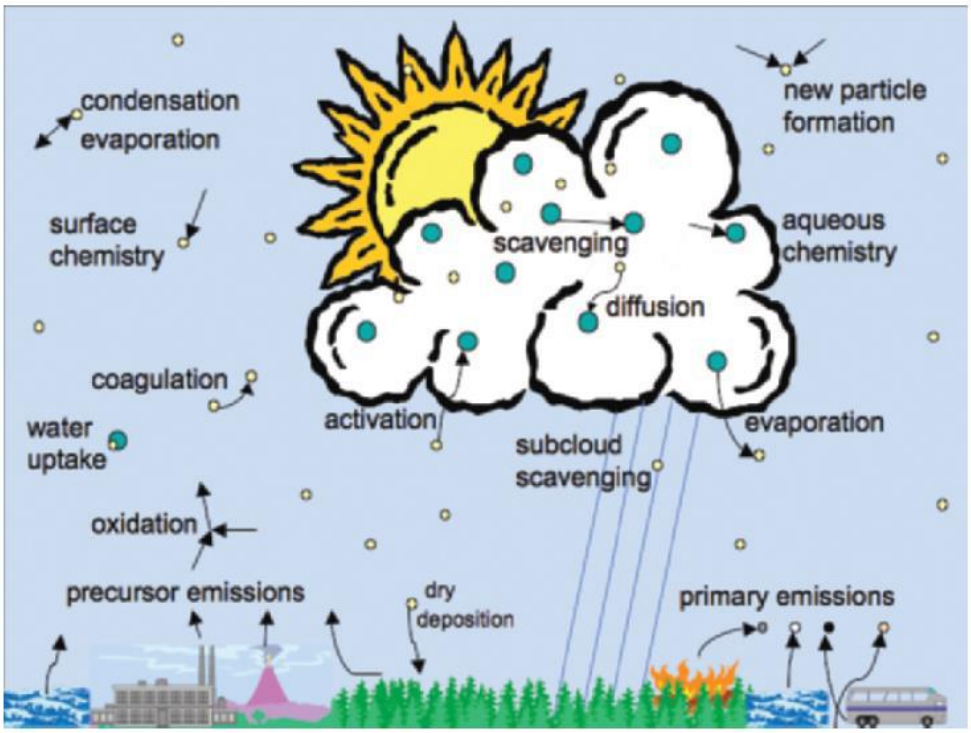

Figure 4. The main atmospheric processes to which aerosols are subject (Ghan et al., 2007).

All aerosol removal mechanisms are determined by the turbulent processes taking place in the PBL (Planetary Boundary-Layer), which is the layer of atmosphere most influenced by the presence of the Earth's surface, by the roughness and the heat emission which characterize it; therefore the aerosol concentration is a function of the quantity of substance released into the atmosphere, but also of the volume in which it is dispersed.

The atmospheric variables on which aerosol particles depends are:

- hydrometeors (without precipitation, the ability of the atmosphere to remove suspended particles is reduced, because wet deposition is less);
- wind (it can carry the aerosol over long distances, as well as causing the lifting of eroded dust);
- temperature (high temperature favours the mixing of particles, low temperature can cause thermal inversion phenomena which tend to "restrain" pollutants);
- mixing height (it coincides with the thickness of the atmosphere layer closest to the Earth's surface and has a direct influence on the concentration of pollutants released near the surface; its maximum value is about 2.5 km, the minimum 50 m, according to the day-night cycle and seasonal cycles).

It is deduced that knowing the chemical composition of atmospheric aerosol and physical-chemicals processes that can modify it is important in order to identify the different sources that have contributed to its formation and to understand its possible effects on the environment and human health (Fig. 5).

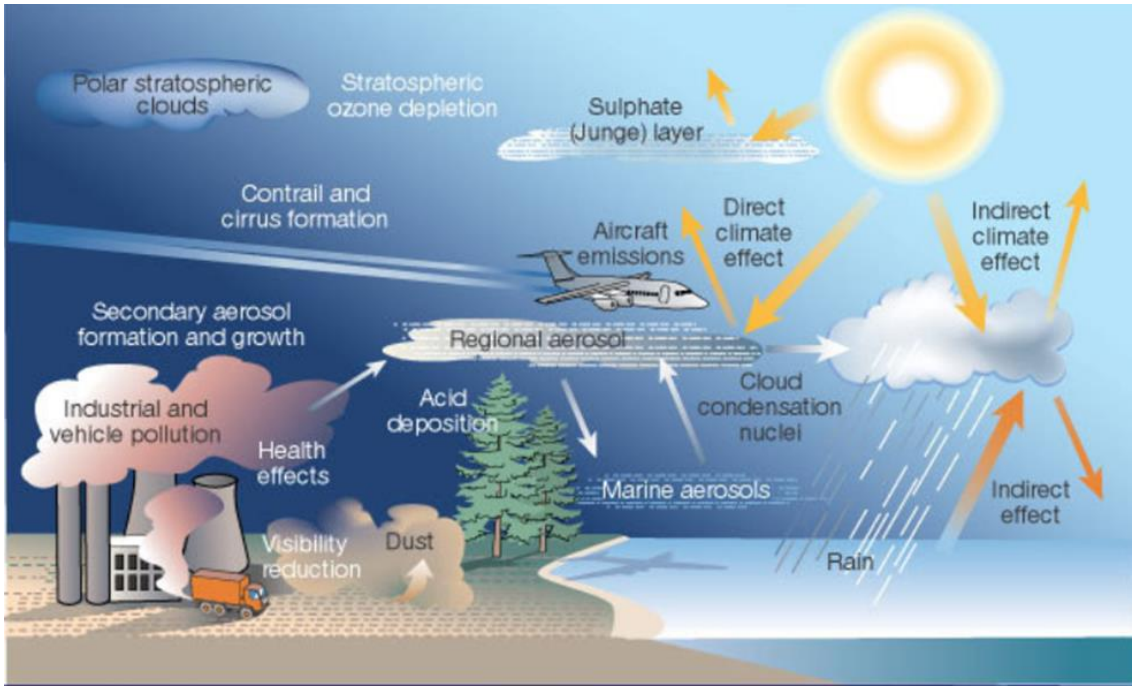

Figure 5. Aerosol effects (http://fst.unife.it/it/orientamento/progetto-lauree-scientifiche/corso-di-eccellenza/allegati/eccellenza2008-DiMatteo.pdf).

It has been found that the presence of aerosol in the air causes a reduction in visibility (Mahowald et al., 2007; Vautard et al., 2009; Manara et al., 2019), due to the reflection of solar radiation by particles of sizes in the order of the visible wavelength (400-780 nm), with consequent problems for aviation and road traffic.

In addition, ecosystems and surfaces are also subject to the action of aerosol; in fact, due to dry or wet deposition, aerosol can contribute to acidification (especially associated with H_2SO_4 and HNO_3) and eutrophication (associated with nitrate salts) of the terrestrial and aquatic environment. Soil acidification can lead to the release of toxic elements such as aluminum, causing serious damage to plants and various forms of aquatic life.

Aerosols can degrade the artistic, architectural and archaeological heritage, causing the disintegration of stone materials, in particular those with a calcareous component, due to

their acidity (determined by emissions of sulphur dioxide, nitrogen oxides and carbon dioxide). In addition, the blackening of the surfaces is very frequent and is dangerous to the cultural heritage for 2.5 times more than the erosion (Report on the State of the Environment in Lombardy, 2001).

The effects on human health are added to the environmental impact. Exposure to air pollution affects the whole population, is inevitable and cannot be eliminated. The research carried out until now shows the existence of statistical-epidemiological associations, or a causal consequence between the increase in pollution and the increase in pathologies. Aerosol is the main pollutant that contributes to diseases and premature deaths with damage to the cardiovascular and respiratory system (Lelieveld et al., 2019).

Effects on health depend mainly on particle size and chemical composition. The first determines the particle's ability to penetrate and settle inside the respiratory system, the deeper the particles penetrate and the greater the toxic effect they exert (Fig. 6).

Fine particles have a high specific surface on which the adsorption and condensation processes take place and therefore have a higher content of pollutants. They are characterized by a higher level of acidity (coarse particles, being essentially crust material, are alkaline), and considering the degree of neutralization of acid compounds, are considered to be more responsible for the negative health effects. These particles, belonging to the inhalable fraction, reach up to the alveoli, where they come into contact with the blood compartment and thus transport toxic and often carcinogenic substances adsorbed on their surface inside the organism.

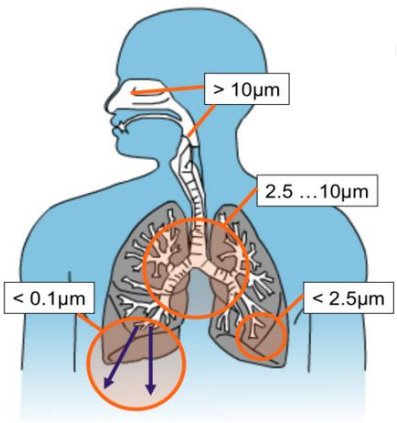

Figure 6. Illustration of inhalation of aerosol particles into the respiratory system.

Concerning the chemical composition of particles, the risk is associated in particular with the content of trace heavy metals (Pb, Cd, As, Zn, Hg...) and carcinogenic substances, including PAHs (Polycyclic Aromatic Hydrocarbons).

Depending on the mode of exposure to pollutants, two types of effects can be distinguished, although these tend to overlap. Acute effects occur over a short period of time as a result of short (days or weeks) but intense exposure to air pollution; on the other

hand, chronic effects are those which damage human health due to prolonged exposure (months or years) and which are not affected by daily changes in atmospheric concentrations of pollutants, but would suffer a significant decrease over the years as a result of a significant improvement in air quality.

WHO (World Health Organization) guidelines report annual tolerable maximum values of 10 $\mu g/m^3$ for fine particles and 20 $\mu g/m^3$ for coarse particles (https://www.who.int/en/news-room/fact-sheets/detail/ambient-(outdoor)-air-quality-and-health).

In addition to all these problems, atmospheric aerosol in its various forms is one of the main causes of climate change that has always, but especially in recent decades, affected our planet.

Therefore, in order to identify specific control and mitigation procedures or environmental policy measures for sustainable development, monitoring through ground-based and satellite observation tools is of considerable importance, combined with simulations, through numerical models capable of reproducing atmospheric events, once modules have been implemented within them to represent as accurately as possible the properties of aerosol and the processes to which it is subject (Ghan et al., 2007).

The present study focuses in particular on the influence of mineral dust on extreme weather events above the Mediterranean region.

1.2. Climate effects: direct, semi-direct and indirect

In addition to the effects on the environment and health, aerosols have a significant impact on the climate, both regionally and globally, as they modify the global radiative budget and the microphysics of clouds (Boucher et al., 2013); in fact, together with water vapour, carbon dioxide, ozone and other trace gases, aerosols influence atmospheric stability with consequent direct, semi-direct and indirect effects on the climate (Fig. 7).

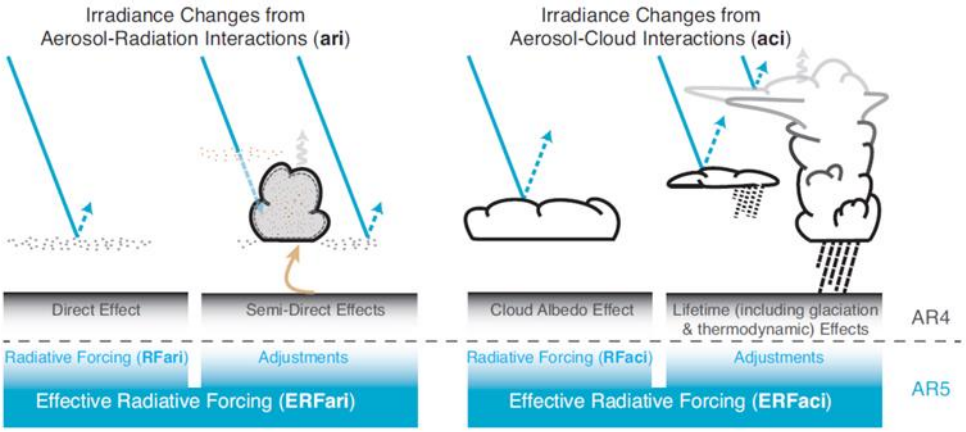

Figure 7. Scheme of the aerosol–radiation and aerosol–cloud interactions. The blue arrows depict solar radiation, the grey arrows terrestrial radiation and the brown arrow symbolizes the importance of couplings between the surface and the cloud layer for rapid adjustments (Boucher et al., 2013).

Direct effects consist in the change of Earth's energy balance due to the absorption and scattering of solar (short-wave) and terrestrial (long-wave) radiation by aerosol particles, depending on their size and chemical composition and the radiation wavelength. The variation in the radiative fluxes is known as Radiative Forcing (RF). Thus, positive RF means a warming effect over the Earth's atmosphere, whilst negative RF represents a cooling effect (Forster et al., 2007). The aerosol particles are the centres of diffusion of solar and thermal radiation which are diverted in a different direction, while only a small part contribute to the absorption of these radiation (Fig. 8). As a result, when an episode of intense aerosol emission occurs in the air, the amount of sunlight reaching the Earth's surface can be greatly reduced, because it is reflected towards space and as a result cooling can occur in the Earth's climate system.

The absorption of solar radiation by some aerosol species increase the temperature and reduce the relative humidity on the troposphere, but at the same time lead to a cooling effect on Earth' surface. This modifies the vertical stability in the atmospheric boundary layer, affecting the formation and the lifetime of the clouds and is indicated as a semi-direct effect of the aerosols (Fig. 8).

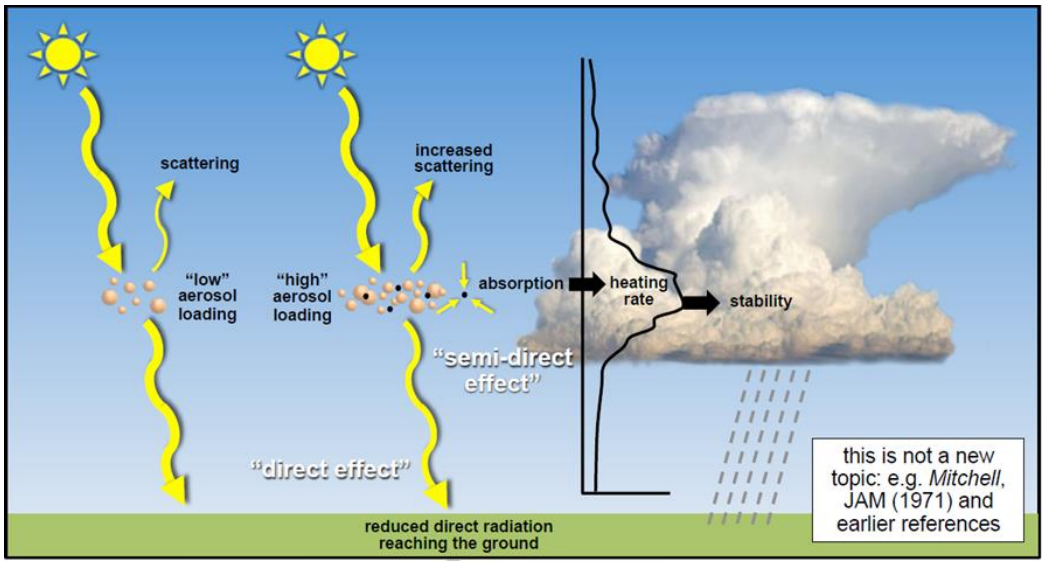

Figure 8. Direct and semi-direct effects of aerosol (Fast et al., 2015).

The gradual reduction in the amount of global direct irradiance at the Earth's surface is known as global dimming and has a negative impact on the hydrogeological cycle and climate by reducing evaporation and rainfall, as shown by some climatic models that associate this phenomenon with the lack of monsoon formation in sub-Saharan Africa during the 1970s and 1980s, with consequent famines such as that caused by the tragic drought in the Sahel, as well as much of the global climate cooling recorded in the 30 years between 1945 and 1975 (https://it.wikipedia.org/wiki/Oscuramento_globale).

The reduction of surface irradiation partly compensates for global warming, which indicates a change in climate characterized by the increase in Earth's average temperature and the associated atmospheric phenomena such as floods, drought, desertification, melting glaciers and rising oceans (https://it.wikipedia.org/wiki/Riscaldamento_globale).

There was an increase of 0.7 ± 0.2°C during the XX century, but the warming is not uniform on the whole planet, it has a peak in the northern hemisphere, more pronounced on the mainland than on the seas and oceans, and a lower level in the southern hemisphere, with an opposite tendency to cooling (IPCC, 2007).

The last report from the International Panel on Climate Change (IPCC, 2013) highlights the Mediterranean as one of the most vulnerable regions in the world to the impacts of global warming. In the Mediterranean region, average annual temperatures are now 1.4 °C higher than during the period 1880-1899, well above current global warming trends (Fig. 9).

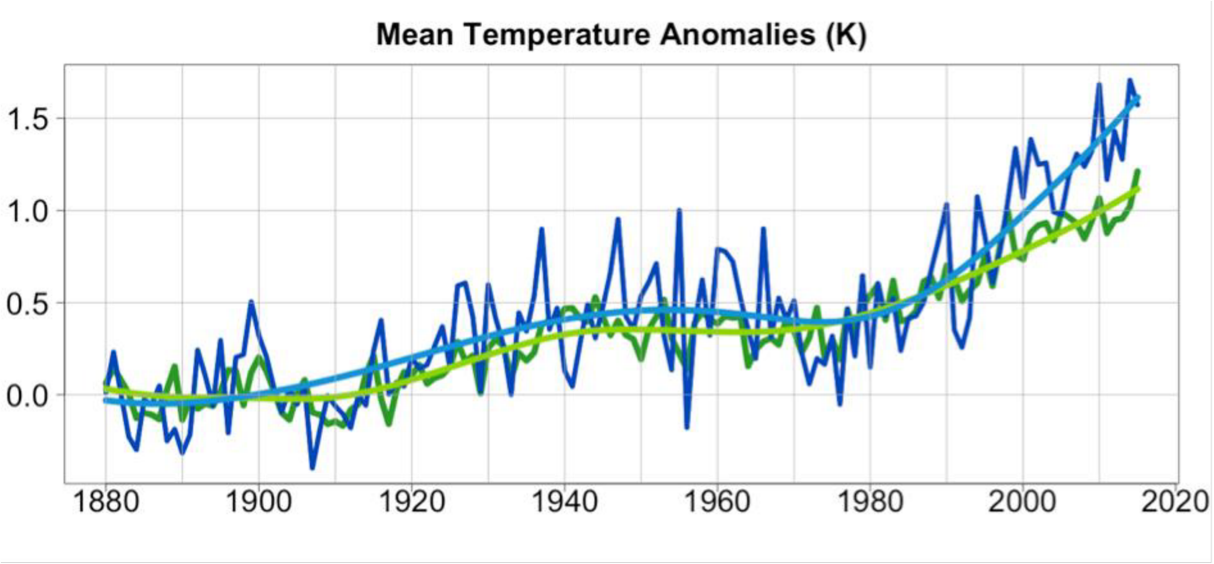

Figure 9. Warming of the atmosphere (annual mean temperature anomalies with respect to the period 1880-1899), in the Mediterranean Basin (blue lines, with and without smoothing) and for the globe (green line). Data from Berkeley Earth available at http://berkeleyearth.org.

As for the future projections, the 2 °C global mean temperature target (Vautard et al., 2014) implies 3 °C warming in hot temperature extremes in the Mediterranean region (Seneviratne et al. 2016). Depending on the climate scenario and the season, a rise in temperature from 2 to 6 ° C by 2100 is expected in the Mediterranean.

It can be said that the radiative forcing (RF) of natural and anthropogenic aerosols is characterized by a strong seasonal and geographic variability and locally can even exceed that of greenhouse gases (Ramanathan et al., 2001). The RF entity depends on both the aerosol load AOT (Aerosol Optical Thickness) and the single dispersion of albedo ω_0 (reflecting surface), related to the distribution and chemical composition of the aerosol (Yoon et al., 2019). In fact, not all species have the same effect: for example, sulphate (SO_4) tends to divert radiation (sw) towards space with consequent cooling of the Earth's surface (negative radiative forcing estimated around –0.41 Wm^{-2} on average across the globe), on the contrary, black carbon tends to absorb radiation (lw), heating local air masses (positive radiative forcing about 0.64 Wm^{-2} on average) (IPCC, 2013; Fig. 10).

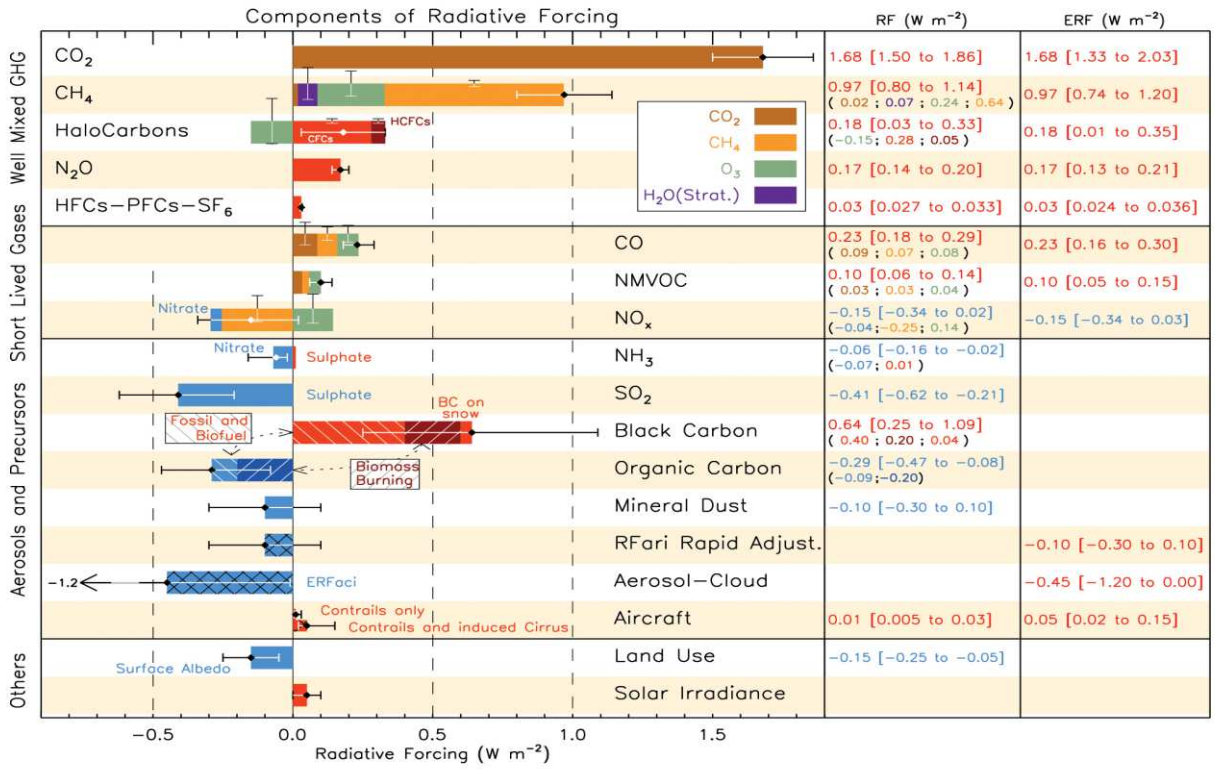

Figure 10. Global mean radiative forcing from various emitted components between 1750 and 2011. From: V Assessment Report - Climate Change 2013 (IPCC, 2013).

These are global mean values because the distribution is very heterogeneous. Regional variations in aerosol concentration may be due to the fact that aerosols mainly affect radiation in the visible spectrum (wavelengths between 400 and 780 nm) and, unlike the other substances previously mentioned, they have a spatial and temporal variability much larger and difficult to simulate (Fast et al., 2015).

As a result, the combined effect of these factors varies, in a complex way, according to altitude, location, brightness and atmospheric variability (night, day, and seasons). Usually during the day the absorption of sunlight prevails (with the effect of mitigating the heating on the Earth's surface), instead at night the back reflection of the Earth's radiation reduces the heat loss of the Earth.

There is therefore a change in the Earth's radiative balance, with a consequent direct effect on the climate, which will depend on the amount of light energy reflected towards space (backscattering) with respect to that absorbed.

The aerosol is very concentrated in the lower atmosphere near its primary source, the Earth's surface. However, even the high atmosphere is not free from these particles, thanks to the ascending air currents that can carry them up to great heights.

Many of these particles act indirectly as cloud condensation nuclei (CCN) and ice nuclei (IN) for water vapour molecules (Karydis et al., 2011). The ice nuclei are aerosol particles that promote transformation from the vapour or liquid phase directly to the ice phase (sublimation); instead condensation nuclei are organic or inorganic hygroscopic particles, which promote the formation of droplets in clouds.

When hygroscopic nuclei are many the water vapour condenses rapidly on them, in some cases even under sub-saturation conditions, leading to the formation of clouds containing more water droplets, but smaller than clouds with the same water content formed in cleaner areas. Since the reflection of solar radiation by such clouds is more efficient (they have a higher albedo), even compared to that of the oceans and lands, a negative radiative forcing results, with a cooling of the Earth's surface, which is defined as the first indirect effect (Fig. 11). Recent estimates of radiative forcing associated with this indirect effect are between –0.3 and –1.8 Wm^{-2}, with a better estimate of approximately –0.7 Wm^{-2}.

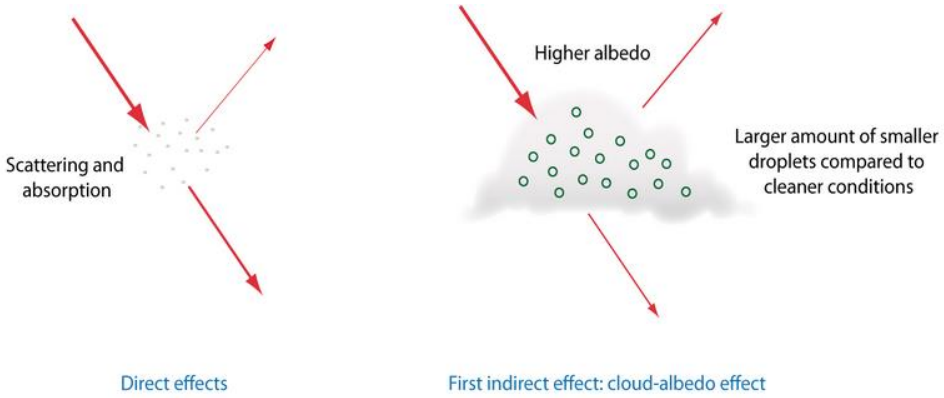

Figure 11. Schematic representation of the direct and first indirect effect of aerosols on the albedo of clouds (http://www.climate.be/textbook/chapter4_node3_2.html).

The aerosols effect of increasing the cloud lifetime and reducing the precipitation (Rosenfeld et al., 2001) has been classically defined as the second indirect effect, which induces negative radiative forcing, but its rate is still difficult to estimate (http://www.climate.be/textbook/chapter4_node3_2.html).

For the semi-direct effect, the sign of the radiative forcing is not currently known, but its magnitude is probably less than that of the indirect effects.

Therefore the influence on the Earth's energy balance, due to changes in the size of the clouds and in the way they absorb and reflect sunlight, in their albedo and in their average lifetime, leads to an indirect effect on the climate.

Aerosols can also act as nuclei for chemical reactions; the most significant are those which lead to the destruction of ozone. During winter in the polar regions aerosols grow to form polar stratospheric clouds on whose large surfaces occur chemical reactions leading to the formation of large amount of reactive chlorine and ultimately to the destruction of ozone in the stratosphere.

The effects caused by aerosols are comparable to those of greenhouse gases in terms of magnitude, but unlike the latter, which cause general overheating, extended almost everywhere, aerosols can generate cooling, which varies from region to region, depending on the proximity to industrial and downwind areas (https://www.nasa.gov/centers/langley/news/factsheets/Aerosols.html).

It is the task of climate models to predict as accurately as possible the transport of these particles and scientific research is moving towards significant progress, although the difficulties derive from the fact that data provided by the observational tools are still often fragmented.

1.3. Characteristics of mineral dust

Considering the total mass of particles present in the atmosphere, mineral dust is the main natural aerosol (Buseck and Posfai, 1999), in fact, according to satellite observations, it constitutes up to 75% of the global aerosol mass (Ginoux et al., 2012).

It has a significant impact on climate, meteorology and biogeochemical processes of the Earth system at different temporal and spatial scales (Wang et al., 2017), as well as on visibility (Mahowald et al., 2007; 2010), on the performance of observational instruments, on agriculture and human health due to the deficit in air quality (De Longueville et al., 2013; Mallone et al., 2011, Stafoggia et al., 2016, Middleton, 2017).

Concerning direct and indirect effects on climate (Weger et al., 2018; Schepanski, 2018), the above paragraph shall apply.

Mineral dust also plays an important role in fertilizing both terrestrial ecosystems, due to the presence of phosphorus (Okin et al., 2004) and marine ecosystems, since their deposition on ocean surfaces is a source of both nutrients and contaminants (Paytan et al., 2009) and being nutrients for phytoplankton, they increase its carbon absorption capacity, with consequent positive implications on air quality and climate (Falkowski et al., 1998; Bishop et al., 2002; Jickells et al., 2005). At the same time the carbonates they carry are a source of carbon that can buffer the atmospheric acidity and increase the alkalinity of the seawater. Both negative and positive effects may be attributed.

For all these reasons it has become an important field of research for the scientific community, even if, despite innumerable studies, the effects related to mineral dust are difficult to quantify, both for the lack of observation data and for the uncertainties concerning physical and chemical processes.

The features to be considered in the study of mineral dust are the extension of the sources, the chemical composition, the load and particle size distribution, the complexity of the optical and physical properties, and the atmospheric processes to which they may be subject (Sokolik et al., 2001). All this is possible through the development of techniques that allow interpreting the information obtained from satellite remote sensing, in situ measurements and models simulations.

The representation of the dust cycle in the atmosphere is a continuous challenge for numerical models, whose surface emission estimates can vary by a factor of 2. This results in a corresponding uncertainty regarding the climatic effects of dust. The difficulty in comparing estimates of dust emissions and concentrations arises from the different assumptions made by the models, for example the distinction between natural (wind erosion, deserts, eruption, etc.) and anthropogenic (soil working, removal of vegetation, drying of water bodies, etc.) origins of dust or the particle size (a diameter less than 10 μm is recommended) (Zender et al., 2004).

Estimates made in 2001 indicate a total dust emission between 1000 and 2150 Tg yr^{-1} and of these have an anthropogenic origin from less than 10% (Tegen et al., 2004) to 50% (Mahowald, 2004) (Fig. 12).

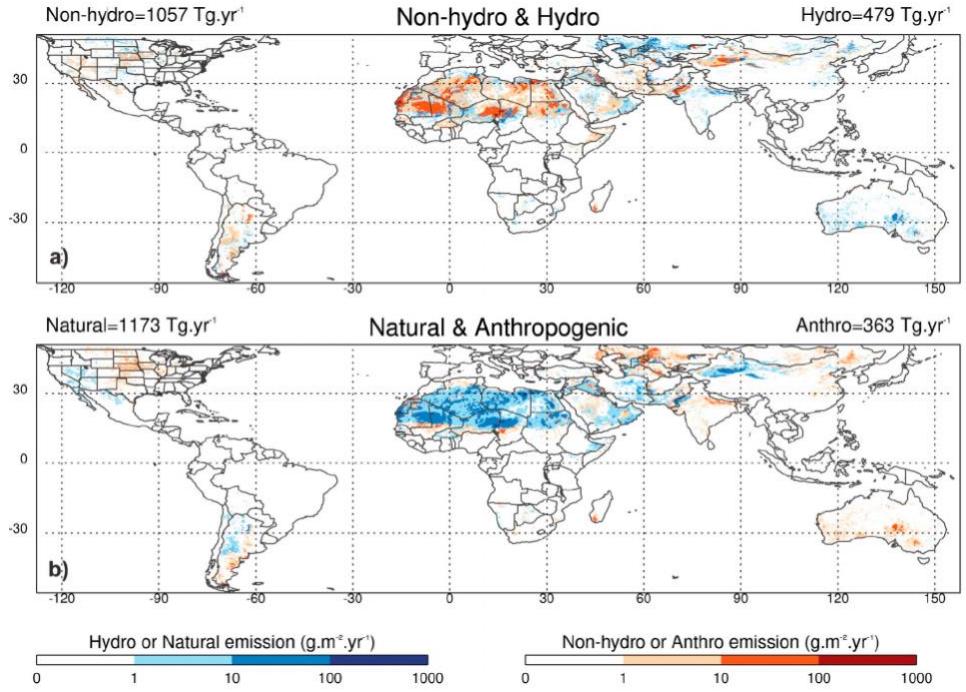

Figure 12. Annual mean dust emission (a) from ephemeral water bodies and (b) from land use. The M-DB2 emissions are colored in blue for hydrologic and natural sources and in red for non-hydrologic and anthropogenic sources (Ginoux et al., 2012).

This gap may be due to the lack of a detailed characterization of the sources.

The desert and semi-desert regions are the main source of dust, but some contribution is also made by the areas subject to desertification, where vegetation is decreasing due to climate change and man's activity (Fig. 13). Dust can also come from topographic depressions in which alluvial deposits have formed due to intermitted floods (Prospero et al., 2002; Ginoux et al., 2012).

Many studies show that dust emission depends on sediment characteristics, soil moisture, groundwater and vegetation.

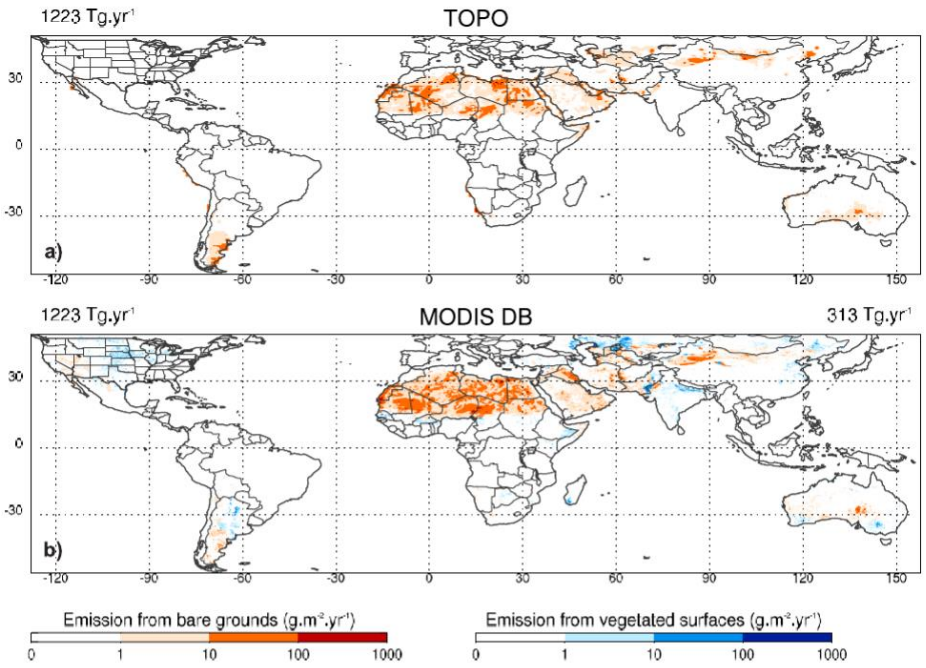

Figure 13. Annual mean dust emission using (a) topographic depression sources and (b) M-DB2 FoO that DOD > 0.2. The M-DB2 emissions are colored in blue or red shading if they are within or outside topographic depression coverage, respectively (Ginoux et al., 2012).

The nine regions that mainly contribute to the mineral dust emission are North and South Africa, the Arabian Peninsula, Central Asia, Eastern and Western China, North and South America and Australia, but in particular, through some simulations, it has been found that the greatest contribution comes from the Sahara desert (North Africa) with 50-60% of the total load present in the atmosphere (Tanaka and Chiba, 2006).

In East Asia the main sources of mineral dust are the Gobi Desert and the Taklimakan Desert, through which Eastern China contributes to the 11% and Western China to 6% of total emissions, with values ranging from 100 Mt yr^{-1} to 460 Mt yr^{-1} (Laurent et al., 2006); this dust is transported mainly over Mongolia, Korea, Japan and the North Pacific Ocean.

With reference to the Arabian Peninsula, the most active local source is the Rub Al Khali desert, but the western part of the region is also affected by dust from the Sahara desert, as in the northern and eastern parts there are also contributions given by the Iraqi deserts. These emissions are dominant from February to June, in particular during the winter season they affect the Red Sea area, during the spring they are concentrated above the An Nafud desert in the north of Saudi Arabia, while in the summer they are transported east to the surroundings of the desert Ad Dahna (Notaro et al., 2013).

Australia is a minor source compared to North Africa and East Asia (Prospero et al., 2002), in fact research carried out by Tanaka and Chiba in 2006 suggests annual emissions of around 106 Tg against 1087 Tg in North Africa and 575 Tg in Asia. However, it remains the main source of mineral dust in the southern hemisphere, with the largest contribution from the Lake Eyre basin between winter and spring and the Murray river basin between spring and summer (McTainsh et al., 1989).

The chemical composition of the dust particles depends on their source region (Tab. 1). Most of them are aggregates of different minerals, while a lesser fraction are pure minerals such as quartz, calcite and dolomite. The main components found in the analyses are iron (Fe), especially on the surface of the particles, calcium (Ca), magnesium (Mg), potassium (K), aluminum (Al), silicon (Si) and sodium (Na) which are an integral part of the particles. If sodium chloride and hydrogen sulphide are absent, it may mean that the dust did not interact with clouds or sea air. Any black residues on the surface may be organic material due to a probable biological activity in the soil of origin.

As a result of chemical reactions with oxidizing gases present in the atmosphere, the particles may be subject to a variation in mineral properties (evident when nitrates and sulphates are found); therefore it is recommended to perform analysis of individual particles using, for example, an Energy-Dispersive Spectrometer (EDS) on a standard Scanning Electron Microscope (SEM) to obtain useful information on the composition and morphology of particles, which are not provided by methods of mass analysis (Falkovich et al., 2001; Krueger et al., 2004).

Table 1. Average chemical composition of mineral dust particles from four source regions (Krueger et al., 2004).

Atomic percent	% Si	% Al	% Mg	% Ca	% Na	% Fe	% K
Mineral dust							
(a) Saharan	69	15	3	2	2	5	2
(b) Coastal Saudi	31	7	13	39	4	3	1
(c) Inland Saudi	53	22	7	3	2	9	3
(d) China Loess	46	17	6	17	2	7	3
Atomic ratio relative to Si	Si:Si	Al:Si	Mg:Si	Ca:Si	Na:Si	Fe:Si	K:Si
Mineral dust							
(a) Saharan	1	0.22	0.04	0.03	0.02	0.07	0.02
(b) Coastal Saudi	1	0.23	0.42	1.25	0.14	0.10	0.04
(c) Inland Saudi	1	0.41	0.14	0.06	0.03	0.17	0.05
(d) China Loess	1	0.37	0.12	0.37	0.05	0.15	0.07

Mineral dust particles are generated by wind erosion and other phenomena on the ground. Soil disintegration releases into the atmosphere particles of less than 5 μm (clay) to more than 75 μm (silt and sand), which can be transported over long distances and subject to change, with a tendency for coarse particles to settle more easily (Maring et al., 2003), while only those with a diameter less than 10 μm are able to remain suspended for longer times (Zender et al., 2003).

The emission of soil-derived particles is a power function of the wind friction velocity (U*) but occurs only when a threshold value in wind friction velocity (U^*_t) is reached. This erosion threshold mainly depends on the dry soil size distribution, on the roughness induced by the presence of non-erodible elements over the erodible surface, and on the soil moisture. Once the erosion threshold is reached, the soil grains enter into a horizontal movement called saltation. When the saltating soil grains strikes the surface, their kinetic energy is transferred to the surface. The soil aggregates can then be disrupted if the energy provided exceeds the energy of the cohesive forces linking the dust particles into aggregates. This process, called sandblasting, is by far the main process responsible for the vertical flux of produced fine particles that can be transported over long distances.

The total amount of material mobilized by wind, or horizontal flux (G), mainly depends on the wind friction velocity and on the dry soil size distribution while the intensity of the dust flux, or vertical flux (F), is mainly controlled by the ability of the soil to release fine transportable particles (Laurent et al., 2008).

The removal of particles, instead, occurs by gravitational settling and by dry and wet deposition.

The representation of all these mobilization mechanisms within the numerical weather prediction (NWP) models is subject to modifications, especially due to the difficulty in determining the required surface characteristics (soil structure, roughness, particle size distribution, wind friction speed, vegetation cover, soil moisture, etc.) and transfer processes from the micro-scale to the global scale (Richter and Gill, 2018).

Modern models implement simplified representations of environmental features and physical processes, called parameterizations that may be associated with known factors in order to consider their “essential” aspect. Each parameterization can be suitable for a

specific application but not for others, so the models are designed to be configurable with different parameterizations to be able to simulate various scenarios and environmental conditions.

Several dust emission schemes have been developed in recent decades for forecasting and research purposes (Marticorena and Bergametti, 1995; Woodward, 2001; Ginoux et al., 2001, 2004; Nickovic et al., 2001; Shao, 2001, 2004, 2011; Kok et al., 2014). To date, lots of case studies have been published on the simulations of intense episodes of mineral dust intrusion (Cavazos et al. 2009; Shao 2007; Kumar et al. 2014; Rizza et al. 2016, 2017).

Some of these concern dust storms in North Africa and surrounding regions (Barkan et al., 2005; Rizza et al., 2017; Gkikas et al., 2018) because half of the mineral dust emissions come from the Sahara Desert (Goudie, 2009) with values between 400 Tg yr^{-1} (Huneeus et al., 2011) and 4500 Tg yr^{-1} (Evan et al., 2014), of which about 100 Tg yr^{-1} are exported toward the western and central Mediterranean (Schepanski et al., 2016).

The atmosphere of this region is particularly interesting, as it is characterized by extreme features, such as high temperatures, the Earth's deepest "Planetary Boundary Layer" (PBL), 4-6 km above the Earth's surface (Gamo, 1996), a very high Aerosol Optical Thickness (AOT) during most of the year and the "Saharan Heat Low" (SHL) which produces a peak of aerosol concentrations and is essential for the monsoon system of West Africa (Peyrillé et al., 2007; Biasutti et al., 2009). Strong surface heating generates a convective system that can lift dust particles for several kilometres in the free troposphere, where they are transported over long distances to the continental and intercontinental scale (Goudie and Middleton, 2001; Engelstaedter et al., 2006).

The trajectories followed are mainly four: the large part (60%) of mineral dust produced by the Sahara remains in Africa, since it is transported and deposited in the Sahel countries along the famous "meningitis belt" (Molesworth et al., 2003), another significant fraction (25%) is pushed west across the Atlantic Ocean (Prospero and Mayol-Bacero, 2013; Yu et al., 2015), but a significant amount of mineral dust (10%) is also transported, across the Mediterranean Sea, to Europe (Moulin et al., 1998, Barnaba and Gobbi, 2004; Israelevich et al., 2012), while the remaining 5% reaches the Middle East.

The passage of Saharan dust across the Mediterranean Sea is mainly determined by a low pressure system over the Atlantic and North Africa and high pressure on the Mediterranean regions (Moulin et al., 1998; Barkan and Alpert, 2008; Querol et al., 2009; Pey et al., 2013; Salvador et al., 2014).

Once released into the atmosphere, the Saharan mineral dust interacts with the cloud systems over a wide region (DeMott et al., 2009). In low clouds, such as cumulus and stratocumulus, higher dust concentrations cause a reduction in precipitation and an increase in drought by dispersing water among many dust particles preventing droplets from becoming heavy enough to fall (Ramanathan et al., 2001; Rosenfeld et al., 2001).

In high clouds, such as cirrus, cirrostratus and deep convective clouds, mineral dust particles provide surfaces for the formation of ice crystals. The crystals grow rapidly, drawing moisture from surrounding cloud droplets. They become heavier and finally fall, generating more rain and reducing the total amount of high clouds (Mahowald and Kiehl, 2003).

These effects, together with those on the Earth's radiation budget, imply changes in the climate system (Fig. 14).

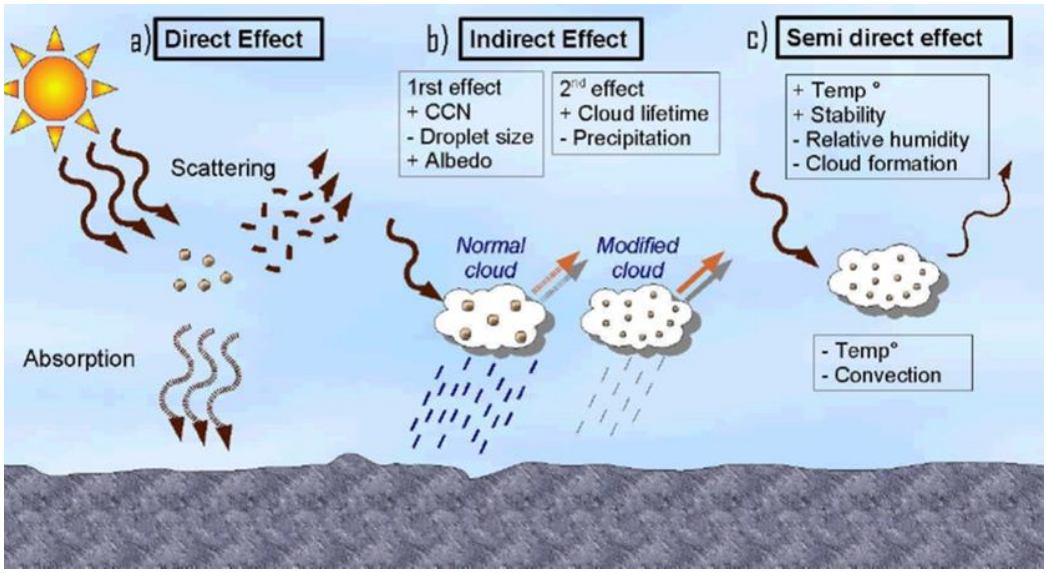

Figure 14. Radiative effects of mineral dust in the atmosphere (Cavazos Guerra, 2011).

The study of dust transport modeling above the vast Saharan region is particularly challenging due to the complex meteorology and poor observation networks.

Since the distribution and effects of dust are heterogeneous, both spatially and temporally, a promising strategy for improving our knowledge is to carry out comprehensive studies on the regions affected by mineral dust. Given the influence of Saharan mineral dust on the Mediterranean basin, in this study it was chosen to investigate the topic through the simulation of an intense dust outbreak occurred during an extreme meteorological event that affected the Italian peninsula.

2. EVENT DESCRIPTION

The weather event under investigation, generally known as “Vaia” (Institut für Meteorologie of the Freie Universität of Berlin, http://www.met.fu-berlin.de/wetterpate/tief2018/), happened between 27 and 30 October 2018 and can be considered among the most severe storm occurred over Italy in the last century.

It was a typical autumn synoptic pattern that affected the western Mediterranean Sea causing floods and serious damage throughout the Italian peninsula.

The storm developed as an explosive cyclogenesis following a cold front from the Gulf of Lion in France (Cavaleri et al., 2019). This extremely intense cyclone originated from a minimum depression at sea level of about 978 hPa, initialized at the West of Sardinia and recorded in the northern part of the Tyrrhenian Sea for more than 24 hours, and was characterized by significant pressure gradients.

In terms of dynamics, the event was very active, characterized by low-level jet, moisture transport, explosive cyclogenesis, storm surge and culminated with an exceptional wind storm over the Alps with gusts exceeding 200 km/h, that uprooted about 11 million trees (Panegrossi et al., 2019; Chirici et al., 2019). Heavy rainfall hit the north-eastern Alps, but also Central Italy and the Liguria region registered more than 250 mm in 24 hours, and over 600 mm in 72 hours were registered in different locations (Panegrossi et al., 2019).

The event was characterized by the sequence of two different phases lapsed of about 8-10 hours, which splitted the first 48 hours of the warm front from the following 12 hours of the cold front. Both fronts have been particularly rich in humidity, with widespread precipitation and strong wind that gave the whole event an absolutely exceptional relevance (https://content.meteotrentino.it/analisiMM/2018_perturbazione_ottobre.pdf).

The large set of available measured data from the sensor MODIS (Salomonson et al., 1989), on board the NASA platforms Terra and Aqua, and the numerical simulations, performed with the WRF-Chem model, have allowed to analyze the meteorological event and the interactions between mineral dust and atmospheric microphysics, since the episode

analyzed was also characterized by an intense intrusion of Saharan dust on the Mediterranean.

2.1. Synoptic analysis

The meteorological situation that characterized the event was analyzed taking into consideration the data provided by ERA5 (Copernicus Climate Change Service (C3S) (2017): ERA5: Fifth generation of ECMWF atmospheric reanalysis of the global climate. Copernicus Climate Change Service Climate Data Store (CDS), date of access. https://cds.climate.copernicus.eu/cdsapp#!/home), in particular those related to pressure, wind and precipitation.

ERA5 (ECMWF ReAnalysis) is a climatic reanalysis dataset (Tab. 2), related to a period from 1950 until today and is developed by the Copernicus Climate Change Service (C3S). The data currently available are those from 1979 up to about two or three months before the current time. Their processing is carried out by the IFS (Integrated Forecasting System) model of the ECMWF (European Centre for Medium-Range Weather Forecasts), using the 4D-Var in the 41r2 cycle as data assimilation system, with 137 vertical pressure levels, of which the highest at 0.01 hPa.

Atmospheric data are available on these levels and they are also interpolated at 37 pressure, 16 potential temperature and 1 potential vorticity levels. Surface or single-level data are also provided, containing 2D parameters such as precipitation, 2 m temperature, atmosphere radiation and vertical integrals over the entire atmosphere.

The IFS model is coupled to a soil model, whose parameters are also designated as surface parameters, and to an ocean wave model.

Of all the atmospheric data, one part (HRES) is at high resolution (31 km, 0.28125 degrees), while a set of 10 members (EDA) have a reduced resolution (63 km, 0.5625 degrees). This does not apply to oceanic data that is produced on a different grid from that of the atmospheric model, namely a reduced latitude / longitude grid with a resolution of 0.36 degrees (HRES) and 1.0 degrees (EDA).

The model time step is 12 minutes for the HRES and 20 minutes for the EDA, with possible adjustments in case of instability.

The data consist of analysis and short forecasts. The latter are initialized twice daily starting at 6 and 18 UTC, with hourly steps ranging from 0 to 18 hours. The frequency of analysis of HRES data is hourly, as well as of oceanic EDAs, while for atmospheric EDAs it is every 3 hours (https://confluence.ecmwf.int/display/CKB/What+is+ERA5).

Table 2. Comparison between the characteristics of ERA5 and its predecessor ERA-Interim (https://confluence.ecmwf.int/display/CKB/What+is+ERA5?preview=/58140637/58140636/16299-newsletter-no147-spring-2016_p7.pdf).

	ERA-Interim	ERA5
Period	1979 – present	1979 – present
Production period	August 2006 – end 2018	Jan 2016 – end 2017, then continued in near real-time
Assimilation system	IFS Cycle 31r2	IFS Cycle 41r2
Model input	As in operations (inconsistent SST)	Appropriate for climate (e.g. CMIP5 greenhouse gases, volcanic eruptions, SST and sea-ice cover)
Spatial resolution	79 km globally, 60 levels to 0.1 hPa	31 km globally, 137 levels to 0.01 hPa
Uncertainty estimates	None	From a 10-member Ensemble of Data Assimilations (EDA) at 63 km resolution
Output frequency	6-hourly analysis, 3-hourly forecast fields	Hourly analysis and forecast fields, 3-hourly for the EDA
Input observations	As in ERA-40 and from Global Telecommunication System	In addition, various newly reprocessed datasets and recent instruments that could not be ingested in ERA-Interim
Variational bias scheme	Satellite radiances	Also ozone, aircraft and surface pressure data
Satellite data	RTTOV-7, clear-sky	RTTOV-11, all-sky for various components
Additional innovations		Long-term evolution of CO_2 in RTTOV, cell-pressure correction SSU, improved bias correction for radiosondes, EDA perturbations for sea-ice cover

Based on the information obtained from these data it was possible to identify the synoptic framework. The main atmospheric variables that characterized the event are described below.

2.1.1. Pressure

In order to investigate the evolution of the event from the meteorological point of view it is fundamental to analyze the atmospheric pressure, especially its variations, since generally, they bring important dynamic or thermodynamic processes, thus announcing the occurrence of atmospheric phenomena. Among the various meteorological parameters, these variations are certainly the most significant factor, which allows us to give useful prognostic indications on the evolution of local weather.

Atmospheric pressure is the pressure that can be registered at any point on the Earth's surface, equivalent to the weight of an air column over an area of 1 m^2 and is measured in hectoPascals (hPa) (https://www.informazioneambiente.it/pressione-atmosferica/).

It is influenced by various factors such as altitude, humidity and temperature. In particular, it decreases with increasing altitude, since rising altitude reduces the height of the air column above the surface and also the air density is lower; in the same way it decreases with increasing humidity, since water vapour has a lower density than oxygen and nitrogen so the moist air is lighter. Finally it is inversely proportional also to the temperature: being the hot air less heavy compared to the cold one, it follows that with the increase of the temperature the pressure decreases, because the weight exerted by the air column is lower

(https://www.cengage.com/resource_uploads/downloads/0495555061_137182.pdf).

The atmospheric pressure values are indicated on a map through the isobars, concentric lines connecting all the points characterized by the same atmospheric pressure, with respect to the sea level and to the temperature of 0 ° C.

These are useful for identifying low pressure areas (cyclones) and high pressure areas (anticyclones) and then to predicting weather conditions.

Generally, when there is high pressure, the weather is clear, while low pressure areas (values below 1000 hPa) are associated with thunderstorms and cyclones. The latter case is also associated with humidity values higher than about 70% and winds blowing from the south; all conditions that induce a worsening of the meteorological situation, with very strong instabilities.

With reference to this case study, it is noted that at 12.00 UTC on 28 October 2018, a low minimum pressure of about 1000 hPa, recorded near the eastern Alps, heralded the establishment of an unstable front (Fig. 15). A large-scale cyclonic system was slowly developing, leading to a southern flow directed towards the Alps, with consequent intense alpine precipitation.

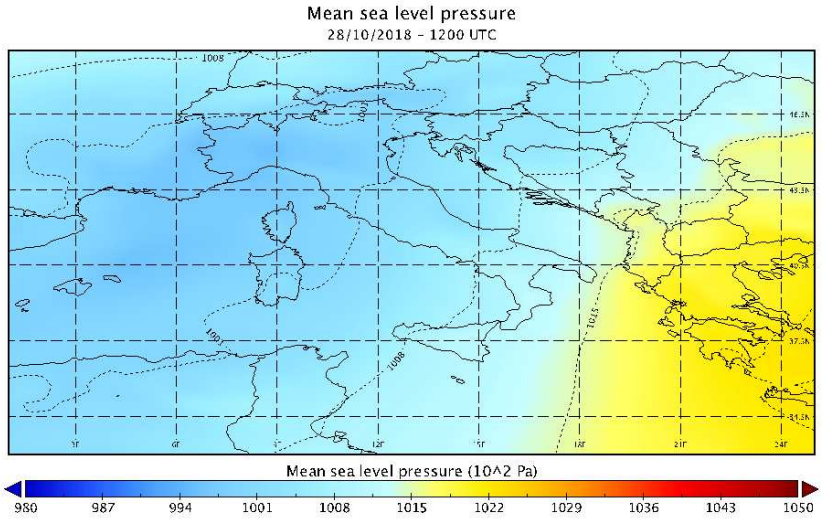

Figure 15. Map showing atmospheric pressure on 28/10/2018 at 12.00 UTC (ERA5).

The weather conditions worsened considerably the following day when a cold front from the Gulf of Lion reached the Mediterranean basin. The minimum depression moved to the West of Sardinia with a value of about 995 hPa (Fig. 16) and remained stationary for most of the day, moving North-East at the evening.

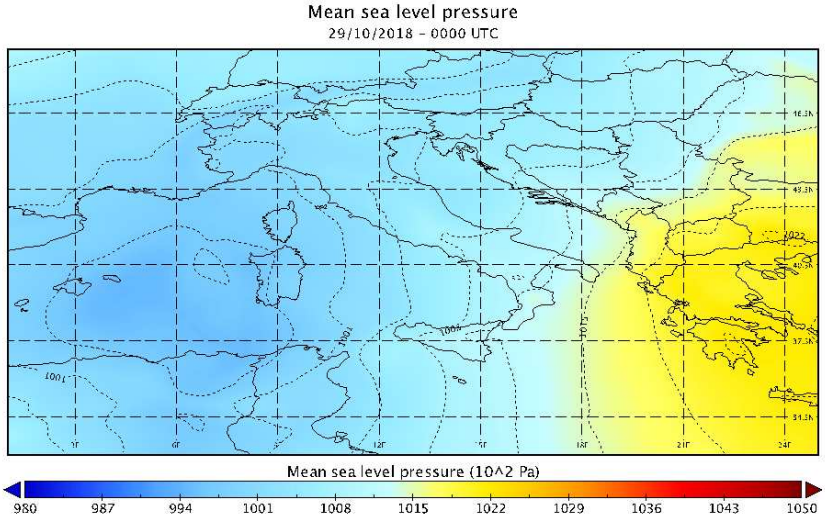

Figure 16. Map showing atmospheric pressure on 29/10/2018 at 00.00 UTC (ERA5).

The measurements evidence the transition from a localized and very deep V-shaped convective system over Liguria and Northern Tuscany, to the extremely intense squall line extending north to south across the Tyrrhenian Sea, and moving eastward over Italy (Panegrossi et al., 2019). The interaction between the cold inflow with the warm and moist marine boundary layer triggered the rapid intensification of the low that, starting from the general field, quickly underwent an explosive cyclogenesis with central pressure estimated at 984 hPa (Fig. 17). The cyclone moved rapidly northward while still deepening down to 977 hPa and further reducing its horizontal scale. The low entered land north of Corsica, followed by a strong and violent flow of cold air from West-South-West. This very energetic cold flow quickly passed over the Apennines, precipitating into the Adriatic basin (Cavaleri et al., 2019).

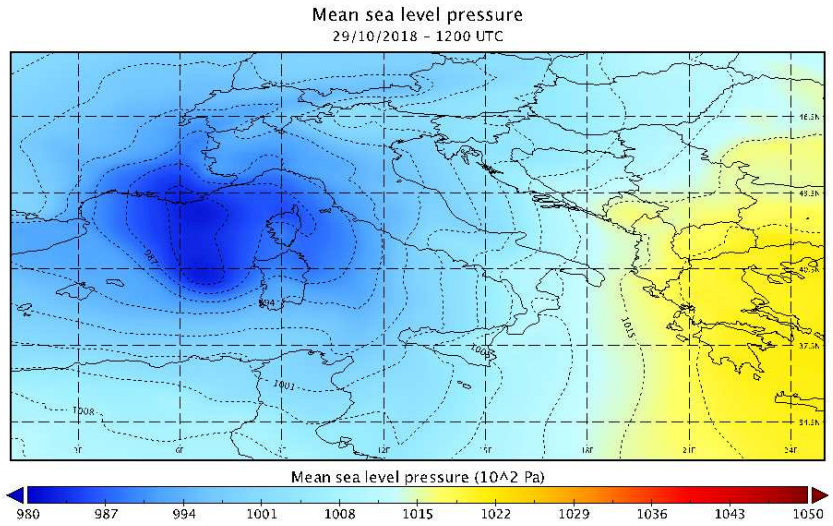

Figure 17. Map showing atmospheric pressure on 29/10/2018 at 12.00 UTC (ERA5).

At the end of 29 October 2018 the minimum depression was located outside the Italian borders, in Swiss territory (Fig. 18), leaving space for a gradual ascent of the geopotential field. The storm has therefore left the Italian peninsula, with the exception of a bit of bad weather still persistent on the northern regions.

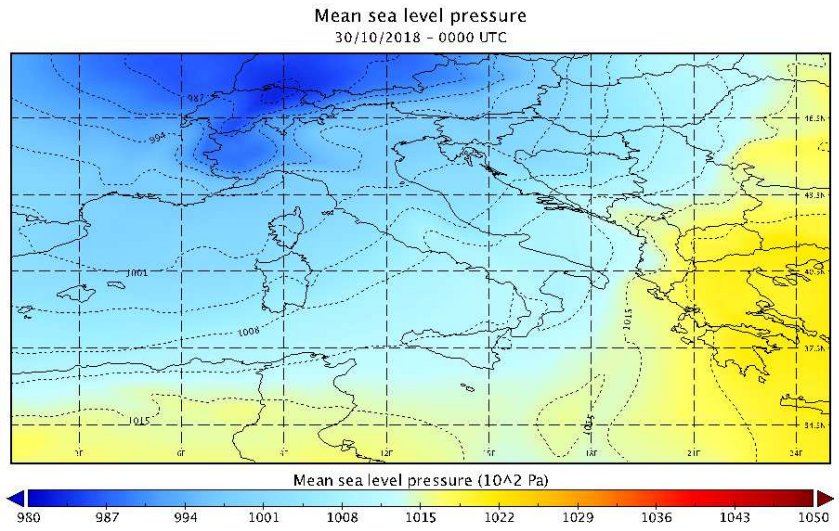

Figure 18. Map showing atmospheric pressure on 30/10/2018 at 00.00 UTC (ERA5).

2.1.2. Wind

The wind is a movement of atmospheric air masses that occurs horizontally, from a high pressure zone to a low pressure area, due to the pressure gradient force.

Closely spaced isobars on a weather map indicate steep pressure gradients, strong forces and high winds, on the other hand widely spaced isobars indicate gentle pressure gradients, weak forces and light winds (Ahrens C. Donald, 2007).

The displacement of the air masses is due first of all to the temperature of the air, since the warm air, being lighter than the cold one, tends to overcome it, creating a void that must be filled because of the continuous search for balance by the forces governing nature. If there were no other forces in action, the air masses would only tend to rise and fall, generating vertical movements known as convective currents. The presence of the Coriolis force deriving from the Earth's rotation, however, leads these air masses to deviate also on the horizontal plane, giving rise to the wind (https://books.google.it/books?id=SpGfKb23Y9QC&printsec=frontcover&dq=Meteorology+Today:+An+Introduction+to+Weather,+Climate,+and+the+Environment,+Eighth+Edition).

The perfect balance between the Coriolis force and the force due to the pressure gradient generates the so-called geostrophic wind, directed parallel to the isobars, while from the differences in atmospheric pressure derives the gradient wind, having a perpendicular

direction with respect to the isobars (https://www.cengage.com/resource_uploads/downloads/0495555061_137182.pdf).

The wind can be characterized through direction and intensity. The direction is influenced by the deviation force due to the Earth's rotation, the roughness of the ground and the friction, and is indicated with the symbols of the cardinal points of the relative octant, while the intensity corresponds to the speed, it is measured in ms^{-1} (or in kmh^{-1} or in knots), it is proportional to the pressure gradient, and depends, like the direction, on latitude, height on the sea and nature of the soil.

Figure 19. The wind rose.

There are various types of wind. For the purposes of our study the interest concerns the local winds that are generated above all in temperate zones due to the vortices resulting from the encounter of cyclonic and anti-cyclonic disturbances. In particular, the winds that blow over the Mediterranean basin are depicted in the wind rose, whose focal point is located at the centre of the Ionian Sea, and are classified according to the geographical point of origin (Fig. 19): *Tramontana* (from the north), *Grecale* (from the north-east), *Levante* (from the east), *Scirocco* (from the south-east), *Ostro* (from the south), *Libeccio* (from the south-west), *Ponente* (from the west) and *Maestrale* (from the North-West).

The very strong winds that raged during the "Vaia" storm were mainly the Scirocco, a wind coming from the African continent, therefore very hot and dry, but which on its way to Italy easily tends to get moisture from the sea, and the Libeccio, a humid and violent wind that comes from the South-West, much feared for the effects that it can cause, such as strong storms and very intense rains.

In fact, from the maps created with the data provided by ERA5, it can be observed that on 28 October at 12.00 UTC the wind came mainly from South-East and South-West, directed both on the Tyrrhenian Sea and on the Adriatic Sea (Fig. 20).

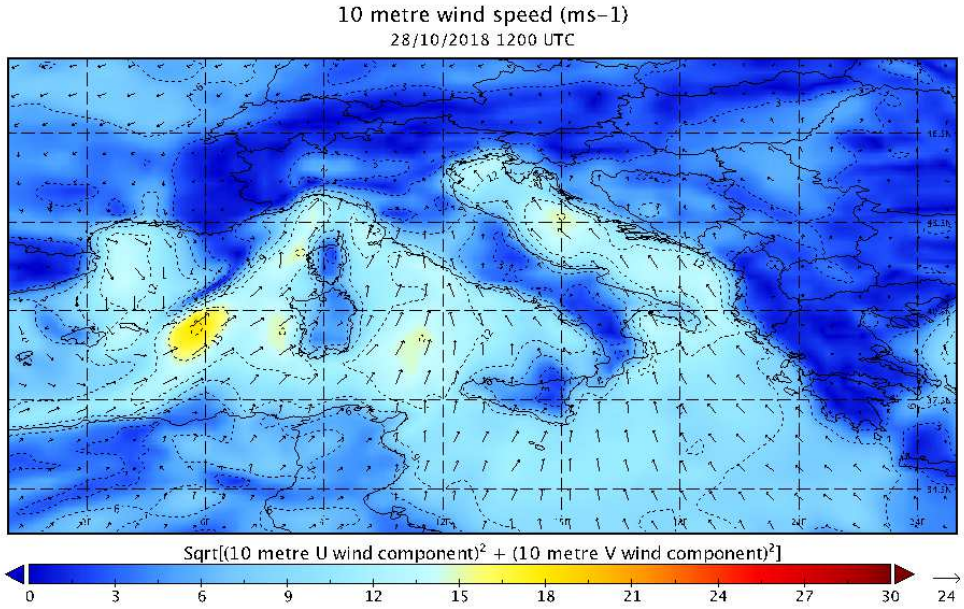

Figure 20. Wind direction and speed at 10 m above the Earth's surface, on 28 October 2018 at 12.00 UTC (ERA5).

The same winds continued to persist even when the depression moved from the Alps above the Western Mediterranean Sea, recording a maximum speed of about 18 ms^{-1} along the Tyrrhenian coast of Tuscany and Liguria (Fig. 21).

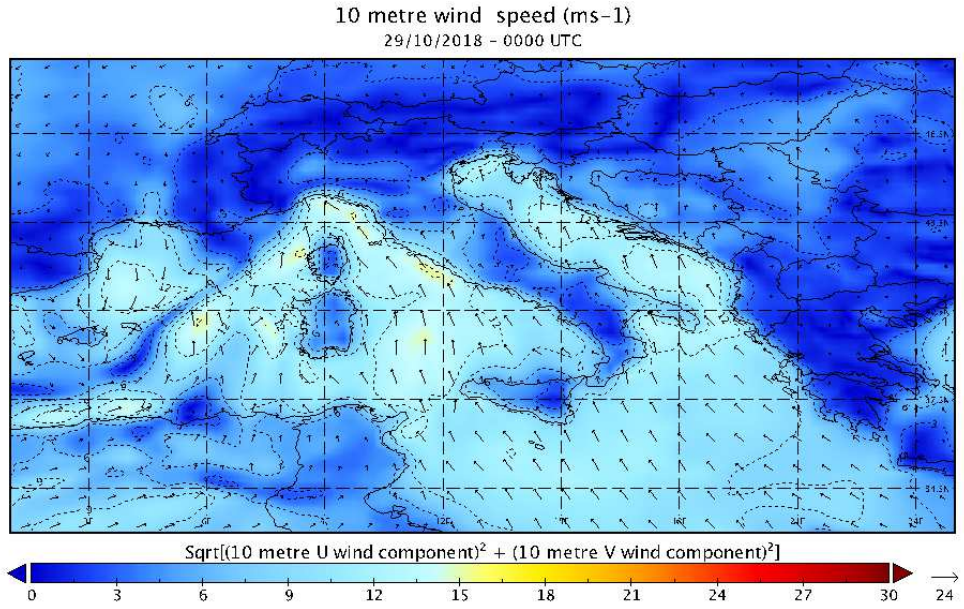

Figure 21. Wind direction and speed at 10 m above the Earth's surface, on 29 October 2018 at 00.00 UTC (ERA5).

The red colour of the following map (Fig. 22) shows how the peak of intensity was reached on 29 October, more exactly at 12.00 UTC the wind has reached speeds above 30 ms^{-1} in correspondence of the minimum pressure localized on the Mediterranean Sea, between the Balearic Islands and Sardinia.

The exceptionally strong wind was caused by the passage of a cold front. A considerable baric gradient both at altitude and on the ground has determined the very high velocities of the air masses; the most violent gusts occurred in the mountains mostly on the eastern sectors, but with significant episodes also on the western ones (https://content.meteotrentino.it/analisiMM/2018_perturbazione_ottobre.pdf).

Moving north, the low forced strong south-easterly winds on its right flank, both on the Tyrrhenian Sea (with the flow squeezed between the low and the Apennines range along the peninsula) and the Adriatic Sea (here enhanced by the high pressure over Eastern Europe). The arrival of a cold air flow from the West-South-West, forcing the *Scirocco* wind into a narrower path against the Eastern Alps, it led to tremendously strong winds in the mountain area (Dolomites and Eastern Alps), with record wind speeds (gusts up to 213 kmh^{-1}) and very extensive forest damage, with an estimated loss of 11 million trees (Cavaleri et al., 2019).

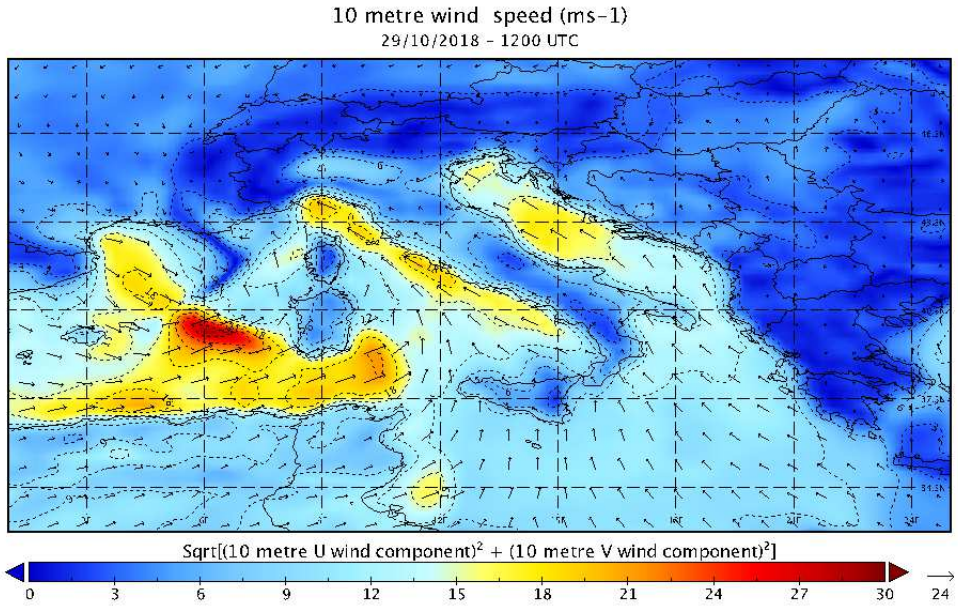

Figure 22. Wind direction and speed at 10 m above the Earth's surface, on 29 October 2018 at 12.00 UTC (ERA5).

On the Adriatic Sea the wind was over at 00.00 UTC of 30 October, but it continued to persist on most of the Mediterranean Sea, even if with lower speeds (Fig. 23).

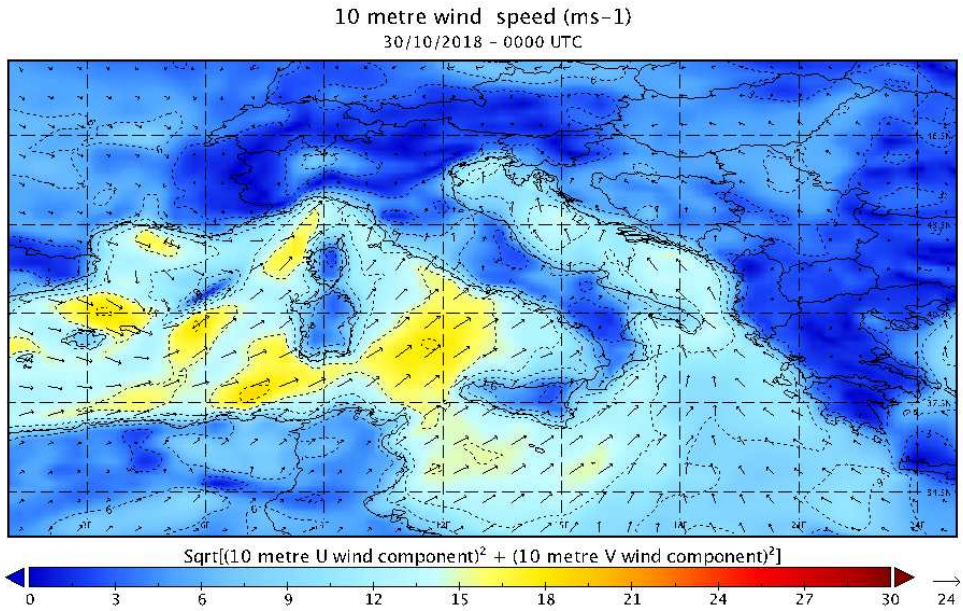

Figure 23. Wind direction and speed at 10 m above the surface, on 30 October 2018 at 00.00 UTC (ERA5).

2.1.3. Precipitation

During the event, the Italian peninsula was affected by violent gusts of wind, but also by abundant precipitations which, as well as being typical of the autumn period, were also favoured by the presence of two particularly intense structures such as the “V -shape" on the morning of 29 October and the "squall line", associated with the passage of the cold front, in the afternoon of the same day (https://allertameteo.regione.emilia-romagna.it/documents/20181/437770/Evento+27-30+ottobre+2018/).

These have generated a powerful storm with strong wind, numerous lightning and intense rainfalls. In three days more than 300 mm of rain have fallen in many places, in particular some rain gauge stations of Liguria and Trentino have measured up to 600 mm. Two main phases of precipitation can be distinguished, namely the more distributed and homogeneous one associated with the warm front of the days preceding 28 October and the more concentrated and locally very intense due to the cold front of 29 October;

separated by an interval of 6-10 hours, with weak or absent rains (https://content.meteotrentino.it/analisiMM/2018_perturbazione_ottobre.pdf).

On 28 October, the transfer of the minimum towards the Italian peninsula caused an intense South-Western flow which, affecting the entire national territory, determined a marked worsening of the weather especially in the areas exposed to these currents, that is the Alps and the western Apennines, where the mm of rainfall at 12.00 UTC is up to 12 mm (Fig. 24).

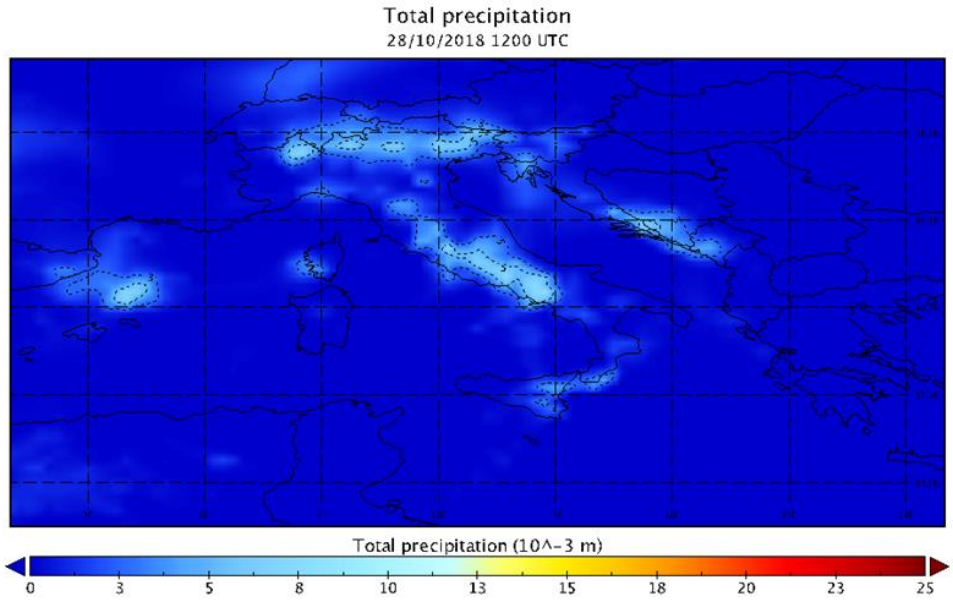

Figure 24. Analysis map (from IFS-ECMWF model) of the precipitation distribution on 28/10/2018 at 12.00 UTC.

From the evening of 28 October until the first morning of the following day the only reported rainfall affected the area where the minimum pressure was allocated (Western Mediterranean Sea), while no significant precipitation was recorded on Italy (Fig. 25), as it is confined between the warm front just passed and the cold one coming from the west.

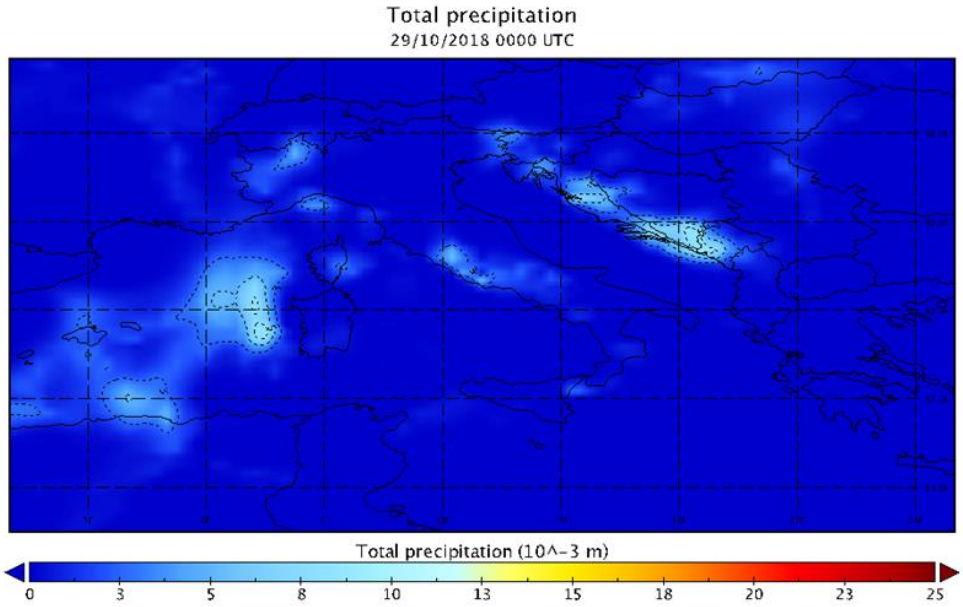

Figure 25. Analysis map (from IFS-ECMWF model) of the precipitation distribution on 29/10/2018 at 00.00 UTC.

After a brief pause, starting from the early morning of 29 October, the deepening of cyclogenesis at the Gulf of Lion, the resulting V-shape system and the passage of the cold front coming from the West led to a resumption of precipitation, which, exalted by the barrier effect of the Apennine chain, have assumed a stormy character (https://allertameteo.regione.emilia-romagna.it/documents/20181/437770/Evento+27-30+ottobre+2018/ab59ec27-27c2-4793-b6f9-b0a91ceef30e). Along the cold front, extended in a meridian sense from Piedmont to Sicily, a "squall line" has developed, that is a very intense thunderstorm line accompanied by heavy rainfall and numerous lightning (https://content.meteotrentino.it/analisiMM/2018_perturbazione_ottobre.pdf).

29 October was therefore the wettest day of the whole event; the rains have affected above all the entire Alpine belt and the regions facing the Northern Tyrrhenian Sea (Fig. 26).

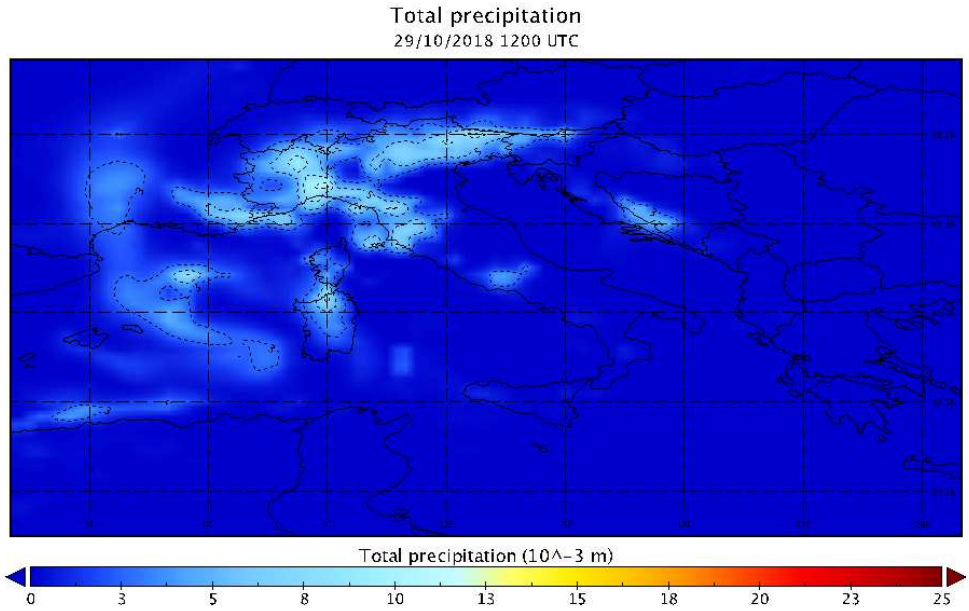

Figure 26. Analysis map (from IFS-ECMWF model) of the precipitation distribution on 29/10/2018 at 12.00 UTC.

The following day, 30 October, the depression moved northwards, so that the storm phenomena gradually attenuated both in number and extent and intensity, leaving space for discontinuous precipitations that were attested on lower quantities (Fig. 27).

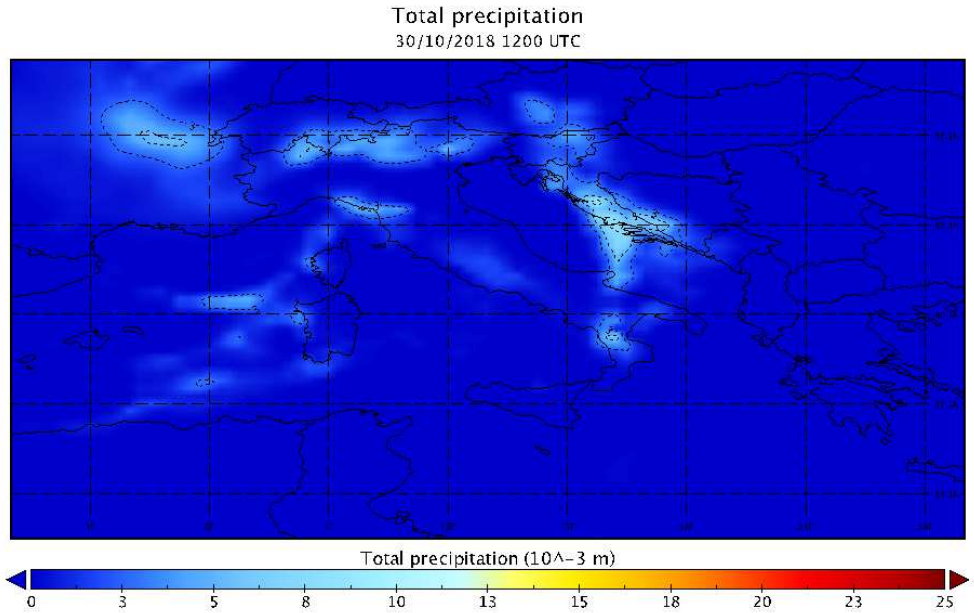

Figure 27. Analysis map (from IFS-ECMWF model) of the precipitation distribution on 30/10/2018 at 12.00 UTC.

2.2. Optical and physical properties of aerosols

The information about aerosols, in particular the dust carried over the Italian peninsula during the event, was obtained from observational data provided by the MODIS sensor (MODerate-Resolution Imaging Spectroradiometer) installed on board the NASA Terra and Aqua satellites (https://modis.gsfc.nasa.gov/about/), launched respectively on 18 December 1999 and 4 May 2002.

Terra's orbit around the Earth is such that it passes from north to south across the equator in the morning, while Aqua passes from south to north over the equator in the afternoon. In this way Terra MODIS and Aqua MODIS display the Earth's surface every one or two days, acquiring data in 36 spectral bands that vary in wavelength from 0.4 μm to 14.4 μm. These data help to improve the knowledge of the dynamics and processes that occur on the surface, in the oceans and in the lower atmosphere.

The MODIS sensor provides high radiometric sensitivity (12 bits) and important information for the development of numerical weather models able to predict global changes in the short and long term so accurately as to assist politicians in making valid decisions concerning the protection of our environment (https://modis.gsfc.nasa.gov/about/).

Responses can be tailored to the individual needs of the user and provide an exceptionally low out-of-band response. Two bands are reproduced at a nominal resolution of 250 m, five bands at 500 m and the remaining 29 bands at 1 km. A ± 55 degree scanning system at the EOS (Earth Observing System) orbit of 705 km achieves a 2330 km swath and provides global coverage every one or two days (https://modis.gsfc.nasa.gov/about/design.php).

The data produced by MODIS (https://modis.gsfc.nasa.gov/data/dataprod/) concern the atmosphere (aerosol, total rainfall, cloud cover, atmospheric profiles, etc.), the cryosphere (snow cover and ice), the Earth's surface (reflectance, albedo, temperature and emissivity, vegetation, evapotranspiration, etc.) and the oceans (temperature, reflectance, organic and inorganic carbon, fluorescence, etc.).

For the purposes of this study, satellite data relating to the AOD were analyzed (Aerosol Optical Depth), which is still the most robust aerosol physical parameter derived from space, used in climate and atmospheric modelling investigations.

2.2.1. Aerosol Optical Depth (AOD)

The aerosol characterization is generally done through the analysis of the Aerosol Optical Depth (AOD), an optical parameter quantifying the aerosol load in the whole atmospheric column. The AOD is unitless, and represents the integral over altitude of the aerosol extinction coefficient (units of length^{-1}), that is the degree to which the aerosols inhibit the transmission of the electromagnetic radiation by absorption or scattering of the same, therefore indicates the attenuation of the radiation passing through a layer of the atmosphere containing aerosol.

Two different approaches are used to retrieve the AOD from MODIS data. These are commonly referred to as “Dark Target” (DT; Kaufman et al., 1997) and “Deep Blue” (DB; Hsu et al., 2004). The algorithm at the basis of the DT approach is further differentiated when applied over ocean (Remer et al., 2005) or land (Levy et al., 2007), and it is not suitable to be applied over bright surfaces (deserts, snow, sun glint). The DB approach was developed to fill this gap (Hsu et al., 2004) and well complements the DT retrievals.

It has been found anyway (Sayer et al., 2013) that MODIS products are not free of problems, in particular the latest collection of the MODIS Deep Blue aerosol product underestimates AOD over the Sahara, while the MODIS Dark Target algorithm overestimates AOD over the ocean especially in dust outflow regions (Levy et al., 2013).

The most recent collection (C006) of MODIS AOD data provides a single AOD product combining both the DT and the DB AOD retrievals and it is considered the “best-of” product for most quantitative purposes (Levy et al., 2013; Rizza et al., 2017).

Three maps, relating to the 28, 29 and 30 October, depicting the distribution and loading of aerosols, in terms of AOD, present in the atmosphere during the event under study, were extrapolated. It can be observed that the MODIS sensor did not record a substantial presence of aerosols during the 28 October, in fact the blue colour corresponds to values of AOD oscillating between 0.1 and 0.5 (Fig. 28).

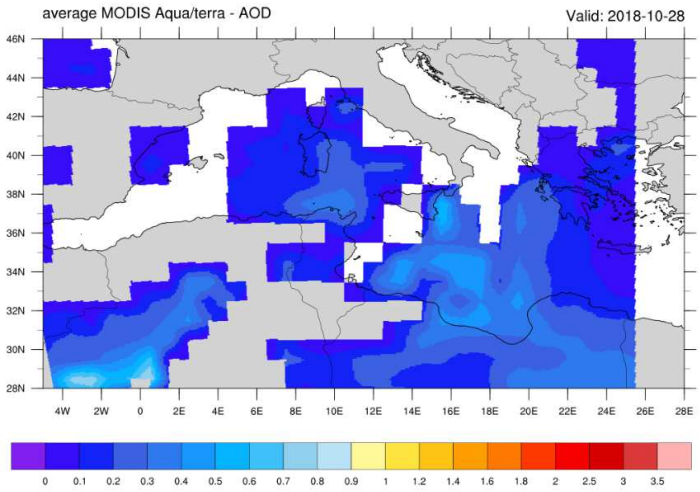

Figure 28. Time-averaged map of the Aerosol Optical Depth recorded on 28 October 2018 by the MODIS Terra and Aqua sensors.

Although the clouds cover didn't make possible to capture the AOD measurements on most of the Italian peninsula, from figure 29 it can be seen that on 29 October, the day on which the storm reached the peak of power, there was also a remarkable amount of aerosol, with a peak of AOD equal to about 3.

This is an extremely high value, such that in these days the skies of some Italian cities have been painted yellowish, due to the southern winds that have pushed the dust of the Sahara up to the Tyrrhenian coasts of Italy.

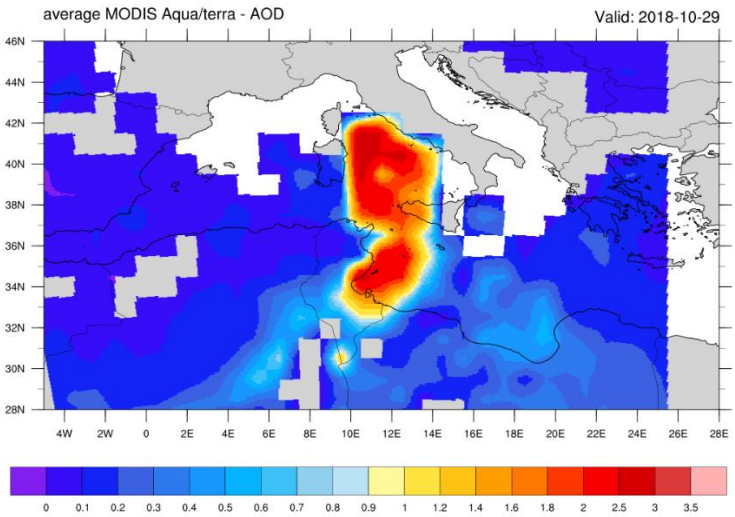

Figure 29. Time-averaged map of the Aerosol Optical Depth recorded on 29 October 2018 by the MODIS sensor.

The AOD values decreased again on 30 October, with a maximum just above 1 which reveals the presence of a little more dust between the Ionian Sea and the Adriatic Sea, as shown in figure 30.

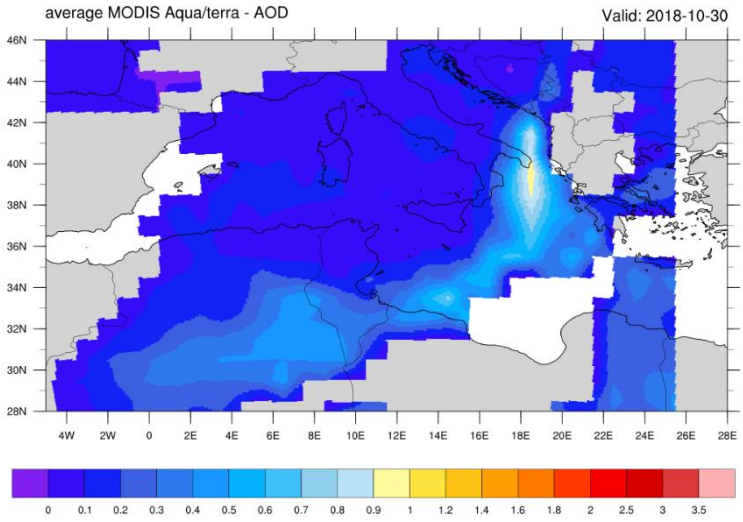

Figure 30. Time-averaged map of the Aerosol Optical Depth recorded on 30 October 2018 by the MODIS sensor.

3. EVENT SIMULATION

Field experiments and satellite measurements have shown that the processes that take place in the atmosphere involve both physical and chemical mechanisms. They are closely related to each other, in fact, atmospheric composition can influence meteorology, for example, through the interaction of aerosols with clouds and solar radiation, in the same way clouds and precipitation affect the chemical transformation and removal processes as well as wind and turbulence act on particles transport.

This was not considered until recently, leading to the development of separate modeling systems, the so-called "offline" models, where physical processes were represented independently of the chemical mechanisms, because of the complexity and the lack of appropriate computer power (Baklanov et al., 2014). The output from the meteorological model, typically available once or twice an hour, is then used to drive the transport in the chemistry simulation. This separation between chemistry and meteorology can lead to a loss of important information relating to atmospheric processes that often have a time scale much lower than the meteorological model's outputs. This can have a perceptible repercussion in forecasting systems, in which horizontal grid sizes on the order of 1 km may be required to match the operational models (Grell et al., 2004).

Today it is a certainty that weather has a strong impact on air quality and atmospheric transport of hazardous materials and that atmospheric composition can influence both weather and climate directly by changing the global radiation budget or indirectly by affecting cloud formation and precipitation (Grell and Baklanov, 2011), therefore, the simulation of a meteorological event must be performed with mathematical forecasting models that take into account both components (physics and chemistry).

This is possible using “online” models where the chemistry is integrated simultaneously with the meteorology, for representing the atmosphere more realistically, since these consider the strong coupling of meteorological and chemical processes in the atmosphere. Although mainly developed by the air quality (AQ) modelling community, these models are also of interest for numerical weather prediction (NWP) and regional climate modelling as

they can consider not only the influence of meteorology on air quality, but also the potentially important effects of atmospheric composition on weather (Baklanov et al., 2018).

The “online” approach has also disadvantages, for example a longer computational time is required to produce the meteorological forecast with an online air quality prediction. On the other side, “offline” chemical transport simulations only require a single meteorological dataset; this is particularly interesting for agencies that need to produce many simulations with different chemical assumptions, such as emissions input (Grell et al., 2004).

Online modelling systems have been developed and used by the research community since the 1990s, but NWP Institutions and air quality forecasting communities are still discussing whether an online approach is important enough to justify the additional computational power required for their implementation (Grell and Baklanov, 2011; Baklanov et al., 2018).

Currently, there are 18 regional online coupled models used in Europe (Baklanov et al., 2014; http://www.mi.uni-hamburg.de/costmodinv); among them, WRF-Chem model was chosen to simulate the meteorological event in question.

3.1. The WRF-Chem model

Several research institutes have collaborated in the development of a new state-of-the-art Weather Research and Forecasting (WRF, https://www.mmm.ucar.edu/weather-research-and-forecasting-model) model. WRF is a numerical weather prediction (NWP) system, non-hydrostatic and includes two dynamical cores [Advanced Research WRF (ARW) and NMM (Non-hydrostatic Mesoscale Model)], a data assimilation system and a software architecture supporting parallel computation and system extensibility. It has several options of physical parameterizations to represent atmospheric processes over a wide range of spatial (from tens of metres to thousands of kilometres) and temporal scales (Skamarock et al., 2008). WRF can produce simulations based on actual atmospheric conditions (i.e., from observations and analyses) or idealized conditions.

The first step toward the implementation of chemistry into WRF was held at the National Center for Atmospheric Research (NCAR) starting from March 2000. Since then, various chemical modules have been implemented into the WRF framework, creating an ‘‘online’’ WRF-Chem model (https://ruc.noaa.gov/wrf/wrf-chem/).

WRF-Chem (Weather Research and Forecasting model coupled with Chemistry) is a fully coupled meteorology-chemistry-aerosol model (Grell et al, 2005). It is able to simulate trace gases, particulates and aerosols transport simultaneously with the meteorological fields, which considers a variety of coupled physical and chemical processes such as transport, deposition, emission, chemical transformation, aerosol interactions, photolysis and radiation (Fast et al., 2006).

The air quality and the meteorological components employ the same transport scheme (mass and scalar conserving flux form of the governing equations), the same grid (horizontal and vertical coordinates), and the same physics schemes for subgrid-scale transport. The components also use the same time step; hence no temporal interpolation is needed. Some schemes for the gas phase chemistry are RADM2 (Regional Acid Deposition Model version 2, Stockwell et al., 1990), RACM (Regional Atmospheric Chemistry Mechanism), MOZART, CBMZ (Carbon-Bond Mechanism version Z), SAPRC99 (extensive VOC chemistry) and MEGAN (Model of Emissions of Gases and Aerosols from Nature).

The aerosol package offers the choice between bulk, modal and sectional schemes; in particular are implemented: MADE (Modal Aerosol Dynamics Modal for Europe, Ackermann et al., 1998), MAM (Modal Aerosol Model from CAM5, Liu et al., 2012), MOSAIC (Model for Simulating Aerosol Interactions and Chemistry, Zaveri et al., 2008) and GOCART (Georgia Tech/Goddard Global Ozone Chemistry Aerosol Radiation and Transport model, Chin et al., 2000). In addition, there are schemes for the gas phase/particle partitioning such as MARS (Model for an Aerosol Reacting System), SORGAM (Secondary Organic Aerosol Model) and VBS (Volatility Basis Set).

Possible applications of WRF-Chem concern:

- the prediction and simulation of weather, or regional and local climate;

- the release and transport of constituents through coupled weather prediction/dispersion model simulations;
- the analysis of the full interaction of chemical species as well as particulate matter through a coupled weather–dispersion–air quality model;
- the study of processes that are important for global climate change issues, including the direct and indirect aerosol forcing.

Due to its versatility WRF-Chem has a large user community world-wide and is continually further developed with additional options implemented.

3.2. Model setup

In this study, the WRF-Chem model version 3.6.1 has been used.

Figure 31 shows the model domain, in Lambert Conformal projection. It covers northern Africa and southern Europe with 300 × 300 grid points centred at 38.6° N, 10.6° E, on a horizontal grid spacing of 10 km in both directions and 40 vertical levels up to 50 hPa. Initial and boundary conditions were provided from NCAR/NCEP Final Analysis (FNL from GFS) (ds083.2), with 1° resolution.

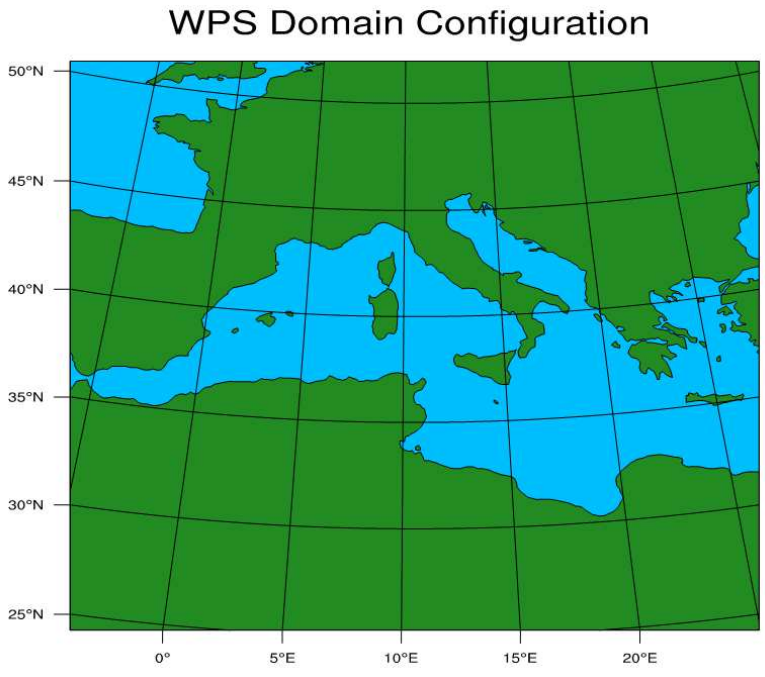

Figure 31. The numerical domain.

In order to investigate the impact of dust mineral effects on the meteorological event, two simulations are compared, both lasted 5 days, starting on 26 October 2018 at 00:00 UTC. The two simulations differ by the dust emission parameterizations that were considered (Tab. 3). A full description of the model configuration, including scheme settings for chemistry and physics, is presented in table 4 and described in next paragraphs.

Table 3. Settings of the two different simulations.

Case	Chem_opt	Dust_opt	Notes
CNTL0	0	Not used	
CNTL1	300	4	Direct effects Shao-2004 dust emission scheme Dust_schme = 2
INTM	300	3	Direct effects GOCART/AFWA dust emission scheme

Table 4. Physics and chemistry parameterizations used in the WRF-Chem setup.

Parameterization	Scheme	Namelist variable	Option
Planetary Boundary Layer	MYNN level 2.5	bl_pbl_physics	5
Surface layer	MYNN	sf_sfclay_physics	5
Land surface	RUC model	sf_surface_physics	3
Microphysics	Two-moment cloud microphysics	mp_physics	10
Shortwave radiation	RRTMG	ra_sw_physics	4
Longwave radiation	RRTMG	ra_lw_physics	4
Cumulus	Grell–Freitas	cu_physics	3
Chemistry/Aerosols	GOCART simple	chem_opt	300
Aerosol optics	Maxwell-Garnett	aer_op_opt	2

3.2.1. Physical parameterizations

The physical schemes adopted for both simulations are listed below and summarized in table 4:

- The Mellor–Yamada–Nakanishi and Niino (MYNN) 2.5 level turbulent kinetic energy (TKE) parameterization was used to describe the planetary boundary layer (Nakanishi and Niino, 2009).
- The MYNN scheme and the RUC (Rapid Update Cycle) land surface model (LSM) were chosen to represent the surface layer physics and the land surface interaction (Benjamin et al., 2004), respectively. The LSM controls the partitioning of energy at

the surface between latent and sensible heat, but also the partitioning of available water into evaporation and runoff (Pitman, 2003).

- The two-moment cloud microphysics scheme (Morrison et al., 2009) was used for the treatment of the microphysics processes.
- The short/long-wave radiation effects were parameterized through the Rapid Radiative Transfer Model for Global (RRTMG, Mlawer et al., 1997, Iacono et al,. 2008).
- The cumulus parameterization of Grell and Freitas (2014), with radiative feedback and shallow convection, allowed the description of the interactions with aerosols through a CCN dependent autoconversion of cloud water to rain as well as an aerosol dependent evaporation of cloud drops.

3.2.2. Aerosol-related model settings

As aerosol/chemistry module, the GOCART simple scheme (Georgia Tech/Goddard Global Ozone Chemistry Aerosol Radiation and Transport model, Chin et al., 2000) has been implemented (chem_opt = 300). It produces output for seven bulk aerosol species (aerosol compounds of which only the total mass is known, therefore there is no information neither on the number of particles nor on the distribution of their dimensions) and for eight sectional aerosols species.

The seven bulk aerosol species are:

- hydrophobic organic carbon (OC1);
- hydrophilic organic carbon (OC2);
- hydrophobic black carbon (BC1);
- hydrophilic black carbon (BC2);
- other GOCART primary species ($PM_{2.5}$, PM_{10});
- sulfate (only secondary aerosol species).

The eight sectional aerosols species are:

- four dust bins (0–2.5, 2.5–5, 5–10, 10–20 μm)
- four sea salt bins (0.1–0.5, 0.5–1.5, 1.5–5, 5–10 μm).

Mineral dust and sea salt emissions are surface wind speed dependent, while the other bulk species are prescribed from emission inventories and their background fields were set using the PREP-CHEM-SRC preprocessing software (Freitas et al., 2011). These fields are provided to the program *convert_emission* (included in WRF-Chem public release) to produce the gridded netCDF emission files for the WRF-Chem domain.

Aerosol optical properties are represented by the Maxwell–Garnett approximation (aer_op_opt = 2; Table 4), which considers small spherical randomly distributed black carbon cores in a particle (Bohren and Huffman, 1983).

Concerning the aerosol removal processes, the deposition schemes takes into account gravitational settling and surface deposition (Wesely, 1989) to simulate the dry removal of desert dust, while a simple wet deposition scheme that considers rainout/washout in large-scale precipitation (Balkanski et al., 1993) was used for both sea-spray and desert dust aerosols (Su and Fung, 2015).

3.2.3. Dust emission parameterizations

Three main mechanisms are responsible for the entrainment of atmospheric dust particles (Fig. 32): aerodynamic lift (Klose and Shao, 2012), saltation bombardment (Marticorena and Bergametti, 1995) and aggregates disintegration (Shao, 2008).

An essential condition for lifting of particles is the action of wind at the surface. Soil particles mobilize when lift, drag, and impact forces overcome the gravitational and interparticle cohesive forces holding them to the soil bed (Kok et al., 2012), so aerodynamic lift is most efficient at lofting larger particles (fine sand grains or aggregates on the order of 60 to 70 μm), because these are characterized by lower cohesive forces (Shao, 2001).

Once lofted, the particles undergo saltation, a process in which the heaviest particles, unable to remain in suspension, fall back upon the land surface with ballistic trajectories. When the impact energy released by collisions with soil exceeds the cohesive and gravitational forces binding particles to the surface, new particles may be engaged into saltation bombardment (Alfaro et al., 1997). This mechanism can mobilize even smaller particles, which were not moved by direct wind shear forcing (aerodynamic lift). As a

result, modeling saltation bombardment can be challenging because it have to represent correctly both wind shear mobilization of larger particles and bombardment interactions between particles of differing size.

The third process causing the dust emission is the aggregates disintegration. It is similar to saltation bombardment, but the dust emitted does not come from the soil surface after particle collisions on it, rather it is part of the saltating particle and originates from dust coatings on solid particles or clay aggregates disintegrating during collisions (Bullard et al., 2007). Modeling this process requires priori knowledge of soil conditions.

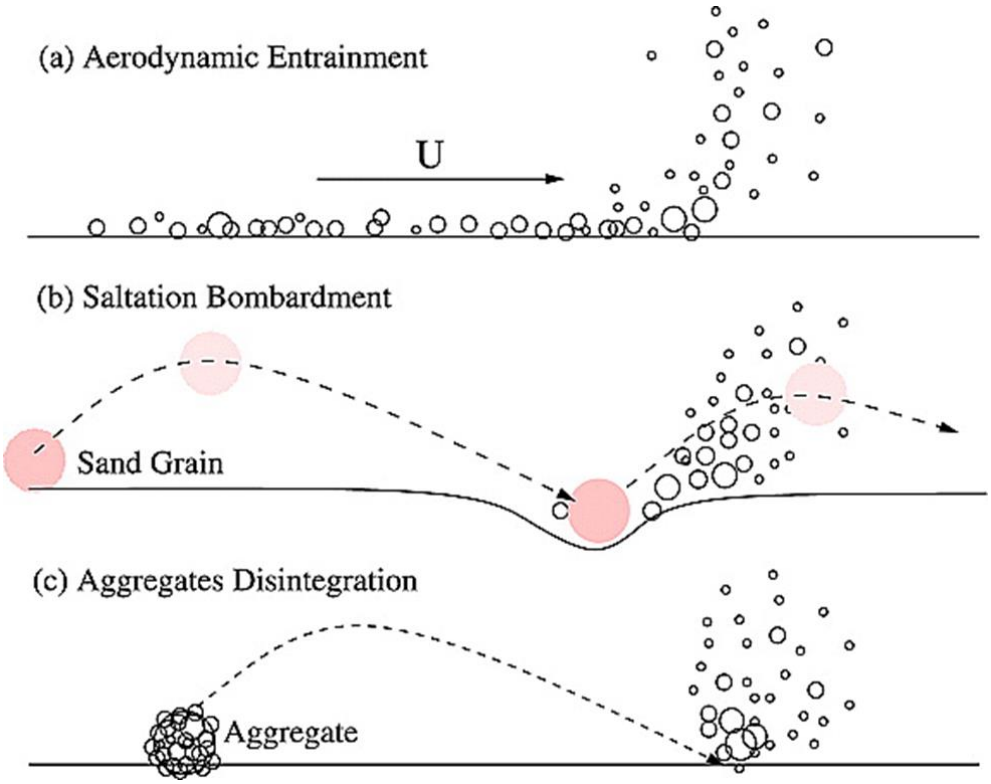

Figure 32. Mechanisms for dust emission: (a) aerodynamic lift, (b) saltation bombardment and (c) aggregate disintegration. Reproduced from Shao (2008).

To adequately represent dust production processes, it is necessary to implement a scheme that takes into account these three mechanisms.

The main parameters that must be considered within any numerical model to describe dust emissions are the threshold friction velocity at which dust particles begin to move and the horizontal and vertical sand dust fluxes.

WRF-Chem model has three different options for the representation of mineral dust emissions: DUST-GOCART, DUST-GOCART/AFWA e DUSTUOC.

The first is the Georgia Institute of Technology-Goddard Global Ozone Chemistry Aerosol (GOCART) model (Ginoux et al., 2001), the second is the Air Force Weather Agency scheme (a new version of the GOCART model), while the last one has been developed at the University of Cologne and is divided into three further parameterizations having among them a progressive level of simplification (Shao, 2001, 2004; Shao et al., 2011).

All three schemes share some commonalities (Letcher and LeGrand, 2018):

- They compute dust-emission flux as a function of wind energy, soil properties (such as soil moisture and particle size) and availability of loose, erodible soil particles;
- They assume that dust emissions are the result of saltation originated when wind speed exceeds critical thresholds;
- Emitted dust particles are divided into five size-based groupings called size bins, with a 1.46 µm, 2.8 µm, 4.8 µm, 9 µm, and 16 µm effective particle diameter size distribution;
- After the injection into the lowest atmospheric model level, simulated atmospheric dust mass concentrations and optical properties are estimated considering separate transport, removal, and radiative transfer schemes.

The two simulations (Tab. 3) of the event under study were performed, one, using the GOCART/AFWA scheme (dust_opt = 3), and the other, with the DUSTUOC scheme based on Shao 2004 (dust_opt = 4, dust_schme = 2).

3.2.3.1. AFWA dust-emission scheme

The AFWA dust-emission scheme (Jones et al., 2010; Jones, 2012) was developed in 2011 by Air Force Weather Agency as an evolution of the original GOCART model, which had detected several issues concerning the representation of dust availability (source strength) and the calculation of dust emissions as a function of wind speed (LeGrand et al., 2019). The equations for the AFWA scheme include the static threshold friction velocity required

for particle entrainment (u_{*t}), the horizontal saltation flux, the resultant bulk vertical dust flux, the emitted dust particle size distribution, and the size-resolved emitted dust flux.

The AFWA scheme utilizes an independent series of bins for saltation based processes (Tab. 5) and emitted dust (Tab. 6), allowing dust emission by saltation bombardment and particle disaggregation to be better represented (LeGrand et al., 2019).

Table 5. Saltation particle size bins and their associated attributes. Particle sizes are presented here in µm but handled in units of centimetres (LeGrand, 2019).

Saltation size bin (p)	Effective diameter ($D_{s,p}$) (µm)	Soil separate class	Soil separate class mass fraction (s_{frac})	Particle density (ρ_p) (g cm^{-3})
1	1.42	Clay	1	2.50
2	2.74	Silt	0.2	2.65
3	5.26	Silt	0.2	2.65
4	10	Silt	0.2	2.65
5	19	Silt	0.2	2.65
6	36.2	Silt	0.2	2.65
7	69	Sand	0.333	2.65
8	131	Sand	0.333	2.65
9	250	Sand	0.333	2.65

Table 6. Dust particle size bins and their associated attributes, presented here in µm but handled in units of centimetres within the model (LeGrand, 2019).

Dust size bin (p)	Lower bound diameter (µm)	Upper bound diameter (µm)	Effective diameter ($D_{d,p}$) (µm)	Particle density (ρ_p) (g cm^{-3})
1	0.2	2	1.46	2.50
2	2	3.6	2.8	2.65
3	3.6	6	4.8	2.65
4	6	12	9	2.65
5	12	20	16	2.65

The threshold friction velocity is calculated with the same equation used in the GOCART scheme:

$$u_{*t}(D_{s,p}) = 0.129 \frac{\left(\frac{\rho_{s,p} g D_{s,p}}{\rho_a}\right)^{0.5} \left(1 + \frac{0.006}{\rho_{s,p} g D_{s,p}^{2.5}}\right)^{0.5}}{\left[1.928\left(a\left(D_{s,p}\right)^{x} + b\right)^{0.092} - 1\right]^{0.5}},$$

Where $D_{s,p}$ is the diameter for saltation size bin, g is acceleration due to gravity, $\rho_{s,p}$ is the particle density of the saltation size bin s, ρ_a is air density, x = 1.56, a = 1331 cm^{-x} , and b = 0.38.

The values thus obtained are then multiplied by a correction function $f(\vartheta)$ to account for the effects of soil moisture on particle cohesion (Fécan et al., 1999):

$$f(\theta) = \begin{cases} \sqrt{1 + 1.21\left(\theta_g - \theta_g'\right)^{0.68}}, & \theta_g > \theta_g' \\ 1, & \theta_g \le \theta_g' \end{cases};$$

where

- θ_g' is the fraction of soil moisture able to be absorbed before capillary forces begin to influence particle detachment:

$$\theta_g' = 0.0014(100c_s)^2 + 0.17\,(100c_s)\,,$$

with c_s (soil clay content mass fraction) derived from the global Food and Agriculture Organization digital Soil Map of the World (FAOSMW) by Reynolds et al. (2000), available at the NASA Land Data Assimilation System (LDAS);

- θ_g is the gravimetric soil moisture fraction:

$$\theta_g = \frac{\theta_v \rho_w}{(2.65 - 0.15c_s)\,(1-\phi)},$$

where θ_v is the volumetric water content, ρ_w is water density equal to 1.0 g cm^{-3}, ϕ is the porosity of the soil medium, and the $2.65 - 0.15c_s$ term represents the soil density.

The horizontal saltation flux is computed via:

$$G = \Sigma_{s,p}\left[H\left(D_{s,p}\right) \mathrm{d}S_{rel}\left(D_{s,p}\right)\right],$$

where

- $H(D_{s,p})$ are the particle-size dependent saltation fluxes (Kawamura, 1951):

$$H\left(D_{s,p}\right) = \begin{cases} C_{mb}\dfrac{\rho_a}{g}u_*^3\left(1+\dfrac{u_{*t,s,p}}{u_*}\right)\left(1-\dfrac{u_{*t,s,p}^2}{u_*^2}\right), & u_* > u_{*t,s,p} \\ 0\,, & u_* \le u_{*t,s,p} \end{cases}$$

with $C_{mb} = 1$.

- $dS_{rel}(D_{s,p})$ are the saltation bin-specific weighting factors, equal to the ratio of the size-resolved basal surface coverage fractions to the total basal surface area of the soil bed:

$$\mathrm{d}S_{rel}\left(D_{s,p}\right) = \frac{\mathrm{d}S_{SFC}\left(D_{s,p}\right)}{N_{SFC}},$$

with

$$\mathrm{d}S_{SFC}\left(D_{s,p}\right) = \frac{\mathrm{d}M\left(D_{s,p}\right)}{\frac{2}{3}\rho_{s,p}D_{s,p}},$$

$$N_{SFC} = \Sigma_{s,p}\left[\mathrm{d}S_{SFC}\left(D_{s,p}\right)\right].$$

The bulk vertical dust flux F_B is calculated as:

$$F_B = \begin{cases} \mathrm{G} \cdot \mathrm{EROD} \cdot \beta, & z_0 \leq 20 \text{ cm} \\ 0, & z_0 > 20 \text{ cm} \end{cases},$$

where EROD is the dust source strength parameterization, varying from 0 to 1, β = $10^{0.134(c_s)-6}$ is the sandblasting efficiency and z_0 is an aerodynamic roughness length.

Once the total dust emission (F_B) has been determined, since it is distributed among suspended dust size bins according to Kok (2011) brittle fragmentation theory, suspended dust distribution weighting factors ($\kappa_{d,p}$) are determined taking the ratio of the normalized volume distributions of each dust size bin ($dV_{d,p}$) to the total normalized volume distribution of emitted dust (N_V):

$$\kappa_{\mathrm{d,p}} = \frac{\mathrm{d}V_{\mathrm{d,p}}}{N_V},$$

where

$$dV_{d,p} = \frac{D_{d,p}}{c_v}\left[1 + \mathrm{erf}\left(\frac{\ln\left(D_{d,p}/\overline{D}_m\right)}{\sqrt{2}\ln\sigma_s}\right)\right]\exp\left[-\left(\frac{D_{d,p}}{\lambda}\right)^3\right]\ln\frac{D_{d,p\_max}}{D_{d,p\_min}},$$

$$N_V = \Sigma_{\mathrm{d,p}}\left[\mathrm{d}V_{\mathrm{d,p}}\right],$$

and $\overline{D}_m$ is the dust particle mass median diameter equal to $3.4 \cdot 10^{-4}$ cm, σ_s is the geometric standard deviation equal to 3.0, c_v is a normalization constant equal to $12.62 \cdot 10^{-4}$ cm, λ is the crack propagation length equal to $12 \cdot 10^{-4}$, erf is the error function, and D_{d,p_max} and D_{d,p_min} are the maximum and minimum effective diameters represented by the dust size bin, respectively.

Finally, size-resolved emitted dust flux ($F_{d,p}$) is obtained as:

$$F_{\mathrm{d,p}} = F_{\mathrm{B}}\kappa_{\mathrm{d,p}}.$$

It is important to point that in the AFWA scheme, the relationship between vertical and horizontal fluxes is only related to the soil clay content. This could be the reason for the over-prediction of the dust concentration by AFWA scheme with respect to DUSTUOC scheme, which considers a more realistic soil texture type (Rizza et al., 2016; Fountoukis et al., 2016).

3.2.3.2. UoC dust-emission scheme by Shao 2004

The UoC (University of Cologne) scheme described in Shao 2004 is an intermediate version, because it incorporates physically based aggregate disintegration algorithms not included in the following Shao 2011 setting, but has less dependence on soil characteristics than that documented in Shao 2001.

The approach is the same as the AFWA scheme, but the more sophisticated UoC sub-options also use size-resolved saltation particle bins to evaluate dust emission from saltating particles of different sizes.

The dry soil threshold friction velocity is calculated following Shao and Lu (2000) as:

$$u_{*\mathrm{t}}(d) = \sqrt{A_{\mathrm{N}}\left(\sigma_{\mathrm{p}} g d + \frac{\gamma_{\mathrm{c}}}{\rho_{\mathrm{p}} d}\right)},$$

where σ_p is the ratio of particle to air density, g is the gravitational constant, d is particle diameter, ρ_p is the particle density, and $A_N = 0.0123$ and $\gamma_c = 1.65 \cdot 10^{-4}$ kg s^{-2} are constant.

The values obtained with this equation are then correct to consider the influence of soil moisture (Fécan et al., 1999) and the surface roughness (Raupach, 1992).

The first correction has the following expression:

$$f_s = \sqrt{1 + a(i)(\theta_v - \theta_r)^{b(i)}}$$

where i = 1.12 is the soil texture index, $a(i)$, $b(i)$ and θ_r are tabulated parameters that explicitly depend on Land Surface Model and θ_v is the volumetric soil moisture.

The roughness correction (r) is calculated following the drag partition theory, being proportional to the frontal area index (x_f), based on the vegetation fraction (c_f):

$$r = \sqrt{1 - 0.5 x_{\mathrm{f}}} \times \sqrt{1 + 100 x_{\mathrm{f}}},$$

$$x_{\mathrm{f}} = 0.35 \times \ln(1 - c_{\mathrm{f}}).$$

This correction factor has a substantial impact on the threshold friction velocity, leading to differences in dust emission between the AFWA and UoC schemes.

The calculation of theoretical saltation fluxes for each particle size bin is similar to that of the AFWA scheme, though UoC uses more size bins (100 vs. 9):

$$q(d) = \begin{cases} (1-c_f)2.3\frac{\rho_a}{g}u_*^3\left(1-\frac{u_{*_t}(d,\theta_v,r)}{u_*}\right)\left(1+\frac{u_{*_t}(d,\theta_v,r)}{u_*}\right)^2, & u_* \geq u_{*_t}(d,\theta_v,r) \\ 0, & u_* < u_{*_t}(d,\theta_v,r) \end{cases}$$

The parent soil particle size distribution is incorporated by multiplying the theoretical saltation flux for each bin by a term representing the availability of saltation particles $p_s(d)$:

$$Q(d) = q(d)\, p_s(d)$$

with

$$p_s(d) = \gamma \times p_m(d) + (1-\gamma) \times p_f(d),$$

where $p_m(d)$ and $p_f(d)$ represent the minimally and fully disturbed particle size distribution and γ is a function describing the binding strength of aggregated particles, calculated as:

$$\gamma = \exp\left[-\left(u_* - u_{*t}\right)^3\right].$$

The dust emission flux from the saltation flux is determined with the following equation:

$$F(d_i, d_s) = c_y \eta_{f,i}\left[(1-\gamma)+\gamma\sigma_p\right]\frac{Q(d_s)\,g}{{u_*}^2}(1+\sigma_m)$$

where c_y is a dimensionless coefficient, u_* is the friction velocity, $\sigma_p = \frac{\eta_{f,i}}{\eta_{m,i}} = \frac{p_f(d_i)}{p_m(d_i)}$ is free dust to aggregated dust ratio and $\sigma_m = 12u_*^2\frac{\rho_b}{p}\left(1+14u_*\sqrt{\frac{\rho_b}{p}}\right)$ is the bombardment efficiency, with bulk soil density ρ_b = 1000 kgm^{-3} and soil plastic pressure p = 30 000 Nm^{-2}. The soil plastic pressure plays an important role in the emission, in particular for a fixed value of the friction speed, the vertical flow decreases as the soil plastic pressure increases. Moreover, this parameter is set to a constant in the WRF-Chem implementation, despite being a parameter well known to be subject to variations with soil type.

The size-resolved dust emission is calculated by integrating dust emissions of each dust bin over all saltation bins:

$$F(j) = \sum_{i=1}^{bins=100} F(i,j).$$

Finally, the total dust emission is calculated by integrating overall emissions bins:

$$F_{\text{total}} = \sum_{j=1}^{\text{bins=dust}} F(j).$$

4. RESULTS AND DISCUSSION

After performing the simulations, it was possible to compare the WRF-Chem model's outputs with satellite retrievals and global model reanalysis, in order to evaluate the performance and consistency of the model in reproducing the weather event under investigation.

It was decided to compare the data relating to wind, water vapour and precipitation, as representative elements of the synoptic framework that characterized the event in question. In fact, they provide information on the type of atmospheric circulation associated with the transport of mineral dust, which was assessed by comparing the AOD data. The atmospheric parameters were compared with only one type of simulation (the one performed with the GOCART/AFWA scheme as dust emission parameterization), since the microphysics setup is the same in both.

Results and discussion are given below.

4.1. Wind

The wind speed at 10 m (ms^{-1}) was evaluated, comparing the data provided by ERA5 (Fig. 33 a, c, e) with the values obtained through the simulations performed with the WRF-Chem model (Fig. 33 b, d, f).

The maps representing reanalysis data show that on 28 October at 12.00 UTC (Fig. 33a) the wind speed did not exceed 16 ms^{-1}, occurred at the Tyrrhenian Sea, the Adriatic Sea and west of Sardinia.

Wind speed increased the following day (Fig. 33c) with a peak of about 25 ms^{-1} between the Balearic Islands and Sardinia, but overall the intensification of the air currents affected the whole Mediterranean basin.

At 16.00 UTC of 29 October (Fig. 33e), we note a further increase of the maximum speed in all sectors; this suggests a wind direction from south-west to north-east.

Although from a qualitative point of view the wind circulation reproduced by the simulations is very close to that of the ERA5 reanalysis, there are inconsistencies in term of

intensity, in particular, the model seems to underestimate the wind speed. This may be caused by an incorrect representation of the roughness parameterization over the sea under high wind conditions (Rizza et al., 2018).

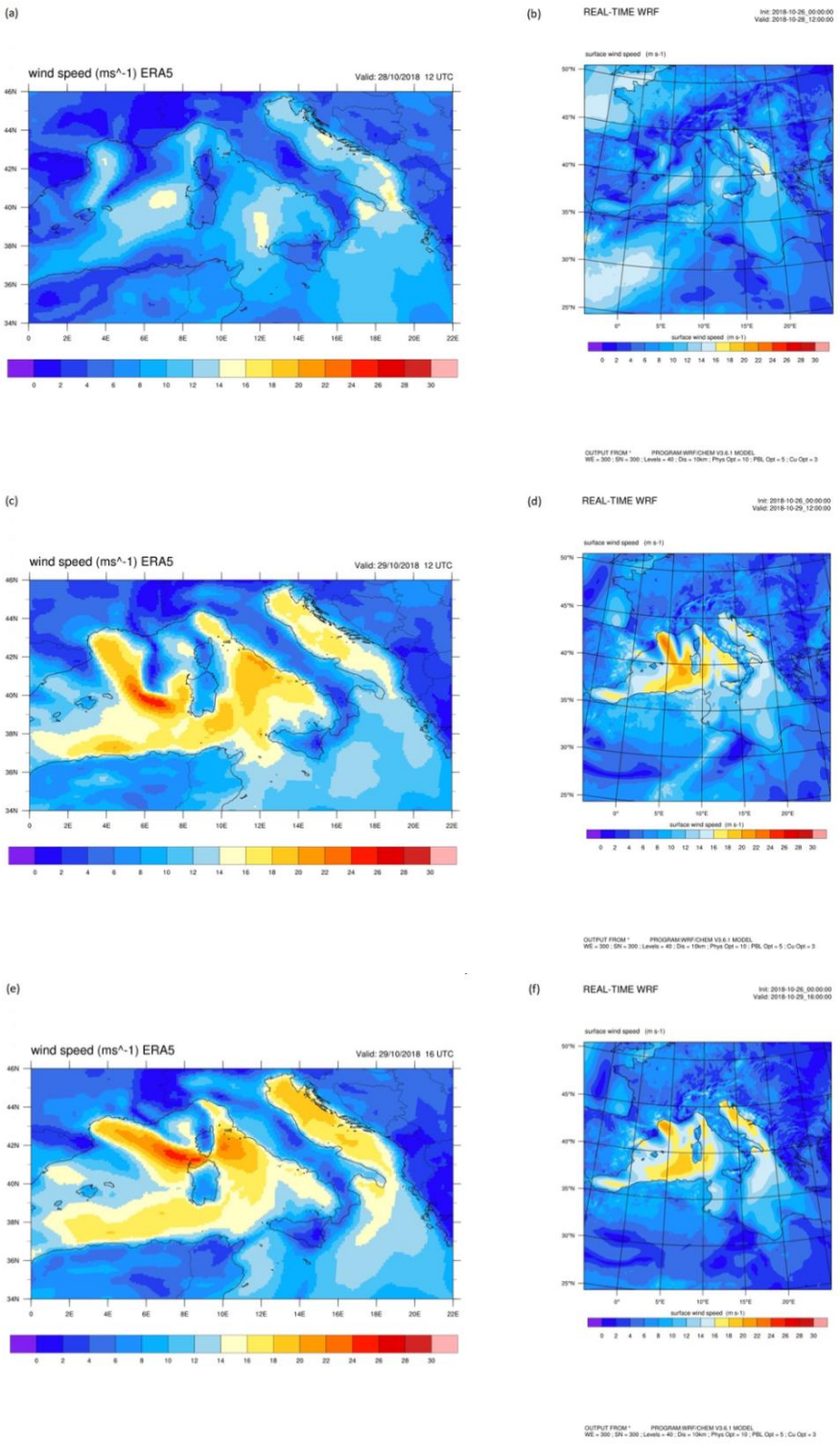

Figure 33. Comparison between the 10 m wind speed provided by ERA5 (a, c, e) and that obtained from the simulations with the WRF-Chem model (b, d, f).

4.2. Water vapour

During the storm “Vaia” the particular combinations of wind, temperature and pressure conditions, typical of extratropical cyclones, led to the formation of "atmospheric rivers" (ARs). These are long and narrow regions (approximately 2.000 km long, less than 1.000 km wide, and averages 3 km in depth) of concentrated moisture (Fig. 34), located within the low-level jet, an area of strong winds in the lower levels of the atmosphere, ahead of the cold front (https://ghrc.nsstc.nasa.gov/home/micro-articles/atmospheric-rivers).

These columns of water vapour move with the weather from the tropics toward the poles and can last around 20 hours over an area (Ralph et al., 2013). When they interact with mountains, the large amount of water vapour is released in form of rain or snow. This extensive precipitation production in relatively short periods of time can lead to flooding and mudslides (https://www.noaa.gov/stories/what-are-atmospheric-rivers). “Atmospheric rivers” are a key feature in the global water cycle, because not all of them cause damage; many are weak systems that often provide beneficial impacts by contributing to the water supply and increasing the snowpack.

Figure 34. Picture of an atmospheric river (https://www.noaa.gov/stories/what-are-atmospheric-rivers).

Within the WRF-Chem model, water vapour is considered through the QVAPOR (water vapour mixing ratio) variable (kg kg^{-1}) which, once multiplied by the density ρ (kg m^{-3}), is integrated over the entire height of the air column at each point of the grid, obtaining the distribution of water vapour on the surface of the domain (kg m^{-2}):

$$< Q_V > (t; x, y) = \int_0^H QVAPOR(t; x, y, z) \cdot \rho(t; x, y, z)\ dz$$

The results were extrapolated starting from 00.00 UTC on 28 October 2018 with a frequency of 12 hours (Fig. 35 b, d, f, h, l).

These maps were compared with the Total Precipitable Water (http://tropic.ssec.wisc.edu/real-time/mimic-tpw/global/main.html) experimental data (expressed in mm) obtained from Cooperative Institute for Meteorological Satellite Studies (CIMSS) (Fig. 35 a, c, e, g, i).

The comparison was possible because 1 kg of rain water over 1 square meter of surface is equal to 1 mm in thickness (1 kg m^{-2} ≡ 1 mm).

It can be observed that on 28 October at 00.00 UTC (Fig. 35a) the south-west wind circulation conveyed very humid air from the Atlantic Ocean to the Mediterranean basin. In particular, the presence of two large streams of water vapour, separated by a region of dry air, that cross the Sahara region and then invade the entire Italian peninsula with values ranging between 30 and 35 mm, is highlighted.

A similar trend is observed at 12.00 UTC (Fig. 35c), but with an intensification of the humidity that exceeded 40 mm in correspondence with central-southern Italy.

The atmosphere above the entire Mediterranean basin continued to be characterized by high humidity values even on the day of 29 October (Fig. 35e), observing from 12.00 UTC (Fig. 35g) a slow movement towards the east, which results even more evident on 30 October (00.00 UTC) when a marked flow of dry air from the west entered the Mediterranean region (Fig. 35i).

The simulations performed with the WRF-Chem model have provided results (Fig. 35 b, d, f, h, l) that fairly faithfully reproduce both the intensity and the extent of the water vapour flows transported during the meteorological event.

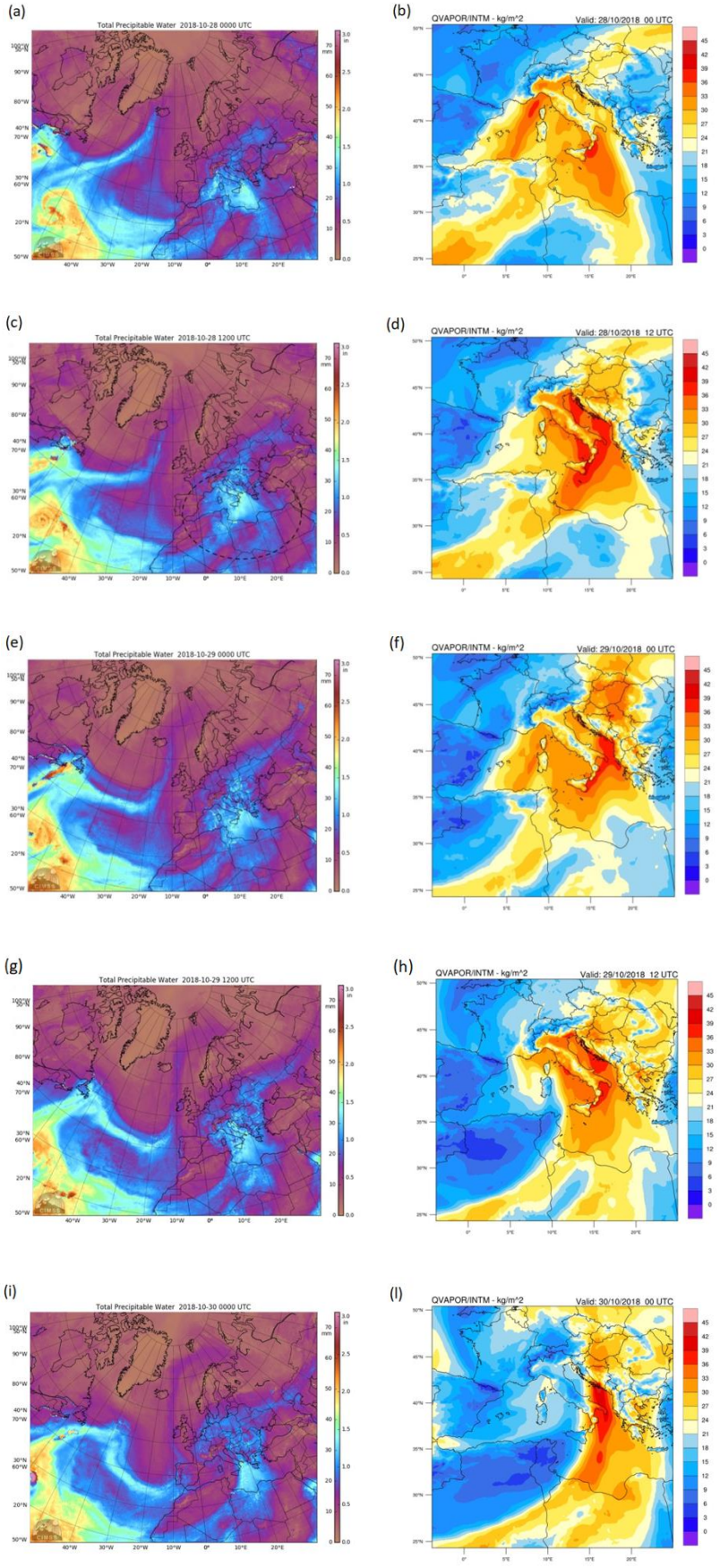

Figure 35. Maps of water vapor on 28-10-2018 at 00.00 UTC and 12.00 UTC, on 29-10-2018 at 00.00 UTC and 12.00 UTC and on 30-10-2018 at 00.00 UTC, from CIMSS (a, c, e, g, i) and WRF-Chem model (b, d, f, h, l).

4.3. Precipitation

The water was represented inside the model both as water vapour and in hydrometeor form, in particular the component of precipitating particles (HMP) was implemented through the variables QRAIN (rain mixing ratio), QSNOW (snow mixing ratio) and QGRAUP (graupel mixing ratio) expressed in kg kg^{-1}. These variables were multiplied by the density ρ (kg m^{-3}) and then integrated over the entire height of the air column at each point of the grid, obtaining the distribution of precipitation over the surface of the domain (kg m^{-2}):

$$HMP = \int_0^H (QRAIN + QSNOW + QGRAUP) \cdot \rho \quad dz$$

The model's outputs (Fig. 36 b, d, f) were compared with the data provided by ERA5 (Fig. 36 a, c, e), analyzing the maps relating to the day 28 October at 00.00 UTC and 18.00 UTC and to 29 October at 12.00 UTC.

From these it is observed that on 28 October (Fig. 36a) the rainfall occurred along the whole mountain range of the Alps, in particular the greater quantity of rain was released in the Italian regions of Piedmont, Lombardy and Liguria with a maximum of 1 kg m^{-2}. Other precipitations were detected at the Balearic Islands, but of less intensity (0.6 kg m^{-2}).

At 18.00 UTC of the same day (fig. 36c) Italy was completely free from heavy shower phenomena, which instead were recorded in the central Mediterranean and on part of North Africa, where the peak exceeded 1 kg m^{-2}.

These rains, on 29 October at 12.00 UTC (Fig. 36e), driven by the southwest winds reached northern Italy where the most abundant rainfall hit the Veneto and Friuli Venezia Giulia regions with maximum values of about 0.8 kg m^{-2}. In general, the intensity decreased throughout the Mediterranean basin.

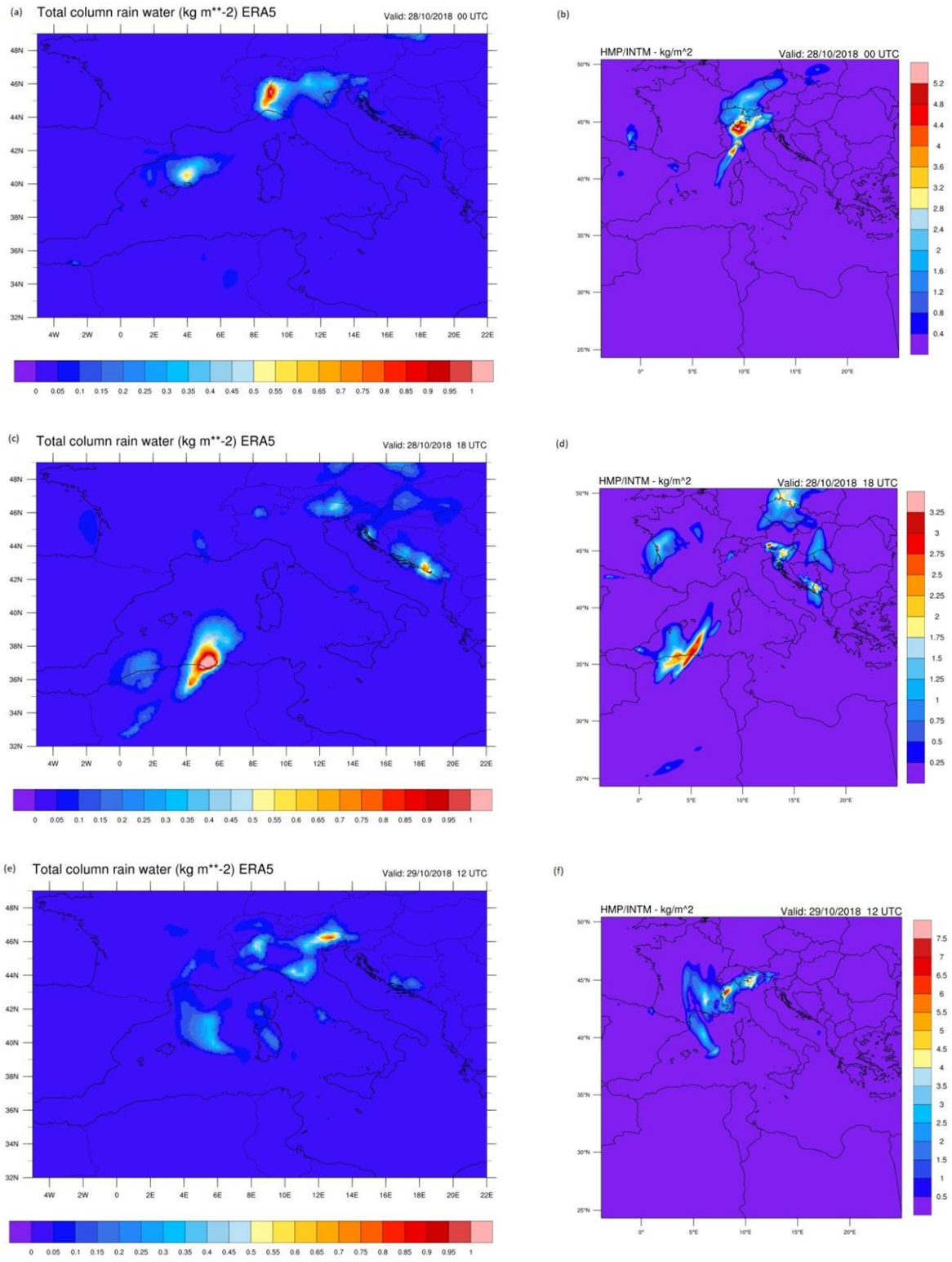

Figure 36. Maps representing the distribution of precipitation according to the data provided by ERA5 (a, c, e) and to the WRF-Chem model (b, d, f).

As for the wind, also for the precipitation there is a biased forecast by the model; in fact the results obtained from the simulations are higher in quantitative terms. HMP (Hydrometeors Precipitating) are always higher than 3 kg m^{-2}, even on 29 October (Fig. 36f)

the map shows a maximum value of about 7 kg m^{-2}: estimates very different from those of ERA5 data.

A further comparison has been made considering the cumulate rain by Tropical Rainfall Measuring Mission (TRMM; Kummerow et al., 1998; Tao and Adler, 2003) and the model cumulate rain at the ground, both expressed in mm.

TRMM is a joint mission between the National Aeronautics and Space Administration (NASA) and the Japan Aerospace Exploration Agency (JAXA) that has developed a platform with remote sensors from space able to obtain precipitation estimations over the ocean and remote continental regions. The passive TRMM Microwave Imager (TMI) is a high-resolution instrument that can provide robust information about hydrometeor content in an atmospheric column, since the amount of scattering due to ice particles in the clouds increases as does the microwave frequency. In this sense, scattering algorithms work over land and water by inferring the precipitation amount based upon computations of in-cloud ice content, and are helpful to define the nature of precipitation (Montero et al., 2011).

In particular, the daily accumulated precipitation product (TRMM_3B42_Daily, https://disc.gsfc.nasa.gov/datasets/TRMM_3B42_Daily_7/summary) used in this study is generated from TRMM Multi-Satellite Precipitation Analysis (TMPA) that is produced at the NASA GES DISC. The daily accumulation is derived by summing valid retrievals in a grid cell for the data day.

Maps extracted from the satellite Tropical Rainfall Measuring Mission (TRMM) datasets (Fig. 37 a, c) show that on 28 October 2018 it was characterized by scattered rainfall over most of Italy and the western Mediterranean Sea, with very limited areas where maximum values of 110 mm/day were measured (Fig. 37a).

Precipitation increased on 29 October 2018, in fact it was measured up to 120 mm/day in much larger areas, especially in the north-western regions of Italy (Fig. 37c).

Also in this case the results obtained from the simulations (Fig. 37 b, d) confirm an overestimation of the cumulate rain, being the maximum values reproduced higher than 150 mm.

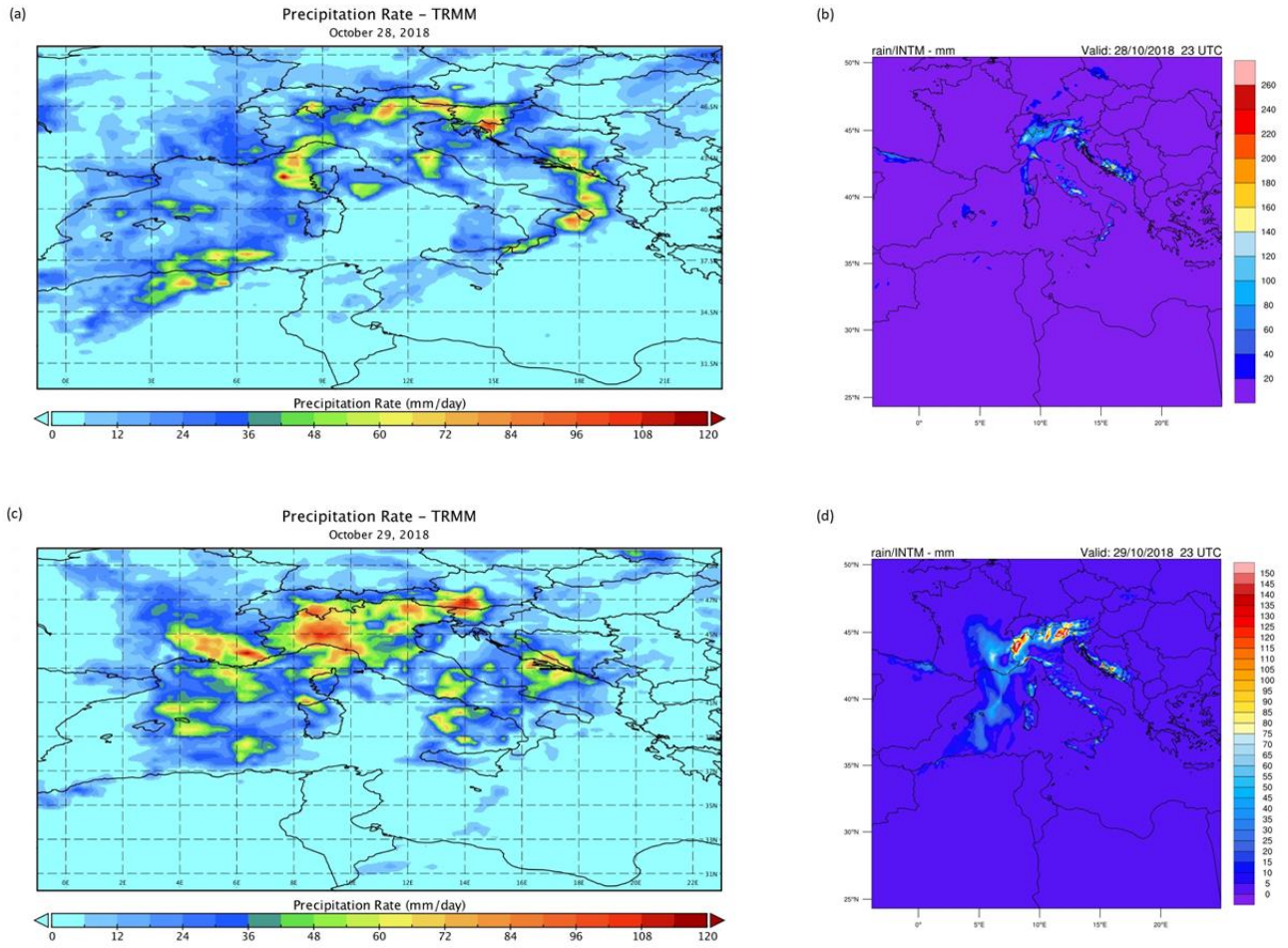

Figure 37. Comparison between the cumulative rain on the ground provided by TRMM (a, c) and that produced by the WRF-Chem model (b, d), on 28 October 2018 and 29 October 2018.

So for both columnar ERA5 data and cumulate rain on the ground (TRMM), there is a good spatial reproduction but an overestimation in quantitative terms by the model; this may be due to the interaction between dust and atmospheric microphysics, in fact, the presence of dust should reduce both quantities since it promotes the formation of cloud condensation nuclei (CCN).

Concerning this, there is work in progress by the joint CNR-ISAC and UNIVPM research group, with the aim of better understanding the indirect effect of aerosols on cloud microphysics so as to improve the parameterization within the WRF-Chem model.

On the other hand, a good result was obtained from the comparison between model simulations and total rainfall accumulations data provided by national rainfall network of the Civil Protection Department (about 2500 tipping bucket stations), mapped on regular 5km x 5km grid with a GRISO (Random Generator of Space Interpolations from Uncertain

Observations) method (Pignone et al., 2010). These data were then remapped again on a 0.1 ° x 0.1 ° grid to compare them with satellite estimates.

The simulations accurately predicted, both for quantity and for spatial distribution, the mm of ground water collected by the rain gauges.

This can be seen from the maps made for the day 29 October 2018 at 23.00 UTC in which the rain gauges (Fig. 38a) measured a maximum value of 150 mm of rain fallen north of the Veneto, Friuli-Venezia Giulia and Piedmont and also on Liguria. The simulation (Fig. 38b) performed with the WRF-Chem model reproduced the same maximum value in the same location, with the exception of a slight underestimate on the Liguria region where the maximum projected was about 130 mm.

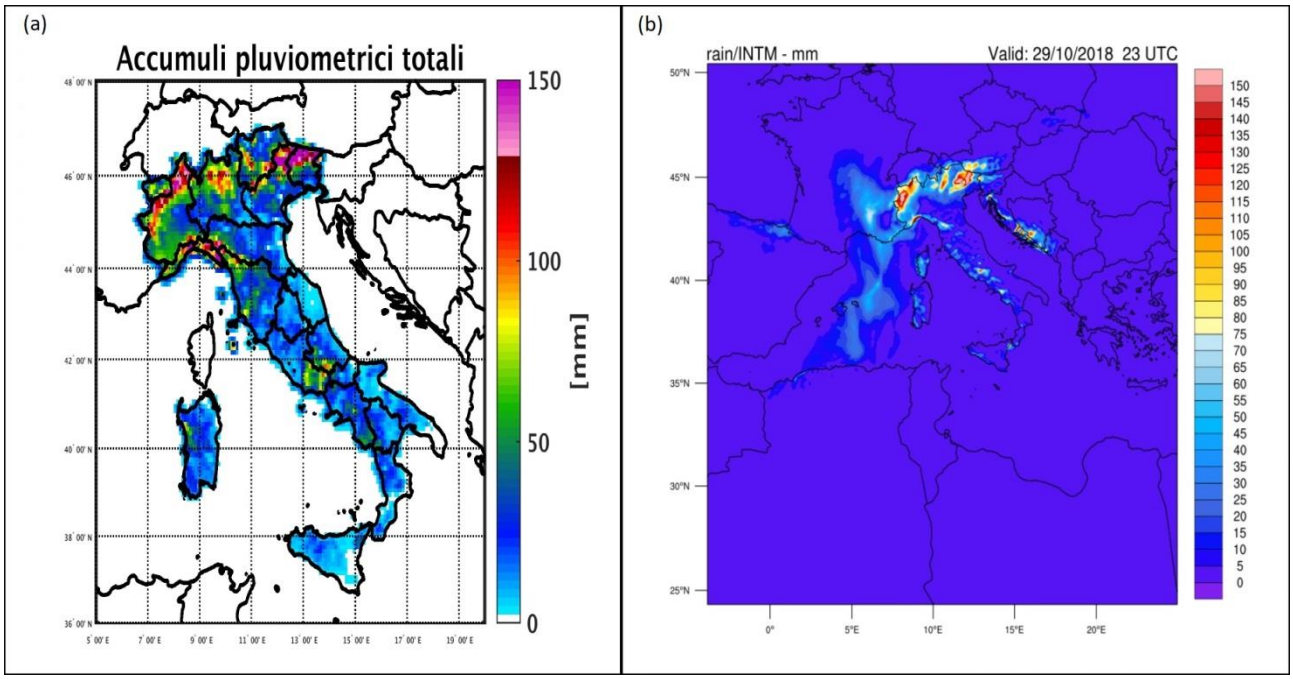

Figure 38. Comparison between the total rainfall accumulations data (mm) provided by national rainfall network of the Civil Protection Department and those forecasted by the WRF-Chem model, on 29 October 2018 at 23.00 UTC.

4.4. Aerosol Optical Depth (AOD)

The AOD data provided by the MODIS sensor on board the Terra and Aqua satellites were averaged for the days 28, 29 and 30 October, obtaining the maps in figure 39 (a, d, g).

In this case, since the main purpose of this study is to assess the influence of Saharan dust on atmospheric dynamics, the comparison was made with respect to both simulations,

carried out with two different dust parameterization schemes (GOCART/AFWA and Shao 2004), in order to evaluate which of the two reproduces more faithfully the transport of mineral dust over the Mediterranean basin.

On 28 October 2018 the large cloud cover in the analyzed region prevents the detection of AOD from space, so it is difficult to refer to satellite data (Fig. 39a), however comparing the two simulations we can observe two dust outflows coming from the desert regions of northern Africa, one of which is very extensive, characterized by high AOD values and transported by south-west wind, and the other less intense driven by south-east wind, exactly as detected by the synoptic analysis previously described. What differs between the two simulations is that the AFWA scheme (Fig. 39b) produces maximum AOD values around 3, quite higher than those obtained with the Shao 2004 scheme (Fig. 39c), which reach a maximum around 2 and where the dust plume from the southeast is almost completely absent.

The satellite data collected on 29 October 2018 (Fig. 39d) show that the dust flow has moved north, to the centre of the Mediterranean Sea and to the Tyrrhenian coast of Italy. The maximum AOD values detected by the MODIS sensor are equal to 3 as well as those provided by the simulation performed with the AFWA scheme (Fig. 39e), even if the latter are extended to a more limited area. Furthermore, in both simulations it appears that passage towards the Mediterranean has a slight delay, since the AOD peak is still present in correspondence of Tunisia and not in proximity of Sardinia, as reported by the observations. Spatially the dust outbreak is well reproduced also by the Shao 2004 scheme (Fig. 39f), but with an evident underestimation of the AOD (maximum equal to 2).

On 30 October 2018, satellite observations (Fig. 39g) show a reduction of the AOD values; the maximum measured is 1 and is located in the Ionian Sea, south of Puglia. This confirms that the perturbation has come to the end and is moving eastward. There is excellent spatial feedback from both simulations, but in this case the AFWA scheme overestimates the amount of dust (Fig. 39h) unlike the Shao 2004 scheme (Fig. 39i) which instead is very close to the satellite data.

In general, it can be said that both setups correctly reproduce the spatial distribution of the desert outbreak; the substantial difference is from a quantitative point of view: the

high AOD values are better estimated by the AFWA setup, while the Shao 2004 scheme can reproduce more precisely the relatively low values of AOD.

The overestimation by the AFWA scheme is due to the fact that the AFWA emission model considers the vertical dust flow related only to the clay content, while the vertical dust flow in the Shao setup (2004) consider four types of soil structure classes, and for each class an appropriate value of the soil plastic pressure (surface hardness), as explained in chapter 3.

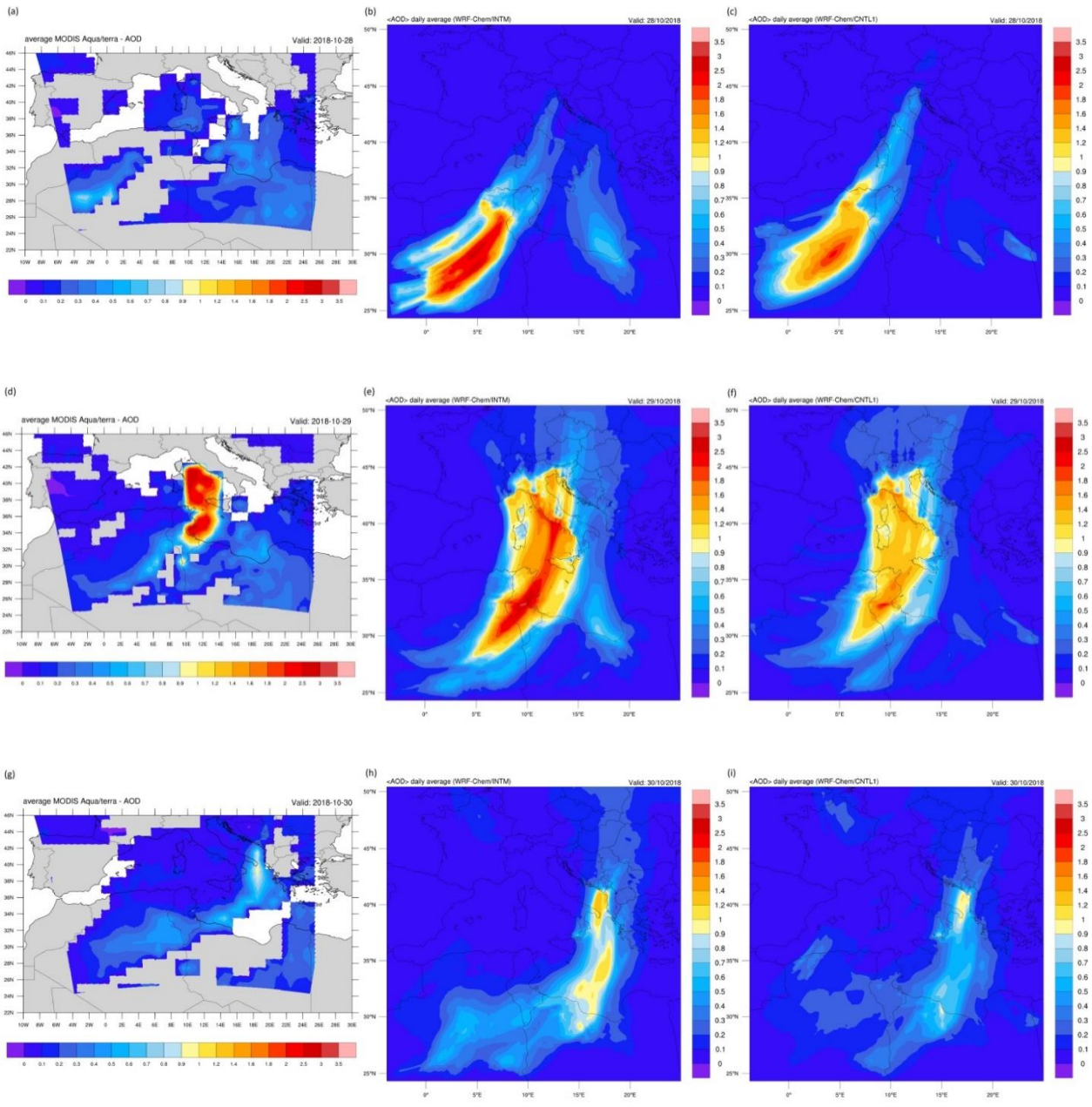

Figure 39. Values and distribution of AOD through MODIS sensor (a, d, g) and WRF-Chem model, with AFWA scheme (b, e, h) and with Shao 2004 scheme (c, f, i).

4.5. Feedback aerosol-clouds: indirect effects

In order to evaluate the indirect effects caused by aerosol particles on cloud microphysics, a simulation was performed implementing a slightly different setup (Tab. 7) within the WRF-Chem model. Specifically, in the physics suite it was adopted the aerosol-aware Thompson–Eidhammer microphysics scheme (mp_physics = 28), which is an "aerosol-aware" scheme designed to include effects of dust aerosols on cloud microphysics. It has been further coupled with the GOCART aerosol model (chem_opt = 300) and Shao (2004) dust emission scheme, following guidelines considered by Su and Fung (2018) and Thompson and Eidhammer (2014). This enable WRF-Chem to simulate the indirect effect of dust aerosol on ice nucleation processes over arid regions during strong wind events. An in-cloud wet scavenging scheme will be implemented in the following days.

Table 7. Setting of the simulation.

Case	Chem_opt	Dust_opt	mp_physics	Wetscav	Notes
CNTL	0	Not used	28	-	No chemistry
SHA3	300	4	28	NO	Indirect on

The Thompson microphysics scheme is a bulk two-moment microphysics scheme that considers the mixing ratios and number concentrations for five water species: cloud water, cloud ice, rain, snow, and a hybrid graupel–hail category (Thompson et al., 2004). The updated Thompson–Eidhammer scheme (herein after MP28) is an aerosol-aware version of the Thompson scheme (Thompson and Eidhammer, 2014), which incorporates the activation of aerosols serving as cloud condensation nuclei (CCN) and ice nuclei (IN), and therefore it explicitly predicts the number concentrations of CCN and IN, as well as the number concentrations of cloud droplets and ice crystals (Su and Fung, 2018). This is realized introducing two additional variables in MP28 namely: the number of the hygroscopic "water friendly" aerosol (N_{wfa}) and the number of the non-hygroscopic ice-nucleating aerosol also called ice-friendly aerosol (N_{ifa}).

The outputs of two additional runs, namely CNTL and SHA3 (table 7) will be depicted and analyzed in figures 40-42. The CNTL setup basically consists in running the WRF model

stand alone, without considering any aerosol effects. On the contrary, on the SHA3 setup the feedbacks radiation-microphysics-aerosol are fully considered.

Results will be analyzed considering the variables: QNIFA (number concentration of ice-friendly aerosols) [kg^{-1}], QNICE (ice number concentration) [kg^{-1}] and QICE (ice mixing ratio) [kg kg^{-1}], properly integrated on the air column. These quantities will be compared considering the above mentioned additional setup.

Figure 40b shows a very high number (22 x 10^{10} m^{-2}) of ice-friendly aerosols, above the desert regions of North Africa.

The number of ice crystals that can form in the atmosphere is highly dependent on the number of particles that can act as ice nuclei (IN), and these results show that dust from Sahara effectively served as IN and affected the formation and development of ice clouds during the event examined.

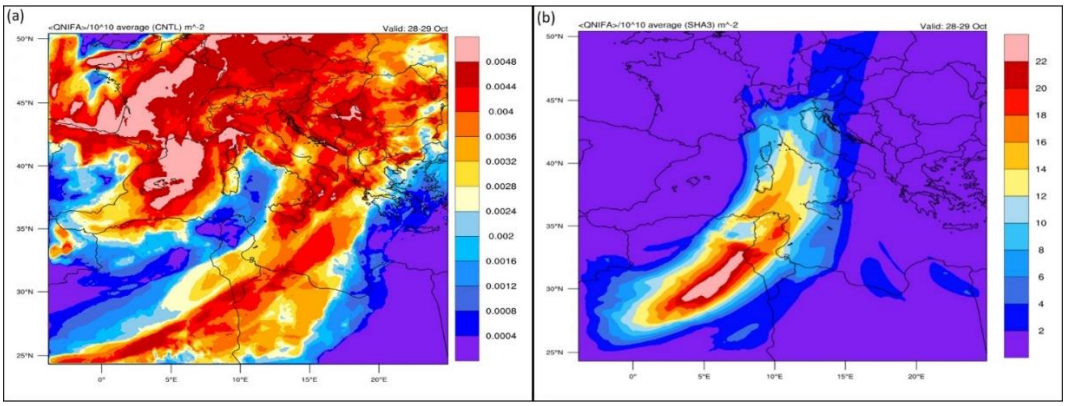

Figure 40. Comparison between the number concentration of ice-friendly aerosols simulated with a default configuration (a) and that produced by implementing the aerosol-aware Thompson–Eidhammer microphysics scheme (b). Average values for the days 28 and 29 October 2018 expressed in m^{-2}.

In fact, by implementing the Thompson scheme, it can also be observed that the model has provided a significantly higher number of ice crystals inside the clouds than expected without considering the aerosol-cloud interaction. In particular, values of about 3 x 10^{8} m^{-2} (Fig. 41d) are reported on the Alps in spite of 0.8 x 10^{8} m^{-2} (Fig. 41c).

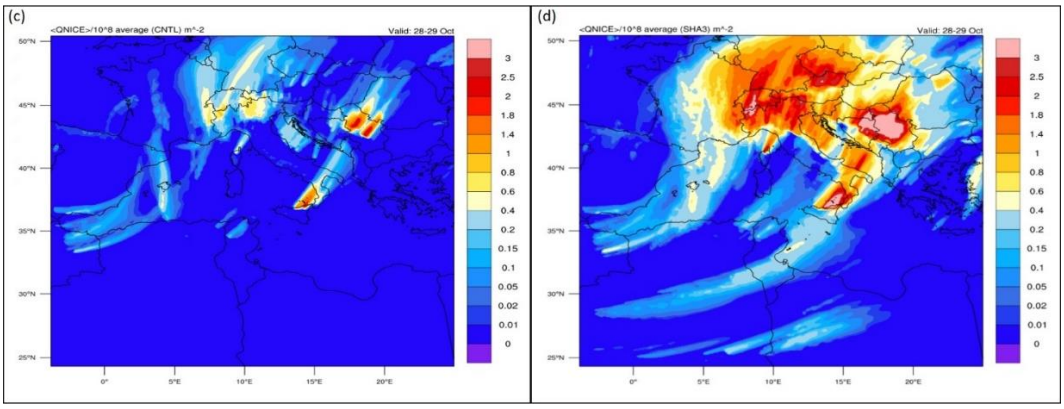

Figure 21. Comparison between the ice number concentration simulated with a default configuration (c) and that produced by implementing the aerosol-aware Thompson–Eidhammer microphysics scheme (d). Average values for the days 28 and 29 October 2018 expressed in m^{-2}.

This also applies to the ice content expressed in g/m^2. In Italy, maximum values of 15 g/m^2 have been predicted (Fig. 42f), which instead are lower (6 g/m^2) in the simulation performed with the default parameterization (Fig. 42e). Clearly the formation of ice crystals is subject to favorable environmental conditions, in fact it is noted that it occurs mainly in correspondence with mountainous areas while it is absent above the sea.

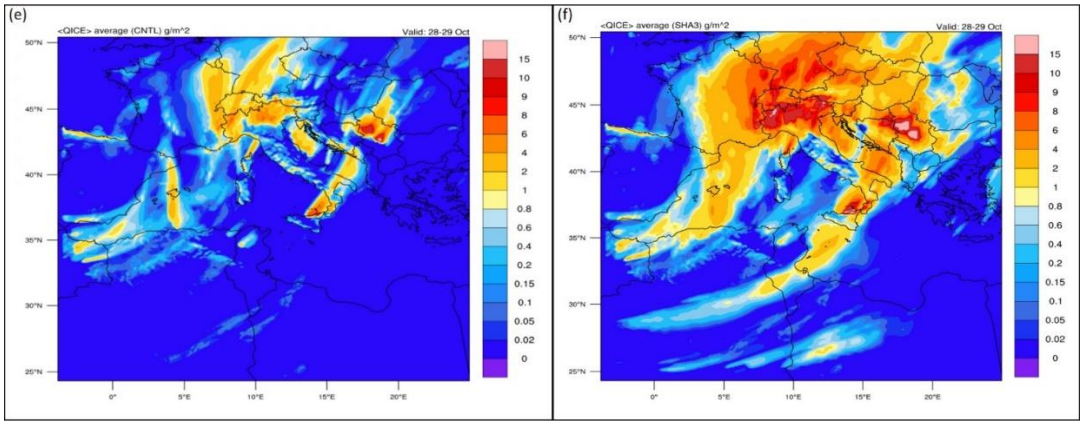

Figure 42. Comparison between the ice mixing ratio simulated with a default configuration (e) and that produced by implementing the aerosol-aware Thompson microphysics scheme (f). Average values for the days 28 and 29 October 2018 expressed in g/m^2.

So it can be seen that with abundant dust particles serving as IN (QNIFA), the simulated ice crystal number concentration (QNICE) and ice water mixing ratio (QICE) increase over the dust source region and downwind areas during the investigated period.

5. CONCLUSIONS

The background of this study is:

- ✓ the need to improve understanding of the interaction between aerosols and atmospheric phenomena, in particular to assess the influence of Saharan mineral dust on the development and evolution of extreme weather events in the Mediterranean basin;
- ✓ to evaluate the forecasting capacity of the WRF-Chem model of both the synoptic framework and the dust transport during a weather event, being a necessary step to respond to the previous point.

This was possible by choosing as subject of study the storm “Vaia” occurred in the period 27-30 October 2018 on the Italian peninsula. For this purpose, two simulations were performed with the WRF-Chem model, changing between them only the dust emission parameterization (GOCART/AFWA and Shao 2004). Subsequently, the results obtained were compared with the reanalysis and satellite data. The comparison of the AOD was made with respect to both simulations, in order to evaluate the validity of the two different dust emission schemes. This was considered superfluous in the case of atmospheric variables because the microphysical scheme used in the two simulations is the same.

Synoptic analysis showed that the episode originated from a cold front coming from the Gulf of Lion, which led to the formation of a depression above the Mediterranean Sea, followed by a cyclogenesis with rainfall and strong south-western and south-eastern wind, which contributed to the transport of water vapour and mineral dust from the Sahara to Italy. In general, the synoptic situation has been well reproduced by the model, although with some inaccuracies:

- underestimation of the wind speed at 10 m; which suggests the need to implement in the model a roughness parameterization that considers the presence of sea spray

in strong wind conditions, as this affects the surface roughness. This aspect was not considered in this study and may be the cause of the model's underestimation;

- overestimation of precipitation (both on the column and on the ground), due to the fact that the model did not correctly consider the secondary effect of mineral dust on atmospheric microphysics, as they constitute cloud condensation nuclei (CCN), which favour the passage from water vapour to liquid/solid phase.

The spatial distribution of the dust outbreak was well predicted by the model, identifying as source regions the desert areas of North Africa, in particular the Sahara, but also the area south of the Atlas Mountains, between Algeria and Tunisia, characterized by a system of ephemeral salt lakes that remains dry in summer, but receives water in winter, playing an important role in the modulation of dust emissions. Some differences between the AOD modeled and that detected by satellites were found in quantitative terms:

- High AOD values (≅ 3) are more easily intercepted by the AFWA scheme, while Shao 2004 tends to underestimate them;
- The relatively lower AOD values (≅ 1) are better reproduced by the Shao scheme (2004), while they are overestimated by the AFWA scheme.

These results confirm the tendency of the AFWA setup to generally produce dust emissions higher than those foreseen by the Shao (2004) scheme.
This overestimation is related to the fact that in the AFWA scheme the impact of the soil is low, since the vertical flow of dust considers only the clay content, so this may under-represent the importance of the soil type. Differently, the Shao (2004) scheme adds corrections such as the vegetation fraction (*greenfract* variable) that influences the threshold friction velocity, in fact, as the vegetation coverage increases, the speed necessary to raise the dust particles increases. Another corrective factor integrated in the Shao (2004) model is that for non-erodible surface elements, which undoubtedly leads to lower estimates of dust emissions.

As a final stage, to quantify the indirect effect (aerosol-clouds), the code was modified by introducing an additional variable, ice-friendly aerosol (GNIFA) from the GOCART model

(Su and Fung, 2018). This allowed to recognize the dust particles as effective ice nuclei (IN) and to evaluate the number of them that play an important role in the ice nucleation process in the atmosphere, directly affecting the dynamics in ice and mixed-phase clouds, such as the formation and development of clouds and precipitation.

The effect of dust on atmospheric cloud ice water content is well reproduced by the aerosol-aware Thompson–Eidhammer microphysics scheme within the WRF-Chem model, but unfortunately, due to the poor understanding of the dust–cloud interactions in microphysics processes, quantifying the microphysical effect of dust remains a difficult problem.

The qualitative analysis of singular episodes, such as the intense intrusion of Saharan dust on the Mediterranean basin can be performed satisfactorily using the WRF-Chem model.

In general, despite the dissimilarities between simulations and observational data from the point of view of intensity, the WRF-Chem model can be considered a valid tool for forecasting and simulating meteorology and climate at regional and local level, as well as the dispersion of pollutants and aerosol (natural and anthropogenic) in the atmosphere.

In conclusion, given the importance of the topic and the gaps that still exist on the part of the WRF-Chem model, it is good to forward the study by applying the necessary adjustments.

Bibliography

Ackermann, I. J., H. Hass, M. Memmesheimer, A. Ebel, F. S. Binkowski, and U. Shankar (1998), Modal aerosol dynamics model for Europe: Development and first applications, Atmos. Environ., 32, 2981–2999.

Ahrens C. Donald, Meteorology Today: An Introduction to Weather, Climate, and the Environment, Eighth Edition, p.198, 203-205.

Alfaro, S. C., Gaudichet, A., Gomes, L., and Maillé, M.: Modeling the size distribution of a soil aerosol produced by sandblasting, J. Geophys. Res.-Atmos., 102, 11239–11249, https://doi.org/10.1029/97JD00403, 1997.

Balkanski, Y. J., Jacob, D. J., Gardner, G. M., Graustein, W. C., and Turekian, K. K.: Transport and residence times of tropospheric aerosols inferred from a global three-dimensional simulation of 210Pb, J. Geophys. Res.-Atmos., 98, 20573–20586, doi:10.1029/93JD02456, 1993.

Baklanov, A., Schlünzen, K., Suppan, P., Baldasano, J., Brunner, D., Aksoyoglu, S., Carmichael, G., Douros, J., Flemming, J., Forkel, R., Galmarini, S., Gauss, M., Grell, G., Hirtl, M., Joffre, S., Jorba, O., Kaas, E., Kaasik, M., Kallos, G., Kong, X., Korsholm, U., Kurganskiy, A., Kushta, J., Lohmann, U., Mahura, A., Manders-Groot, A., Maurizi, A., Moussiopoulos, N., Rao, S. T., Savage, N., Seigneur, C., Sokhi, R. S., Solazzo, E., Solomos, S., Sørensen, B., Tsegas, G., Vignati, E., Vogel, B., and Zhang, Y.: Online coupled regional meteorology chemistry models in Europe: current status and prospects, Atmos. Chem. Phys., 14, 317–398, https://doi.org/10.5194/acp-14-317-2014, 2014.

Baklanov A, Brunner D, Carmichael G, et al. Key Issues for Seamless Integrated Chemistry-Meteorology Modeling. *Bull Am Meteorol Soc*. 2018; 98:2285–2292. doi:10.1175/BAMS-D-15-00166.1.

Barkan, J., P. Alpert, H. Kutiel, and P. Kishcha (2005), Synoptics of dust transportation days from Africa toward Italy and central Europe, J. Geophys. Res., 110, XXXXXX, doi:10.1029/2004JD005222.

Barkan, J. and Alpert, P.: Synoptic patterns associated with dusty and non-dusty seasons in the Sahara, Theor. Appl. Climatol., 94, 153–162, doi:10.1007/s00704-007-0354-9, 2008.

Barnaba, F. and Gobbi, G. P.: Aerosol seasonal variability over the Mediterranean region and relative impact of maritime, continental and Saharan dust particles over the basin from MODIS data in the year 2001, Atmos. Chem. Phys., 4, 2367–2391, doi:10.5194/acp-4-2367-2004, 2004.

Basart, S., Dulac, F., Baldasano, J. M., Nabat, P., Mallet, M., Solmon, F., and Sic, B.: Extensive Comparison Between a Set of European Dust Regional Models and Observations in the Western Mediterranean for the Summer 2012 Pre-ChArMEx/TRAQA Campaign, in: Air Pollution Modeling and its Application XXIV, 79–83, Springer International Publishing, 2016.

Benjamin, S. G., Grell, G. A., Brown, J. M., Smirnova, T. G., and Bleck, R.: Mesoscale weather prediction with the RUC hybrid isentropic-terrain-following coordinate model, Mon. Weather Rev., 132, 473–494, 2004.

Bi, J., Huang, J., Fu, Q., Wang, X., Shi, J., Zhang, W., Huang, Z., and Zhang, B.: Toward characterization of the aerosol optical properties over Loess Plateau of Northwestern China, J. Quant. Spectrosc. Ra., 112, 346–360, 2011.

Biasutti, M., Sobel, A. H., Camargo, S.J., 2009, The Role of the Sahara Low in Summertime Sahel Rainfall Variability and Change in the CMIP3 Models, https://doi.org/10.1175/2009JCLI2969.1.

Bishop, James K. B., Davis, Russ E., Sherman, Jeffrey T., Robotic Observations of Dust Storm Enhancement of Carbon Biomass in the North Pacific, Science 25 Oct 2002: Vol. 298, Issue 5594, pp. 817-821. DOI: 10.1126/science.1074961.

Bohren, C. F. and Huffman, D. R.: Absorption and scattering of light by small particles, Wiley, New York, 1983.

Boucher, O., D. Randall, P. Artaxo, C. Bretherton, G. Feingold, P. Forster, V.-M. Kerminen, Y. Kondo, H. Liao, U. Lohmann, P. Rasch, S.K. Satheesh, S. Sherwood, B. Stevens, and X.Y. Zhang, 2013: Clouds and aerosols. In Climate Change 2013: The Physical Science Basis. Contribution of Working Group I to the Fifth Assessment Report of the Intergovernmental Panel on Climate Change. T.F. Stocker, D. Qin, G.-K. Plattner, M. Tignor, S.K. Allen, J. Doschung, A. Nauels, Y. Xia, V. Bex, and P.M. Midgley, Eds. Cambridge University Press, pp. 571-657, doi:10.1017/CBO9781107415324.016.

Brindley, H., and A. Ignatov, Retrieval of mineral aerosol optical depth and size information from Meteosat Second Generation solar reflectance bands, Rem. Sens. Env., 102, 344–363, 2006.

Bullard, J. E., McTainsh, G. H., and Pudmenzky, C.: Factors affecting the nature and rate of dust production from natural dune sands, Sedimentology, 54, 169–182, https://doi.org/10.1111/j.1365-3091.2006.00827.x, 2007.

Buseck, P. R. and M. Posfai., 1999, Airborne minerals and related aerosol particles: Effects on climate and the environment, Proceedings of the National Academy of Sciences of the United States of America, 96(7), 3372-3379.

Cavaleri, L., Bajo, M., Barbariol, F., Bastianini, M., Benetazzo, A., Bertotti, L., Chiggiato, J., Davolio, S., Ferrarin, C., Magnusson, L., Papa, A., Pezzutto, P., Pomaro, A., Umgiesser, G., The October 29, 2018 storm in Northern Italy – An exceptional event and its Modeling, Progress in Oceanography 178 (2019) 102178, https://doi.org/10.1016/j.pocean.2019.102178.

Cavazos Guerra, C.d.C.; (2011) Modelling the atmospheric controls and climate impact of mineral dust in the Sahara Desert. Doctoral thesis, UCL (University College London).

Cavazos, C., Todd, M. C., & Schepanski, K. (2009). Numerical model simulation of the dust event of 6-11 March 2006 using Regional Climate Model version 3 (RegCM3). Journal of Geophysical Research, 114, D12109. doi: 10.1029/2008JD011078.

Chin, M., Rood, R. B., Lin, S.-J., Muller, J. F., and Thomspon, A. M.: Atmospheric sulfur cycle in the global model GOCART: Model description and global properties, J. Geophys. Res.-Atmos., 105, 24671–24687, 2000.

Chirici G, Giannetti F, Travaglini D, Nocentini S, Francini S, D'Amico G, Calvo E, Fasolini D, Broll M, Maistrelli F, Tonner J, Pietrogiovanna M, Oberlechner K, Andriolo A, Comino R, Faidiga A, Pasutto I, Carraro G, Zen S, Contarin F, Alfonsi L, Wolynski A, Zanin M, Gagliano C, Tonolli S, Zoanetti R, Tonetti R, Cavalli R, Lingua E, Pirotti F, Grigolato S, Bellingeri D, Zini E, Gianelle D, Dalponte M, Pompei E, Stefani A, Motta R, Morresi D, Garbarino M, Alberti G, Valdevit F, Tomelleri E, Torresani M, Tonon G, Marchi M, Corona P, Marchetti M (2019). Stima dei danni della tempesta "Vaia" alle foreste in Italia. Forest@ 16: 3-9. – doi: 10.3832/efor3070-016 [online 2019-02-15].

Claquin, T., Schulz, M., Balkanski, Y., and Boucher, O.: Uncertainties in assessing radiative forcing by mineral dust, Tellus B, 50, 491–505, 1998.

Claquin, T., Schulz, M., Balkanski Y. J., Modeling the mineralogy of atmospheric dust sources, Journal of Geophysical Research, vol. 104, no. d18, pages 22,243-22,256, September 27, 1999.

De Longueville, F., Hountondji, Y.C., Ozer, P., Marticorena, B., Chatenet, B., Henry, S., 2013, Saharan Dust Impacts on Air Quality: What Are the Potential Health Risks in West Africa?, Human and Ecological Risk Assessment: An International Journal, 19:6, 1595-1617, DOI: 10.1080/10807039.2012.716684.

DeMott, P. J., K. Sassen, M. R. Poellot, D. Baumgardner, D. C. Rogers, S. D. Brooks, A. J. Prenni, and S. M. Kreidenweis (2009), Correction to ''African dust aerosols as atmospheric ice nuclei,''Geophys. Res. Lett., 36, L07808,doi:10.1029/2009GL037639.

Dubovik, O., A. Smirnov, B. N. Holben, M. D. King, Y. J. Kaufman, T. F. Eck, and I. Slutsker, 2000: Accuracy assessments of aerosol optical properties retrieved from AERONET sun and sky-radiance measurements. J. Geophys. Res., 105, 9791–9806.

Engelstaedter, S., Tegen, I., andWashington, R.: North African dust emissions and transport, Earth-Sci. Rev., 79, 73–100, 2006.

Evan, A.T., Flamant, C., Fiedler, S., Doherty, O., 2014. An analysis of aeolian dust in climate models. Geophys. Res. Lett. 41 (16), 5996–6001.

Falkovich, A. H., Ganor, E., Levin, Z., Formenti, P., Rudich, R., Chemical and mineralogical analysis of individual mineral dust particles, Journal of Geophysical Research, vol. 106, no. d16, pages 18,029-18,036, august 27, 2001, https://doi.org/10.1029/2000JD900430.

Falkowski, Paul G., Barber, Richard T., Smetacek, V., Biogeochemical Controls and Feedbacks on Ocean Primary Production, Science 10 Jul 1998: Vol. 281, Issue 5374, pp. 200-206 DOI: 10.1126/science.281.5374.200.

Fast, J. D., W. I. Gustafson Jr., R. C. Easter, R. A. Zaveri, J. C. Barnard, E. G. Chapman, G. A. Grell, and S. E. Peckham (2006), Evolution of ozone, particulates, and aerosol direct radiative forcing in the vicinity of Houston using a fully coupled meteorology-chemistry-aerosol model, J. Geophys. Res., 111, D21305, doi:10.1029/2005JD006721.

Fast, J., Barnard, J., Berg, L., Chapman, E., Easter, R., Ghan, S., Gustafson, B., Po-Lun Ma, Singh, B., Rasch, P., Yang, Q., Zaveri, R., Zhao, C., Morrison, H., McKeen, S., Kumar, R., Aerosol-Radiation-Microphysics Interactions, WRF-Chem Tutorial, August 3, 2015, Boulder CO.

Fécan, F., Marticorena, B., and Bergametti, G.: Parametrization of the increase of the aeolian erosion threshold wind friction velocity due to soil moisture for arid and semi-arid areas, Ann. Geophys., 17, 149–157, https://doi.org/10.1007/s00585-999-0149-7, 1999.

Forster, P., V. Ramaswamy, P. Artaxo, T. Berntsen, R. Betts, D.W. Fahey, J. Haywood, J. Lean, D.C. Lowe, G. Myhre, J. Nganga, R. Prinn, G. Raga, M. Schulz and R. Van Dorland, 2007: Changes in Atmospheric Constituents and in Radiative Forcing. In: Climate Change 2007: The Physical Science Basis. Contribution of Working Group I to the Fourth Assessment Report of the Intergovernmental Panel on Climate Change [Solomon, S., D. Qin, M. Manning, Z. Chen, M. Marquis, K.B. Averyt, M.Tignor and H.L. Miller (eds.)]. Cambridge University Press, Cambridge, United Kingdom and New York, NY, USA.

Fountoukis, C., Ackermann, L., Ayoub, M. A., Gladich, I., Hoehn, R. D., and Skillern, A.: Impact of atmospheric dust emission schemes on dust production and concentration over the Arabian Peninsula, Model. Earth Syst. Environ., 2, 1–6, 2016.

Freitas, S. R., Longo, K. M., Alonso, M. F., Pirre, M., Marecal, V., Grell, G., Stockler, R., Mello, R. F., and Sánchez Gácita, M.: PREP-CHEM-SRC – 1.0: a preprocessor of trace gas and aerosol emission fields for regional and global atmospheric chemistry models, Geosci. Model Dev., 4, 419–433, https://doi.org/10.5194/gmd-4-419-2011, 2011.

Gamo, M., Thickness of the dry convection and large-scale subsidence above deserts, Boundary-Layer Meteorology 79: 261-278, 1996.

Ghan, S. J. and Schwartz, S. E., Aerosol Properties and Processes: A Path from Field and Laboratory Measurements to Global Climate Models, B. Am. Meteorol. Soc., 88, p. 1059, 2007.

Ginoux, P., Chin, M., Tegen, I., Prospero, J. M., Holben, B., Dubovik, O., and Lin, S. J.: Sources and distributions of dust aerosols simulated with the GOCART model. J. Geophys. Res.-Atmos., 106, 20255–20273, https://doi.org/10.1029/2000JD000053, 2001.

Ginoux, P., J. Prospero, O. Torres, and M. Chin. 2004. Long-Term Simulation of Global Dust Distribution with the GOCART Model: Correlation with North Atlantic Oscillation. Environmental Modelling and Software 19 (2): 113–128.

Ginoux, P., J. M. Prospero, T. E. Gill, N. C. Hsu, and M. Zhao (2012), Global-scale attribution of anthropogenic and natural dust sources and their emission rates based on MODIS Deep Blue aerosol products, Rev. Geophys., 50, RG3005, doi:10.1029/2012RG000388.

Gkikas, A., Obiso, V., Pérez García-Pando, C., Jorba, O., Hatzianastassiou, N., Vendrell, L., Basart, S., Solomos, S., Gassó, S., and Baldasano, J. M.: Direct radiative effects during intense Mediterranean desert dust outbreaks, Atmos. Chem. Phys., 18, 8757–8787, https://doi.org/10.5194/acp-18-8757-2018, 2018.

Goudie, A. S.: Dust storms: Recent developments, J. Environ. Manage., 90, 89–94, 2009.

Goudie A.S., Middleton N.J., 2001, Saharan dust storms: nature and consequences, Earth-Science Reviews 56 (1–4), 179–204.

Grell, G. A., Knoche, R., Peckham, S. E., and McKeen, S.: Online versus offline air quality modeling on cloud-resolving scales, Geophys. Res. Lett., 31, L16117, doi:10.1029/2004GL020175, 2004.

Grell, G. A., S. E. Peckham, R. Schmitz, S. A. McKeen, G. Frost, W. C. Skamarock, and B. Eder (2005), Fully coupled ‘‘online’’ chemistry within the WRF model, Atmos. Environ., 39, 6957– 6975.

Grell G. A., and Baklanov A., 2011: Integrated modelling for forecasting weather and air quality: A call for fully coupled approaches. Atmos. Environ, 45, 6845–6851, doi:10.1016/j.atmosenv.2011.01.017.

Grell, G.A., Freitas, S.R., 2014. A scale and aerosol aware stochastic convective parameterization for weather and air quality modeling. Atmos. Chem. Phys. 14 (10), 5233–5250.

Haapanala, P., Räisänen, P., Kahnert, M., and Nousiainen, T.: Sensitivity of the shortwave radiative effect of dust on particle shape: Comparison of spheres and spheroids, J. Geophys. Res.-Atmos., 117, D08201, doi:10.1029/2011JD017216, 2012.

Hsu, N. C., M.-J. Jeong, C. Bettenhausen, A. M. Sayer, R. Hansell, C. S. Seftor, J. Huang, and S.-C. Tsay (2013), Enhanced Deep Blue aerosol retrieval algorithm: The second generation, J. Geophys. Res. Atmos., 118, 9296–9315,doi:10.1002/jgrd.50712.

Hsu, N. C., Jeong, M.-J., Bettenhausen, C., Sayer, A. M., Hansell, R., Seftor, C. S., Huang, J., Tsay, S.-C., Enhanced Deep Blue aerosol retrieval algorithm: The second generation, JOURNAL OF GEOPHYSICAL RESEARCH: ATMOSPHERES, VOL. 118, 9296–9315, doi:10.1002/jgrd.50712, 2013.

Huneeus, N., Schulz, M., Balkanski, Y., Griesfeller, J., Prospero, J., Kinne, S., Bauer, S., Boucher, O., Chin, M., Dentener, F., Diehl, T., Easter, R., Fillmore, D., Ghan, S., Ginoux, P., Grini, A., Horowitz, L., Koch, D., Krol, M.C., Landing, W., Liu, X., Mahowald, N., Miller, R., Morcrette, J.-J., Myhre, G., Penner, J., Perlwitz, J., Stier, P., Takemura, T., Zender, C.S., 2011. Global dust model intercomparison in AeroCom phase I. Atmos. Chem. Phys. 11, 7781–7816.

Iacono, M.J., Delamere, J.S., Mlawer, E.J., Shephard, M.W., Clough, S.A., Collins, W.D., 2008. Radiative forcing by long–lived greenhouse gases: calculations with the AER radiative transfer models. J. Geophys. Res. 113, D13103.

IPCC: Climate Change 2007: The Physical Science Basis. Contribution of Working Group I to the Fourth Assessment Report of the Intergovernmental Panel on Climate Change, edited by: Solomon, S., Qin, D., Manning, M., Chen, Z., Marquis, M., Averyt, K. B., Tignor, M., and Miller, H. L., Cambridge University Press, Cambridge, United Kingdom and New York, NY, USA, 2007.

IPCC: Climate Change 2013: The Physical Science Basis. Contribution of Working Group I to the Fifth Assessment Report of the Intergovernmental Panel on Climate Change [Stocker, T.F., D. Qin, G.-K. Plattner, M. Tignor, S. K. Allen, J. Boschung, A. Nauels, Y. Xia, V. Bex and P.M. Midgley (eds.)]. Cambridge University Press, Cambridge, United Kingdom and New York, NY, USA.

Israelevich, P., Ganor, E., Alpert, P., Kishcha, P., and Stupp, A.: Predominant transport paths of Saharan dust over the Mediterranean Sea to Europe, J. Geophys. Res., 117, D02205, doi:10.1029/2011JD016482, 2012.

Jickells, T. D., An, Z. S., Andersen, K. K., Baker, A. R., Bergametti, G., Brooks, N., Cao, J. J., Boyd, P. W., Duce, R. A., Hunter, K. A., Kawahata, H., Kubilay, N., laRoche, J., Liss, P. S., Mahowald, N., Prospero, J. M., Ridgwell, A. J., Tegen, I., Torres, R., Global Iron Connections Between Desert Dust, Ocean Biogeochemistry, and Climate, Science 01 Apr 2005: Vol. 308, Issue 5718, pp. 67-71 DOI: 10.1126/science.1105959.

Jones, S. L., et al. (2010). Adapting WRF-CHEM GOCART for Fine-Scale Dust Forecasting. AGU Fall Meeting Abstracts. Vol. 1.

Jones, S. L. 2012. Performance Assessment of WRF-Chem GOCART. TR-SP-64. Offutt Air Force Base, NE: U.S. Air Force Weather Agency.

Kahn, R., A. Petzold, M. Wendisch, E. Bierwirth, T. Dinter, M. Esselborn, M. Fiebig, B. Heese, P. Knippertz, D. Müller, A. Schladitz, and W. von Hoyningen-Huene, Desert dust aerosol air mass mapping in the western Sahara, using particle properties derived from space-based multi-angle imaging, Tellus, 61B, 239–251, 2009.

Kalashnikova, O. V., and R. A. Kahn, Mineral dust plume evolution over the Atlantic from MISR and MODIS aerosol retrievals, J. Geophys. Res., 113, D24204, doi:10.1029/2008JD010083, 2008.

Karydis, V. A., Kumar, P., Barahona, D., Sokolik, I. N., and Nenes, A.: On the effect of dust particles on global cloud condensation nuclei and cloud droplet number, J. Geophys. Res.-Atmos., 116, D23204, doi:10.1029/2011JD016283, 2011.

Kaufman, Y. J., A. E. Wald, L. A. Remer, Bo-Cai Gao, Rong-Rong Li and L. Flynn, "The MODIS 2.1-/spl mu/m channel-correlation with visible reflectance for use in remote sensing of aerosol," in *IEEE Transactions on Geoscience and Remote Sensing*, vol. 35, no. 5, pp. 1286-1298, Sept. 1997, doi: 10.1109/36.628795.

Kawamura, R.: Study on sand movement by wind, Inst. Sci. Technol., Rep. 5, 95–112, Tokyo, 1951.

Klose, M. and Shao, Y.: Stochastic parameterization of dust emission and application to convective atmospheric conditions, Atmos. Chem. Phys., 12, 7309–7320, https://doi.org/10.5194/acp-12-7309-2012, 2012.

Knippertz, P. and Todd, M. C., Mineral dust aerosol over the Sahara: Processes of emission and transport, and implications for modeling, Reviews of Geophysics, DOI: 10.1029/2011RG000362.

Koch, D., T. C. Bond, D. Streets, N. Unger, and G. R. van der Werf (2007), Global impacts of aerosols from particular source regions and sectors, J. Geophys. Res., 112, D02205, doi:10.1029/2005JD007024.

Kok, J. F.: A scaling theory for the size distribution of emitted dust aerosols suggests climate models underestimate the size of the global dust cycle, Proc. Natl. Acad. Sci. USA, 108, 1016–1021, https://doi.org/10.1073/pnas.1014798108, 2011.

Kok, J. F., Parteli, E. J., Michaels, T. I., and Karam, D. B.: The physics of wind-blown sand and dust, Rep. Prog. Phys., 75, 106901, https://doi.org/10.1088/0034-4885/75/10/106901, 2012.

Kok, J. F., N. M. Mahowald, G. Fratini, J. A. Gillies, M. Ishizuka, J. F. Leys, M. Mikami, M.-S. Park, S.-U. Park, R. S. Van Pelt, and T. M. Zobeck. 2014. An Improved Dust Emission Model–Part 1: Model Description and Comparison Against Measurements. Atmospheric Chemistry and Physics 14 (23): 13023–13041.

Krueger, B.J., Grassian, V.H., Cowin, J.P., Laskin, A., (2004), Heterogeneous chemistry of individual mineral dust particles from different dust source regions: the importance of particle mineralogy, https://doi.org/10.1016/j.atmosenv.2004.07.010.

Kumar, R., M. C. Barth, G. G. Pfister, M. Naja, and G. P. Brasseur. 2014. WRF-Chem Simulations of a Typical Pre-Monsoon Dust Storm in Northern India: Influences on Aerosol Optical Properties and Radiation Budget. Atmospheric Chemistry and Physics 14 (5): 2431–2446.

Kummerow, C., Barnes, W., Kozu, T., Shiue, J. and Simpson, J. 1998. The Tropical Rainfall Measuring Mission (TRMM) sensor package. Journal of Atmospheric and Oceanic Technology, 15: 809–817.

Laurent, B. & Marticorena, Beatrice & Bergametti, Gilles & Léon, Jean-François & Mahowald, Natalie. (2008). Modeling mineral dust emission from the Sahara desert using new surface properties and soil database. Journal of Geophysical Research. 113. 10.1029/2007JD009484.

Laurent, B. & Marticorena, Beatrice & Bergametti, Gilles & Mei, F. (2006). Modeling Mineral Dust Emissions From Chinese and Mongolian Deserts. Global and Planetary Change. 52. 121-141. 10.1016/j.gloplacha.2006.02.012.

LeGrand, S., Polashenski, C., Letcher, T., Creighton, G., Peckham, S., Cetola, J. (2019). The AFWA dust emission scheme for the GOCART aerosol model in WRF-Chem v3.8.1. Geoscientific Model Development. 12. 131-166. 10.5194/gmd-12-131-2019.

Lelieveld, J., Klingmüller, K., Pozzer, A., Pöschl, U., Fnais, M., Daiber, A., Münzel T., Cardiovascular disease burden from ambient air pollution in Europe reassessed using novel hazard ratio functions, European Heart Journal, Volume 40, Issue 20, 21 May 2019, Pages 1590–1596, https://doi.org/10.1093/eurheartj/ehz135.

Letcher, T. W. and LeGrand, S. L.: A comparison of simulated dust produced by three dust-emission schemes in WRF-Chem, ERDC/CRREL TR-18-13, U.S. Army Engineer Research and Development Center, Hanover, New Hampshire, USA, 2018.

Levy, R. C., L. A. Remer, S. Mattoo, E. F. Vermote, and Y. J. Kaufman (2007), Second-generation operational algorithm: Retrieval of aerosol properties over land from inversion of Moderate Resolution Imaging Spectroradiometer spectral reflectance, J. Geophys. Res., 112, D13211, doi:10.1029/2006JD007811.

Levy, Robert & Mattoo, S. & Munchak, Leigh & Remer, Lorraine & Sayer, A.M. & Patadia, Falguni & Hsu, N.C.. (2013). The Collection 6 MODIS aerosol products over land and ocean. Atmospheric Measurement Techniques. 6. 10.5194/amt-6-2989-2013.

Liu, Xiaohong & Easter, Richard & Ghan, Steven & Zaveri, Rahul & Rasch, P. & Shi, Xiangjun & Lamarque, Jean-François & Gettelman, Andrew & Morrison, Hugh & Vitt, Francis & Conley, Andrew & Neale, Richard. (2012). Toward a Minimal Representation of Aerosols in Climate Models: Description and Evaluation in the Community Atmosphere Model CAM5. Geoscientific Model Development.

Mahowald, N. M., and L. M. Kiehl, Mineral aerosol and cloud interactions, Geophys. Res. Lett., 30(9), 1475, doi:10.1029/2002GL016762, 2003.

Mahowald, N. M., G. D. R. Rivera, and C. Luo (2004), Comment on ‘‘Relative importance of climate and land use in determining present and future global soil dust emission’’ by I. Tegen et al., Geophys. Res. Lett., 31, L24105, doi:10.1029/2004GL021272.

Mahowald, N. M., J. A. Ballantine, J. Feddema, and N. Ramankutty, Global trends in visibility: implications for dust sources, Atmos. Chem. Phys., 7, 3309–3339, 2007.

Mahowald, N. M., et al., Observed 20th century desert dust variability: impact on climate and biogeochemistry, *Atmos. Chem. Phys., 10,* 10875–10893, 2010.

Mallone, S., Stafoggia, M., Faustini, A., Gobbi, G. P., Marconi, A., and Forastiere, F.: Saharan dust and associations between particulate matter and daily mortality in Rome, Italy, Environ. Health Persp., 119, 1409–1414, 2011.

Manara, V.; Brunetti, M.; Gilardoni, S.; Landi, T.C.; Maugeri, M. 1951–2017 changes in the frequency of days with visibility higher than 10 km and 20 km in Italy. Atmos. Environ. 2019,214, 116861.

Maring, H., D. L. Savoie, M. A. Izaguirre, L. Custals, and J. S. Reid, Mineral dust aerosol size distribution change during atmospheric transport, J. Geophys. Res., 108(D19), 8592, doi:10.1029/2002JD002536, 2003.

Marticorena, B., and G. Bergametti. 1995. Modeling the Atmospheric Dust Cycle: 1. Design of a Soil-Derived Dust Emission Scheme. Journal of Geophysical Research: Atmospheres 100 (D8): 16415–16430.

McTainsh, G. H., R. Burgess, and J. R. Pitblado (1989), Aridity, drought and dust storms in Australia (1960–1984), J. Arid Environ., 16, 11–22.

Middleton, N. J. 2017. Desert Dust Hazards: A Global Review. Aeolian Research 24:53–63.

Mlawer, E. J., Taubman, S. J., Brown, P. D., Iacono, M. J., and Clough, S. A.: Radiative transfer for inhomogeneous atmospheres: RRTM, a validated correlated-k model for the longwave, J. Geophys. Res.-Atmos., 102, 16663–16682, 1997.

Molesworth, A. M., L. E. Cuevas, A. P. Morse, J. R. Herman, and M. C. Thomson, Correspondence: Dust clouds and spread of infection, *The Lancet, 359,* 81–82, 2002.

Molesworth, A. M., Cuevas, L. E., Connor, S. J., Morse, A. P., and Thomson, M. C.: Environmental risk and meningitis epidemics in Africa, Emerg. Infect Dis., 9, 1287–1293, 2003.

Montero G., V. Zarraluqui, E. S. Caetano and F. García, 2011. Hydrometeor vertical characterization of precipitating clouds over the Mexico Basin. Int. J. Rem. Sens. 32, 6367-6378, http://dx.doi.org/10.1080/01431161.2010.510489.

Morrison, H., Thompson, G., Tatarskii, V., 2009. Impact of cloud microphysics on the development of trailing stratiform precipitation in a simulated squall line: comparison of one-and two-moment schemes. Mon. Weather Rev. 137 (3), 991–1007.

Moulin, C., Lambert, C. E., Dayan, U., Masson, V., Ramonet, M., Bousquet, P., Legrand, M., Balkanski, Y. J., Guelle, W., Marticorena, B., Bergametti, G., and Dulac, F.: Satellite climatology of African dust transport in the Mediterranean atmosphere, J. Geophys. Res.-Atmos., 103, 13137–13144, 1998.

Nakanishi, M. and Niino, H.: Development of an improved turbulence closure model for the atmospheric boundary layer, J. Meteorol. Soc. Jpn., 87.5, 895–912, 2009.

Nickovic, S., G. Kallos, A. Papadopoulos, and O. Kakaliagou. 2001. A Model for Prediction of Desert Dust Cycle in the Atmosphere. Journal of Geophysical Research: Atmospheres 106 (D16): 18113–18129.

Notaro, M., F. Alkolibi, E. Fadda, and F. Bakhrjy (2013), Trajectory analysis of Saudi Arabian dust storms, J. Geophys. Res. Atmos., 118, 6028–6043, doi:10.1002/jgrd.50346.

Okin, G. S., N. Mahowald, O. A. Chadwick, and P. Artaxo (2004), Impact of desert dust on the biogeochemistry of phosphorus in terrestrial ecosystem, Global Biogeochem. Cycles, 18, GB2005, doi:10.1029/2003GB002145.

Panegrossi, G., Marra, A. C., Barnaba, F., Rizza, U., Gallicchio, D., Hourngir, D., Sanò, P., Casella, D., D'Adderio, L. P., Dietrich, S., Di Liberto, L., Morichetti, M., Passerini, G., Multi-sensor analysis of the exceptional 29 October 2018 event over Italy, 2° Congresso Nazionale AISAM 2019.

Paytan, A., Katherine R. M. Mackey, Chen, Y., Ivan D. Lima, Scott C. Doney, Mahowald, N., Labiosa, R., and Anton F. Post, Toxicity of atmospheric aerosols on marine phytoplankton, PNAS March 24, 2009, 106 (12) 4601-4605; https://doi.org/10.1073/pnas.0811486106.

Pey, J., Querol, X., Alastuey, A., Forastiere, F., and Stafoggia, M.: African dust outbreaks over the Mediterranean Basin during 2001–2011: PM10 concentrations, phenomenology and trends, and its relation with synoptic and mesoscale meteorology, Atmos. Chem. Phys., 13, 1395–1410, doi:10.5194/acp-13-1395-2013, 2013.

Peyrillé, P., and Lafore, J. P., 2007, An Idealized Two-Dimensional Framework to Study the West African Monsoon. Part II: Large-Scale Advection and the Diurnal Cycle, https://doi.org/10.1175/JAS4052.1.

Pignone, F., Rebora, N., Silvestro, F., Castelli, F., 2010. GRISO – Rain, CIMA Research Foundation, Savona, Italy. Operational Agreement 778/2009 DPC-CIMA, Year-1 Activity Report 272/2010.

Pitman, A.J., 2003. The evolution of, and revolution in, land surface schemes designed for climate models. Int. J. Climatol. 23 (5), 479–510.

Prospero, J. M., P. Ginoux, O. Torres, S. E. Nicholson, and T. E. Gill (2002), Environmental characterization of global sources of atmospheric soil dust identified with the NIMBUS 7 Total Ozone Mapping Spectrometer (TOMS) absorbing aerosol product, Rev. Geophys., 40(1), 1002, doi:10.1029/2000RG000095.

Prospero, J. M. and Mayol-Bracero, O. L.: Understanding the transport and impact of African dust on the Caribbean basin, B. Am. Meteorol. Soc., 94, 1329–1337, 2013.

Querol, X., Pey, J., Pandolfi, M., Alastuey, A., Cusack, M., Pérez, N., Moreno, T., Viana, M., Mihalopoulos, N., Kallos, G., and Kleanthous, S.: African dust contributions to mean ambient PM_{10} mass-levels across the Mediterranean Basin, Atmos. Environ., 43, 4266–4277, 2009.

Ralph, F. M., Coleman, T., Neiman, P. J., Zamora, R., & Dettinger, M. D. (2013). Observed impacts of duration and seasonality of atmospheric-river landfalls on soil moisture and runoff in coastal northern California. Journal of Hydrometeorology, 14(2), 443– 459; https://doi.org/10.1175/jhm-d-12-076.1.

Ramanathan, V., Crutzen, P. J., Kiehl, J. T., Rosenfeld D., Aerosols, Climate, and the Hydrological Cycle, Science 294, 2119 (2001), DOI: 10.1126/science.1064034.

Raupach, M.R. Drag and drag partition on rough surfaces. Boundary-Layer Meteorol 60, 375–395 (1992); https://doi.org/10.1007/BF00155203.

Remer, L. A., Kaufman, Y. J., Tanré, D., Mattoo, S., Chu, D. A., Martins, J. V., Li, R.-R., Ichoku, C., Levy, R. C., Kleidman, R. G., Eck, T. F., Vermote, E., and Holben, B. N.: The MODIS Aerosol Algorithm, Products, and Validation, J. Atmos. Sci., 62, 947–973, https://doi.org/10.1175/JAS3385.1, 2005.

Reynolds, C. A., Jackson, T. J., and Rawls, W. J.: Estimating soil water-holding capacities by linking the Food and Agriculture Organization soil map of the world with global pedon databases and continuous pedotransfer functions, Water Resour. Res., 36, 3653–3662, https://doi.org/10.1029/2000WR900130, 2000.

Richter, D., and T. Gill. 2018. Challenges and Opportunities in Atmospheric Dust Emission, Chemistry, and Transport. Bulletin of the American Meteorological Society, in press. doi:10.1175/BAMS-D-18-0007.1.

Rizza, U., Anabor, V., Mangia, C., Miglietta, M. M., Degrazia, G. A., and Passerini, G.: WRF-Chem Simulation of a saharan dust outbreak over the mediterranean regions, Vol. 38, Special Edition, 330–336, Ciência e Natura, doi:10.5902/2179460X20249, 2016.

Rizza, U., F. Barnaba, M. M. Miglietta, C. Mangia, L. Di Liberto, D. Dionisi, F. Costabile, F. Grasso, and G. Paolo Gobbi. 2017. WRF-Chem Model Simulations of a Dust Outbreak over the Central Mediterranean and Comparison with Multi-Sensor Desert Dust Observations. Atmospheric Chemistry and Physics 17 (1): 93–115.

Rizza, U., Canepa, E., Ricchi, A., Bonaldo, D., Carniel, S., Morichetti, M., Passerini, G., Santiloni, L., Puhales, F. S., and Miglietta, M.: Influence of Wave State and Sea Spray on the Roughness Length: Feedback on Medicanes, Atmosphere, 9, 301, https://doi.org/10.3390/atmos9080301, 2018.

Rosenfeld, D., Rudich, Y., and Lahav, R.: Desert dust suppressing precipitation: A possible desertification feedback loop, P. Natl. Acad. Sci. USA, 98, 5975–5980, 2001.

Salomonson, V. V., Barnes, W. L., Maymon, P. W., Montgomery, H. E., and Ostrow, H.: MODIS: Advanced facility instrument for studies of the Earth as a system, IEEE T. Geosci. Remote, 27, 145–153, 1989.

Salvador, P., Alonso-Pérez, S., Pey, J., Artíñano, B., de Bustos, J. J., Alastuey, A., and Querol, X.: African dust outbreaks over the western Mediterranean Basin: 11-year characterization of atmospheric circulation patterns and dust source areas, Atmos. Chem. Phys., 14, 6759–6775, doi:10.5194/acp-14-6759-2014, 2014.

Sayer, A. M., N. C. Hsu, C. Bettenhausen, and M.-J. Jeong (2013), Validation and uncertainty estimates for MODIS Collection 6 “Deep Blue” aerosol data, J. Geophys. Res. Atmos., 118, 7864–7872, doi:10.1002/jgrd.50600.

Scanza, R. A., Mahowald, N., Ghan, S., Zender, C. S., Kok, J. F., Liu, X., Zhang, Y., and Albani, S.: Modeling dust as component minerals in the Community Atmosphere Model: development of framework and impact on radiative forcing, Atmos. Chem. Phys., 15, 537-561, https://doi.org/10.5194/acp-15-537-2015, 2015.

Schepanski, K., Mallet, M., Heinold, B., Ulrich, M., 2016. North African dust transport toward the western Mediterranean basin: atmospheric controls on dust source activation and transport pathways during June–July 2013. Atmos. Chem. Phys. 16 (22), 14147–14168.

Schepanski, Kerstin. (2018). Transport of Mineral Dust and Its Impact on Climate. Geosciences. 8. 151. 10.3390/geosciences8050151.

Schulz, M., Chin, M., and Kinne, S.: The Aerosol Model Comparison Project, AeroCom, Phase II: Clearing up diversity, IGAC Newsl., 41, 2–11, 2009.

Seneviratne, S., Donat, M., Pitman, A. et al. Allowable CO2 emissions based on regional and impact-related climate targets. Nature 529, 477–483 (2016). https://doi.org/10.1038/nature16542.

Shao, Y. and Lu, H.: A simple expression for wind erosion threshold friction velocity, J. Geophys. Res.-Atmos., 105, 22437–22443, https://doi.org/10.1029/2000JD900304, 2000.

Shao, Y.: A model for mineral dust emission, J. Geophys. Res.-Atmos., 106, 20239–20254, https://doi.org/10.1029/2001JD900171, 2001.

Shao, Y.: Simplification of a dust emission scheme and comparison with data, J. Geophys. Res.-Atmos., 109, D10202, https://doi.org/10.1029/2003JD004372, 2004.

Shao, Y., J. F. Leys, G. H. McTainsh, and K. Tews. 2007. Numerical Simulation of the October 2002 Dust Event in Australia. Journal of Geophysical Research: Atmospheres 112 (D8): D08207.

Shao, Y. (2008), Physics and Modelling of Wind Erosion, 2 ed., 452 pp., Springer-Verlag, Berlin.

Shao, Y., Ishizuka, M., Mikami, M., and Leys, J. F.: Parameterization of size-resolved dust emission and validation with measurements, J. Geophys. Res.-Atmos., 116, D08203, https://doi.org/10.1029/2010JD014527, 2011.

Skamarock, W. C.: Klemp, J. B., Dudhia, J., Gill, D. O., Barker, D. M., Duda, M. G., Huang, X.-Y., Wang, W., and Powers, J. G.: A description of the Advanced Research WRF version 3, National Center for Atmospheric Research Tech. Note, NCAR/TN-475+STR, 113 pp., 2008.

Sokolik, I. N., D. M. Winker, G. Bergametti, D.A. Gillette, G. Carmichael,Y. J. Kaufman, L. Gomes, L. Schuetz and J. E. Penner, (2001), Introduction to special section: Outstanding problems in quantifying the radiative impacts of mineral dust, Journal of Geophysical Research-Atmospheres, 106(D16), 18015-18027.

Stafoggia, M., Zauli-Sajani, S., Pey, J., Samoli, E., Alessandrini, E., Basagaña, X., Cernigliaro, A., Chiusolo, M., Demaria, M., Díaz, J., Faustini, A., Katsouyanni, K., Kelessis, A. G., Linares, C., Marchesi, S., Medina, S., Pandolfi, P., Pérez, N., Querol, X., Randi, G., Ranzi, A., Tobias, A., and Forastiere, F.: MEDPARTICLES Study Group, Desert dust outbreaks in Southern Europe: contribution to daily PM10 concentrations and short term associations with mortality and hospital admissions, Environ Health Persp., 124, 413–419, doi:10.1289/ehp.1409164, 2016.

Stockwell, W. R., P. Middleton, J. S. Chang, and X. Tang (1990), The second generation regional acid deposition model chemical mechanism for regional air quality modeling, J. Geophys. Res., 95, 16,343– 16,367.

Su, L. and Fung, J. C. H.: Sensitivities of WRF-Chem to dust emission schemes and land surface properties in simulating dust cycles during springtime over East Asia, J. Geophys. Res.-Atmos., 120, 11215–11230, doi:10.1002/2015JD023446, 2015.

Su, L. and Fung, J. C. H.: Investigating the role of dust in ice nucleation within clouds and further effects on the regional weather system over East Asia – Part 1: model development and validation, Atmos. Chem. Phys., 18, 8707–8725, https://doi.org/10.5194/acp-18-8707-2018, 2018.

Tanaka, T.Y., Chiba, M., 2006, A numerical study of the contributions of dust source regions to the global dust budget, https://doi.org/10.1016/j.gloplacha.2006.02.002.

Tao, W.-K. and Adler, R. (Eds.), 2003, Cloud Systems, Hurricanes, and the Tropical Rainfall Measuring Mission (TRMM). Part V. TRMM - History and Management, Meteorological Monographs, 29, pp. 175–234 (Boston, MA: American Meteorological Society).

Tegen, I., Werner, M., Harrison, S. P., Kohfeld, K. E., 2004, Relative importance of climate and land use in determining present and future global soil dust emission, https://doi.org/10.1029/2003GL019216.

Textor, C., et al., Analysis and quantification of the diversities of aerosol life cycles within AeroCom, *Atmos. Chem. Phys., 6,* 1777–1813, 2006.

Thomas G. E., C. A. Poulsen, R. L. Curier, G. De Lewuw, S. H. Marsh, E. Carboni, R. G., and R. Siddans, Comparison of AATSR and SEVIRI aerosol retrievals over the Northern Adriatic, Quart. J. Roy. Meteorol. Soc., 133, 85–95, 2007.

Thompson, G., Rasmussen, R. M., and Manning, K.: Explicit forecasts of winter precipitation using an improved bulk microphysics scheme. Part I: Description and sensitivity analysis, Mon. Weather Rev., 132, 519–542, 2004.

Thompson, G. and Eidhammer, T.: A study of aerosol impacts on clouds and precipitation development in a large winter cyclone, J. Atmos. Sci., 71, 3636–3658, 2014.

Todd, M., et al., Quantifying uncertainty in estimates of mineral dust flux: An intercomparison of model performance over the Bodélé Depression, northern Chad, *J. Geophys. Res., 113,* D24107, doi:10.1029/2008JD010476, 2008.

UNEP/MAP-Plan Bleu: State of the Environment and Development in the Mediterranean, UNEP/MAP-Plan Bleu, Athens, 2009.

UNEP/MAP, 2012. State of the Mediterranean Marine and Coastal Environment. UNEP/MAP – Barcelona Convention, Athens, 2012.

Vautard, R., Yiou, P., and Oldenborgh, G. J. v.: Decline of fog, mist and haze in Europe over the past 30 years, Nat. Geosci., 2, 115–119, 2009.

Vautard, Robert & Gobiet, Andreas & Sobolowski, Stefan & Kjellström, Erik & Stegehuis, Annemiek & Watkiss, Paul & Mendlik, Thomas & Landgren, Oskar & Nikulin, Grigory & Teichmann, Claas & Jacob, Daniela. (2014). The European climate under a 2 °C global warming. Environmental Research Letters. 9. 034006. 10.1088/1748-9326/9/3/034006.

Wang, F., X. Zhao, C. Gerlein-Safdi, Y. Mu, D. Wang, and Q. Lu. 2017. Global Sources, Emissions, Transport and Deposition of Dust and Sand and Their Effects on the Climate and Environment: A Review. Frontiers of Environmental Science and Engineering 11 (1): 13. doi:10.1007/s11783-017-0904-z.

Washington, R., M. C. Todd, A. S. Goudie, and N. Middleton, Global dust storm source areas determined by the total ozone monitoring spectrometer and ground observations. Ann. Assoc. Am. Geogr., 93, 297–313, 2003.

Weger, M., Heinold, B., Engler, C., Schumann, U., Seifert, A., Fößig, R., Voigt, C., Baars, H., Blahak, U., Borrmann, S., Hoose, C., Kaufmann, S., Krämer, M., Seifert, P., Senf, F., Schneider, J., and Tegen, I.: The impact of mineral dust on cloud formation during the Saharan dust event in April 2014 over Europe, Atmos. Chem. Phys., 18, 17545–17572, https://doi.org/10.5194/acp-18-17545-2018, 2018.

Wesely, M. L.: Parameterization of surface resistances to gaseous dry deposition in regional-scale numerical models, Atmos. Environ., 41, S52–S63, 1989.

Winker, D. M., M. A. Vaughan, A. Omar, Y. Hu, K. A. Powell, Z. Liu, W. H. Hunt, and S. A. Young, Overview of the CALIPSO Mission and CALIOP Data Processing Algorithms, J. Atmos. Oceanic Technol., 26, 2310–2323, 2009.

Woodward, Stephanie. (2001). Modeling the atmospheric life cycle and radiative impact of mineral dust in the Hadley Centre Climate Model. Journal of Geophysical Research. 106. 18155-18166. 10.1029/2000JD900795.

Yoon, J., Chang, D.Y., Lelieveld, J., Pozzer, A., Kim, J., Yum, S.S., Empirical evidence of a positive climate forcing of aerosols at elevated albedo, Atmospheric Research 229 (2019) 269–279, https://doi.org/10.1016/j.atmosres.2019.07.001.

Yu, H., Chin, M., Bian, H., Yuan, T., Prospero, J. M., Omar, A. H., and Remer, L. A.: Quantification of trans-Atlantic dust transport from seven-year (2007–2013) record of CALIPSO lidar measurements, Remote Sens. Environ., 159, 232–249, 2015.

Zaveri, R. A., R. C. Easter, J. D. Fast, and L. K. Peters (2008), Model for Simulating Aerosol Interactions and Chemistry (MOSAIC), J. Geophys. Res., 113, D13204, doi:10.1029/2007JD008782.

Zender, C. S., H. Bian, and D. Newman, Mineral Dust Entrainment and Deposition (DEAD) model: Description and 1990s dust climatology, J. Geophys. Res., 108(D14), 4416, doi:10.1029/2002JD002775, 2003.

Zender, C. S., R. L. Miller, and I. Tegen (2004), Quantifying mineral dust mass budgets: Systematic terminology, constraints, and current estimates, Eos Trans. AGU, 85(48), 509–512.

Sitography

https://www.centrometeoitaliano.it/notizie-meteo/sabbia-polvere-deserto-cieli-italia-pulviscolo-arrivo-sahara-29-10-2018-68196/

https://digilander.libero.it/silvanodgl3/aeropsol_atmosferico1.htm

http://fst.unife.it/it/orientamento/progetto-lauree-scientifiche/corso-di-eccellenza/allegati/eccellenza2008-DiMatteo.pdf

http://www.climate.be/textbook/chapter4_node3_2.html

https://www.who.int/en/news-room/fact-sheets/detail/ambient-(outdoor)-air-quality-and-health

https://it.wikipedia.org/wiki/Oscuramento_globale

https://it.wikipedia.org/wiki/Riscaldamento_globale

http://berkeleyearth.org

https://www.nasa.gov/centers/langley/news/factsheets/Aerosols.html

http://www.met.fu-berlin.de/wetterpate/tief2018/

https://content.meteotrentino.it/analisiMM/2018_perturbazione_ottobre.pdf

https://cds.climate.copernicus.eu/cdsapp#!/home

https://confluence.ecmwf.int/display/CKB/What+is+ERA5

https://www.informazioneambiente.it/pressione-atmosferica/
https://www.cengage.com/resource_uploads/downloads/0495555061_137182.pdf

https://books.google.it/books?id=SpGfKb23Y9QC&printsec=frontcover&dq=Meteorology+Today:+An+Introduction+to+Weather,+Climate,+and+the+Environment,+Eighth+Edition

https://allertameteo.regione.emilia-romagna.it/documents/20181/437770/Evento+27-30+ottobre+2018/

https://modis.gsfc.nasa.gov/about/

https://modis.gsfc.nasa.gov/about/design.php

https://modis.gsfc.nasa.gov/data/dataprod/

http://www.mi.uni-hamburg.de/costmodinv

https://www.mmm.ucar.edu/weather-research-and-forecasting-model

https://ruc.noaa.gov/wrf/wrf-chem/

http://tropic.ssec.wisc.edu/real-time/mimic-tpw/global/main.html

https://disc.gsfc.nasa.gov/datasets/TRMM_3B42_Daily_7/summary

https://ghrc.nsstc.nasa.gov/home/micro-articles/atmospheric-rivers

https://www.noaa.gov/stories/what-are-atmospheric-rivers

Acknowledgments

Thanks to the supervisor Prof. Eng. Giorgio Passerini, for the consideration and the trust given me during the realization of this thesis, allowing me to work in a peaceful as well as efficient environment, confirming the competence and strong human qualities that qualify him as a person and as a professor.

My gratitude also goes to Dr. Umberto Rizza, co-supervisor of this thesis and first researcher at the National Research Council – Institute of Atmospheric Sciences and Climate (CNR – ISAC, Unit of Lecce), for his availability to clarify all my doubts and for having followed me with particular attention and kindness during the writing of this thesis.

Thanks to Dr. Giulia Panegrossi and Dr. Francesca Barnaba, both researchers at the CNR-ISAC (Unit of Rome) for having collaborated by providing essential data and information.